NTNU – Trondheim
Norwegian University of
Science and Technology

Lessons from Nature, the Wetting of Springtail Cuticles

Kristin Fjellvang

Master of Science in Product Design and Manufacturing
Submission date: June 2012
Supervisor: Christian Thaulow, IPM

Norwegian University of Science and Technology
Department of Engineering Design and Materials

THE NORWEGIAN UNIVERSITY
OF SCIENCE AND TECHNOLOGY
DEPARTMENT OF ENGINEERING DESIGN
AND MATERIALS

MASTER THESIS SPRING 2012
FOR
STUD.TECHN. KRISTIN FJELLVANG

Lessons from Nature, the Wetting of Springtail Cuticles

Lære av naturen, overflatefuktning av kutikula til spretthaler

Nature often exhibits very sophisticated solutions to complex problems. Millions of years of evolution have resulted in structures and materials that are ideally suited for the environments they are exposed to. There is much to learn from nature for a materials scientist, this has led to the establishment of the field of biomimetics. Biomimetics involves the study and replication of natural mechanisms, structures and materials. In many engineering challenges nature has already solved a similar problem, the biomimetics scientist will learn from nature's lessons in her search for efficient solutions.

Springtails (Collembola) are small earth-dwelling arthropods whose cuticle shows several interesting properties, the replication of which would be useful in as diverse fields as corrosion-protection, anti-fouling, self-cleaning, anti-icing and possibly hydrate-inhibition. The cuticle combines superhydrophobicity with a low contact angle hysteresis (necessary for self-cleaning), a robust capacity for air-retention (i.e. the "plastron" effect), gas permeability and structural strength superior to that of more well-studied surfaces in the field of superhydrophobicity.

- Present the wetting-properties of the springtail cuticle and discuss the value of these properties in industrial applications.
- Perform studies of the surface structures of springtail cuticles, using advanced methods such as focused ion beam (FIB) machining combined with scanning electron microscopy (SEM).
- Consider the effect of surface geometry on the wetting-properties of a solid, with special focus on the unique geometric pattern of springtail cuticles. Present the relationships between geometry, surfaces tensions and wetting-properties.

The thesis should include the signed problem text, and be written as a research report with summary both in English and Norwegian, conclusion, literature references, table of contents, etc. During preparation of the text, the candidate should make efforts to create a well arranged and well written report. To ease the evaluation of the thesis, it is important to cross-reference text, tables and figures. For evaluation of the work a thorough discussion of results is appreciated.

Three weeks after start of the thesis work, an A3 sheet illustrating the work is to be handed in. A template for this presentation is available on the IPM's web site under the menu "Undervisning". This sheet should be updated when the Master's thesis is submitted.

The thesis shall be submitted electronically via DAIM, NTNU's system for Digital Archiving and Submission of Master's thesis.

The contact person is
PhD student Håkon Holm Gundersen, NTNU

Torgeir Welo
Head of Division

Christian Thaulow
Professor/Supervisor

NTNU
Norges teknisk-
naturvitenskapelige universitet
Institutt for produktutvikling
og materialer

Abstract

Surfaces that display super-hydrophobic properties have numerous areas of application in the industry. Nature have trough millions of years of evolution developed structures and materials perfectly adapted to different species' environment, and by learning from nature similar hydrophobic surfaces can be manufactures. The Collembolas, a small arthropod, have showed to possess a sophisticated nanoscaled, geometrical pattern of granules connected with ridges on their cuticle, their skin. These patterns make the surface structure roughened, which is by traditional wetting theory stated as the reason its of super-hydrophobic properties. In addition to a rough surface, the collembolans are said to have an overhang on the granules. These overhangs make the granule appear as a nano sized "mushroom", and should provide a further resistance to wettability. This overhang has however not been documented by imaging, besides one image taken by Transmission Electron Microscopy. To confirm the overhang is an important part of this thesis, as well as a study of its relation to super-hydrophobic properties.

To investigate the existence of the overhang, a Focused Ion Beam (FIB) was used together with Scanning Electron Microscopy (SEM). By utilizing properties provided by the FIB and its software, a survey of the granules on the cuticle was obtainable. There are in total seven different species distributed on eight samples was examined. Four out of eight samples proved to display an overhang, but by a comparison with measured values of hydrophobicity, no direct relationship between the degree of overhang displayed and the resistance to wetting was found. The overhang is very likely a factor contributing to hydrophobicity, but the collembolans are not depending on them to exhibit such properties. This fact is important to establish before an overhang is rewarded as the reason for the collembolans super-hydrophobic properties.

Sammendrag

Overflater som viser superhydrofobiske egenskaper har et stort antall bruksområder I industrien. Gjennom millioner av år med evolusjon har naturen utviklet overflater og materialer perfekt tilpasset ulike artes miljø, og ved å lære av naturen kan lignende hydrofobiske overflater bli fremstilt. Kollemboler, en liten arthropod, har vist seg å inneha et sofistikert, nanoskalert mønster av granuler knyttet sammen av lister på deres kutikula (hud). Disse mønstrene gjør overflatestrukturen ru, hvilket i følge tradisjonell fuktningsteori skal føre til super-hydrofobiske egenskaper. I tillegg til en ru overflate, skal kollembolene visstnok ha et overheng på granulene. Disse overhengene fører til at granulene blir seende ut som «sopper» av nanostørrelse, og skal føre til en ytterligere motstand mot fuktning. Dette overhenget har derimot aldri blitt dokumentert ved avbildning, utenom ett bilde tatt av Transmission Electron Microscopy. Å bekrefte overhenget er en viktig del av denne masteroppgaven, sammen med en studie av overhengets relasjon til superhydrofobiske egenskaper.

For å undersøke eksistensen av overhenget ble det benyttet en Focused Ion Beam (FIB) sammen med Scanning Electron Microscopy (SEM). Ved å benytte egenskapene gitt av FIB'en og tilhørende software var det mulig å undersøke granulene på kutikulaen. Totalt ble syv ulike arter fordelt på åtte prøver undersøkt. Fire av åtte prøver viste seg å inneha et overheng, men ved en sammenligning med målte verdier for hydrofobisitet, ble ingen dirkete sammenheng mellom graden av overheng og motstand mot fuktning funnet. Overhenget er svært sannsynlig en faktor som bidrar til hydrofobisitet, men kollembolene er ikke avhengig av dem for å vise slike egenskaper. Dette er et viktig faktum å etablere før overhenget blir omtalt som årsaken for kollembolenes superhydrofobiske egenskaper.

Preface

This master thesis is produced throughout the spring semester 2012 at the Norwegian University of Science and Technology, Department of Engineering Design and Materials. To be allowed at the nano lab at NTNU, clean room courses and FIB training was required, and the latter with a subsequent exam.

I would like thank my supervisor Christian Thaulow for showing great enthusiasm and interest in my work, co supervisor Håkon Gundersen who always takes his time to help me with my work and supplying me with data from his own research, Runar Sandnes for the cooperation between his and my results, Bjørn Rogne for teaching me to use and understand the FIB and Vidar Tonaas Fauske for teaching me to use integrated FIB software.

Table of contents

Figure list

Symbol and abbreviation list

BSE – Backscattered Electron

f_1 – Total area of solid-liquid interface

f_2 – Total area of liquid-vapour interface

FIB – Focused Ion Beam

F_{lv} - Free energy in liquid-solid interface

F_{sl} - Free energy in solid-liquid interface

F_{sv} – Free energy in solid-vapour interface

Ga - Gallium

kV – Kilo Volt

LMIS – Liquid Metal Ion Source

nA – Nano Ampere

pA – Pico Ampere

r_f – Roughness factor

Rel. Int. Diam – Relative Interaction Diameter

S&V – Slice and View

S.A. – Sliding angle

SE – Secondary Electron

SEM – Scanning Electron Microscopy

$\Delta\theta$ - Contact Angle Hysteresis

θ - Contact Angle

θ' – Apparent Contact Angle

θ_0 – Static,Mmetastable Contact Angle

θ_a – Advancing Contact Angle

θ_h – Contact Angle of Homogenous Interface

θ_r – Receding Contact Angle

1. Introduction

Super-hydrophobicity and the application of surfaces with such properties is a popular area for researches, and there have been an substantial increase of published material on the topic.(1) A super-hydrophobic surface has a widely potential area of utilization, from drag reduction of ships to water harvesting. Attempts to copy mechanisms of biological material to achieve their properties have been done for centuries(2), and regarding super-hydrophobicity and modern applications the lotus plant was a pioneer when mimicked for manufacturing a self-cleaning paint in 1999.

To understand the mechanisms behind hydrophobicity a literature study was done. In 1804 Thomas Young first described the theory of capillary phenomena on the principle of surface tension(3). By observing the constancy of contact angles, thus the angle between a liquid-gas interface and a liquid-solid interface when a drop rests on a solid, Young deduced his theories. In 1805 Young and Simon-Pierre Laplace(4) simultaneously derived the theories of how capillary difference pressure is sustained across an interface at equilibrium, resulting in the equation now known as Young-Laplace equation. When surface topography later was credited as a great contributor to super-hydrophobic properties, theories an equations was in 1936 developed by Wenzel on the effect of roughened surface with respect to hydrophobicity(5). He claimed that large contact angles due to a rough surface resulted in resistance of wetting. Inspired by Wenzel, Cassie and Baxter extended his theories in 1944 to include a porous surface with asperities(6). The state of liquid resting on top of asperities, leaving air pockets underneath the drop, is now referred to as the Cassie-Baxter state, and is in general a more realistic state than the Wenzel state where it is assumed that the droplet wets the surface between the roughness. To date describing wetting is by most scientist done by the Wenzel and Cassie-Baxter's equations, despite the critique that have been raised against them due to assumptions of wetting phenomena and condition during wetting(7-10).

In recent years attention has been paid to the wetting properties of the cuticle (skin) of the small animal Collembola(2, 11). Their cuticle is covered with a geometrical pattern of nano scaled granules with ridges between them. Their super-hydrophobic properties are believed to be a consequence of a combination of surface roughness and a unique overhang of their granules. This overhang makes some of the granules look very similar to the shape of a mushroom, more specific as a champignon. Hydrophobic surfaces have already been manufactured in great extent by implanting surface roughness in shapes of everything from honeycomb-patterns to raspberries, tough ordinary cylinder or cubic shapes are most common(12-17). A surface inspired by an overhang is however to my knowledge never been produced.

The overhang of collembolans granules is new information to most, and is investigated in this thesis by the utilization of Focused Ion Beam (FIB) and Scanning Electron Microscopy (SEM). By suitable software 3D models was also made of two of the samples, allowing me to rotate and study structure of the sample from every direction and angle. Helbig et al.(11) have published an image of an overhang taken by Transmission Electron Microscopy (TEM), see Figure 3, but to date no known work of imaging the granules and the ridges between them have been done by FIB milling in combination with SEM imaging. The lack of previously known work made the processing of the samples in FIB both challenging and interesting. If the cuticle ever is to be mimicked for industrial applications, it is essential to fully understand the shape of the features that leads to super-hydrophobicity.

A model of measurements necessary to calculate wetting properties due to the surface geometry of the collembola is proposed. These requirements were given by a student investigating the possibilities to develop a mathematical model for such calculations(18). Measurements were taken by studying SEM images, and the number of required measurements possible to obtain was decided by image quality and the geometrical shape of the granule in question. It proved to be great variations in granule size, both between species, and for some samples it varied internally at different areas of the animal. To support the theory of collembolans being super-hydrophobic and to compare FIB and SEM results with quantitative measurements, contact angle measurements of all species is presented and evaluated. All but two samples showed to be super-hydrophobic, and the two

that were not, were still well within the definition of hydrophobic. One of the species was adapting itself depending on seasons, summer or winter, and displayed a more hydrophobic behavior during winter. FIB and SEM studies could however not discover any differences in geometrical features of the summer and winter adapted species.

The dual FIB used for the experimental part is an instrument combining the properties given by an ion beam and an electron beam. It is a highly technical and sophisticated instrument that requires knowledge from the user to utilize it to its full potential. A source of gallium ions provide an ion beam that can be used for matters as extremely accurate milling, etching, deposition of other metals and imaging(19, 20). The electron beam provided from a tungsten filament, may be used for imaging and deposition of protective metal layers. Briefly explained, the ions and electrons that are sent out, hit the sample and returns to detectors that transform the signal to an image. In general samples are much more sensitive to the ion beam than the electron beam, and hence the ion beam should be used to a minimum for visualization and then at very low currents, 9 pA. It is very beneficial to be able to use the SEM for imaging, as the electron beam is much gentler to the sample regarding etching damages. When using the FIB for procedures as milling, the result can be inspected by the SEM.

Biological material have been examined by FIB since the late 60's (21, 22), but due to the effect caused by ion etching the applicability of FIB has been limited. Biological samples are more sensitive to ion beam than metal samples (23, 24), and the usage of currents should therefore be restrictive. Earlier publications have described methods for using FIB to study biological samples (23, 25-28), but none of them could directly be linked to this work, and it seems to be very varying how sensitive each individual biological sample is to high currents. Neither wetting theory or biological samples in FIB are new scientifically areas, but the combination of using FIB to inspect biological features that causes the unique property of hydrophobicity have to my knowledge not been done before.

By SEM studies the beautiful geometrical patterns on the cuticle was well displayed. Depending on the species the granules was placed hexagonally, rhombic or as a combination, and with ridges of varying length between them. This surface structure alone makes a roughened surface, and should according to Wenzel and Cassie-Baxter lead to hydrophobic properties. In advance of the experimental part it was expected to be found mushroom shaped granules on most of the samples. Eight samples in total with seven different species were investigated, and only half of them proved to display a clearly shaped overhang. These overhangs did look like a mushroom, but four samples had thus no sign of overhang and were displayed as what reminiscent of thick pancakes placed side by side. This indicates that other factors besides granule overhang are the reason for super-hydrophobic and hydrophobic properties.

2. Background

The Collembola is a small animal in the phylum microarthropods. The oldest fossils ever found of this phylum are 400 million-years old Collembolan, very similar to the ones found to day(29). Springtails can be found almost anywhere on Earth, from the treetops in the rainforest to the cold tundra on Svalbard. In healthy soil they can be abundant, with a density up to several million individuals per square meter, and a species richness from 1-3 to 50-60 species in an ecosystem(30). Members of the Collembola have a varying size, between 0.4-10 mm in length. As for today, there are more than 7000 known species, but there are still areas that are not properly surveyed(11).

The respiration systems of most insects are the tracheae system(29). For transport of oxygen insects utilize branched tubes. These tubes, or tracheoles, have openings called the spiracles, which support the insect with oxygen. Springtails are not classified as insects, but are still relevant to compare their respiration system with traditional insects.

In Collembola the tracheal system is only present in a much reduced form, and only for a few groups(29). They have a unique feature, the ventral tube, or collophore which is utilized for matters as imbibition, excretion, respiration and adhesion to smooth surfaces. In addition to the collophore, the respiration takes place through the cuticle. This cuticle is also hydrophobic, and this matter will be thoroughly discussed in this thesis. Collembola species that have a habitat located submerged in fluid displays plastron-respiration. This is respiration through an air film (plastron) surrounding the animal due to the hydrophobic cuticle. A number of Collembola have the fascinating capability of *anhydrobiosis*. This means they can become completely dry without dying. Before they go into this state they form a capsule around themselves, and when rewetted they resume common activity in a couple of hours.

In an evolutionary aspect the springtail cuticle was developed to withstand the harsh conditions of their habitats. As a consequence of epidermal respiration the springtail depends on the prevention of cuticle wetting as well as surviving drought and freezing(11). The collembola displays a hierarchical structure of nanoscopic granules. The granules exist in the form primary granules, which are interconnected, secondary granules, and in combination with bristles.

The primary granules are triangular and quadrangular in shape with a length of 200-1500 nm covering the whole body(11). These geometrical shapes may occur on the same animal, where rhombic pattern is found on areas that require higher elasticity. They are connected with ridges, forming a hexagonal or rhombic pattern, see Figure 1. Not every species displays the secondary granules, see Figure 2. According to Helbig et al.(11) it seems to be a connection between secondary granules and habitat, where these granules may protect the integrity of the nanostructure. This theory is rejected by others as secondary granules also are displayed on collembolans in a moist habitat, where the granules are not subjected to harsh mechanical wear(31).

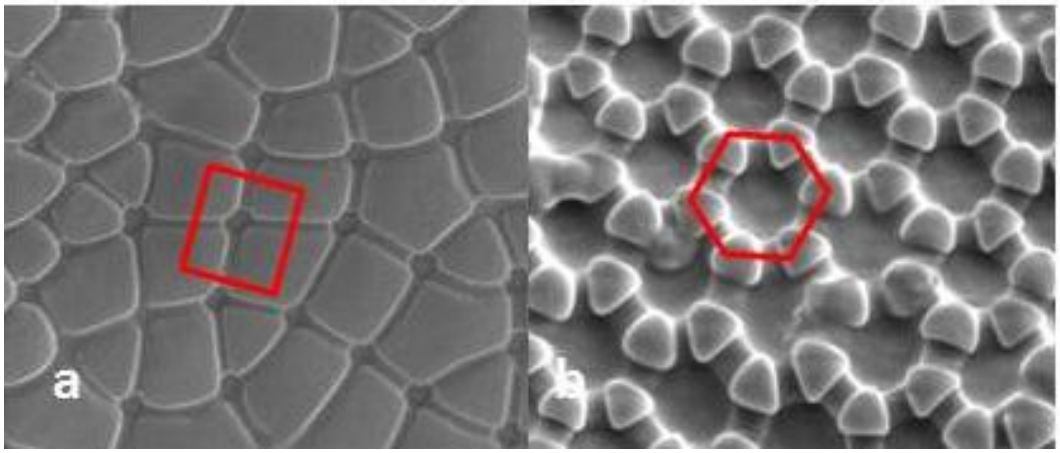

Figure 1 – Geometrical patterns on cuticle a) Rhombic alignment, b) Hexagonally alignment

Figure 2 - Secondary granules (SG) (11)

Helbig et al. (11) showed in 2011 that the combination of bristles and the hexagonal or rhombic mesh can resist wetting from organic liquids at elevated pressure. They revealed the negative overhang in the profile of the ridges and granules to be a very effective design principle of the springtail cuticle. Helbig et al. observed if the collembolans are immersed in liquid, very stable plastrons form around them, resisting elevated pressures higher than 3.5 atmospheres and sustaining for days. This includes polar and non-polar liquids with much lower surface tension. Droplet formation occurred on secondary granules tops, and fusion of droplets during growth was often followed by lateral displacements of the droplets, verifying a very low wetting hysteresis in the wetting behavior.

To facilitate respiration and creating a surface highly resistant to wetting, the primary granules and ridges are equipped with a negative curvature of the overhang, see Figure 3. This negative overhang leads to an energy barrier that must be overcome by the advancing liquid phase before any wetting becomes irreversible(11). It should be noted that Helbig et al.'s article presents the overhang as a feature displayed by all collembolans. Theories on how the overhang contributes to super-hydrophobicity are described later in section 4.1.6.

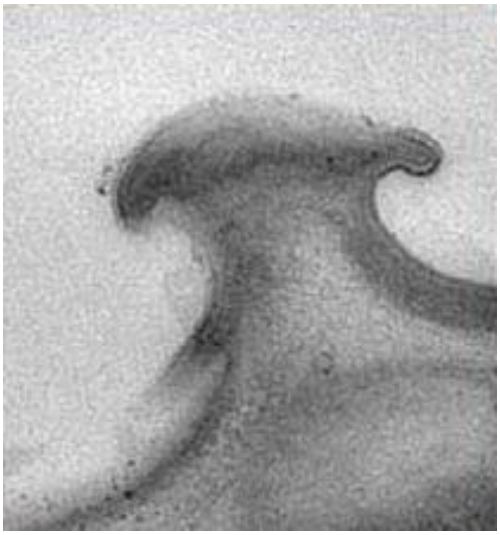

Figure 3 - Collembola overhang (11)

3. Biomimetics

The term "Biomimetic" was first used in the 1960s by Otto Schmitt. Biomimetics is the study of the structure and function of biological systems as models for the design and engineering of materials and machines. Biomimetic is derived from ancient Greek; *bios*, meaning life, and *mimetikos*, meaning to imitate(32). Biomimetics is used in several fields; architecture, algorithms, fabric, biofuel, paint, artificial tissue, material structure and many more. In relation to super-hydrophobic surfaces the surface features of certain plants have already been imitated to obtain their properties(11). Plants have however nanoscaled wax crystals forming a rather fragile and continuously renewed structure. These epicuticular wax crystals cannot be replicated due to their poor mechanical stability(33). Collembolans cuticle is sustainable and more mechanically stable due to incorporated, flexible bristles and the alignment of granules(11). The following sections describe areas where biomimetic may be utilized to develop surfaces of different applications, where section 3.1-3.3 is related to the properties of the collembolans.

3.1 Self-cleaning

In modern industry, the Lotus leaf has already been copied due to its well-known capability of self-cleaning, called the Lotus effect™, the trademark owned by Wilhelm Barthlott. Self-cleaning is the mechanism where water drops completely roll of the surface, carrying with them particles of dirt and soil, leaving a clean surface(34). The self-cleaning properties have been used in painting industry since 1999(2). Self-cleaning paint will reduce the need of chemical cleaning and hence have a positive effect on environment as well as a self-cleaning surface result in less maintenance. Another industry that will benefit from self-cleaning material is producers of solar panels and windows. These industries will however require an optically transparent surface.

3.2 Anti-icing

Challenges related to ice vary from problems as reduced visibility on the front wind-shield of vehicles due to frosting(2), to ice building up on solid materials causing mechanical failure or insulator flashovers(35). It is a challenge to construct solid surfaces with anti-icing properties, but produced biomimetic super-hydrophobic surfaces have proven to reduce accumulation of ice and snow and to completely prevent formation of ice on solid surfaces. In the offshore industry ice in several forms is a major issue. It is estimated that 20 % of remaining oil- and gas recourses is found north of the Arctic Circle, where 85 % of these recourses is located offshore(36). This means that in addition to different forms of ice impact on cities and populated areas, there is an enormous industry seeking materials with anti-icing properties.

3.3 Drag reduction

Drag reduction would give advantages as reduction of fuel consumption for airplanes and ships, and increased pipeline capacities(37). These industries would have an economic interest in reduction of drag, and as exhaust gases and particles related shipping and aviation have a serious impact on the climate they should be reduced to a minimum.

A super-hydrophobic surface could be utilized to reduce the effect of drag for ships(2). It is assumed that the flow velocity is equal to zero at a solid-liquid interface (no-slip condition), and that it continuously increases when increasing from the surface. On super-hydrophobic surfaces fluid flow display a boundary slip, which means that the fluid velocity near the solid surface is unequal to solid surface velocity, which then reduce drag in fluid flow. Surfaces with nano sized air bubbles have showed to reduce drag as these bubbles decrease the solid-liquid interaction and lead to reduced friction between fluid and solid walls at the solid-liquid interface(38).

3.4 Super-oleophobicity

Fish scales have proven to be super-oleophobic (oil contact angle larger than 150°), and allows the fish to survive in oil-polluted water(39). It is the hierarchal nanostructure of the fish scales in combination with their chemical composition that results in this super-oleophobicity. Submerged in an aqueous environment, the wettability of oil on a material surface have many applications; droplet manipulation in microfluids, cell and protein adhesion control on surfaces, preparation of electrowetting-based displays and separation of oil and water(40).

3.5 Adhesive properties

The common super-hydrophobic surface should have high contact angle and very low slide angle (SA<10°), but a new class of biomimetic super-hydrophobic surface combined with adhesive surface as well has been reported(35). Boduroglu et al.(41) demonstrated how they could control the adhesion properties through nanoscale modulation of roughness, changes in composition and alteration of surface chemistry of the films used in their study. Van der Waals force and/or the capillary force interactions between the nanostructured film surface and water causes the strong adhesion.

A surface combining super-hydrophobicity and adhesion may be used for handling small liquid droplets, inducing selective permeability in a membrane and in operation of wall-climbing robots(41). A surface well-known for its amazing adhesive features is the toe of a gecko(42). The toes of a live *Tokay* gecko is highly hydrophobic, and adheres equally well to highly hydrophobic- and highly hydrophilic, polarizable surfaces. Autumn et al. (42) attributes a van der Waals mechanism for the extraordinary adhesive properties of gecko setae[1]. This implies that the adhesive property is merely a result of the size and shape of the setae tip, and not strongly affected by surface chemistry.

[1] The hair-like structures on the gecko toes.

[2] A Taylor cone is the cone observed in electrospraying (here ion spraying) before the jet and plume is formed

3.6 Anti-corrosion

It is estimated that corrosion alone makes up 4 % of Norway's gross domestic product, resulting in total of 60 billion NOK every year(43). Industries that will benefit from anti-corrosion products, either by coating or anti-corrosive materials is e.g. pipeline, shipping, containers, onshore construction and offshore construction with stationary and floating oil platforms.

Previous work has proved modified copper to exhibit hydrophobic behavior(44). Surface structure at a nanoscale level was selective etched onto film in the shape of flowers, flowerlike clusters and straw-like structure. Such structures can trap a large amount of air, and results in contact angle of 158°. These samples were then immersed in seawater, and after a month the super-hydrophobic film was intact, and the contact angle had not changed. By a comparison of bare and modified copper samples, the corrosion rate of the copper with a super-hydrophobic surface was dramatically decreased.

By deposition of Ni-P composite coating on carbon steel, great results have been obtained trying to develop surfaces with anti-corrosive properties(45). The microstructure of the film had micro-particles with diameters of 1-12 μm spread over the surface, and the contact angle was reduced by only 2-3° after 45 days in room temperature. Samples with triple layer of super-hydrophobic film proved to have a 45 hours delay of corrosion compared to a bare surface.

Manufactured surfaces of super-hydrophobic properties by the use of coating or film have however showed weak adhesion forces between the coated hydrophobic membrane and main solid surface, and the coated membrane were generally electrically insulated(46). Micro-nickel cylinder arrays have been fabricated to mimic the state of Cassie-Baxter, and during tests of droplets on surface contact angles up to 155° was achieved without coating materials with low surface energy. Figure 4 is a SEM image of one of the fabricated surfaces. The height of the cylinder is 10μm, diameter is 10μm, spacing between to cylinders is 20μm and the surface displays a contact angle of 155°. This is not surface structure at a nanolevel, but by improved fabrication process who knows how small structures can be developed?

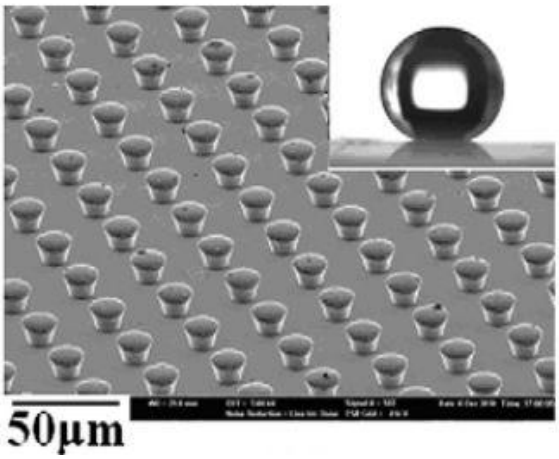

Figure 4 - Prepared cylinder arrays (46)

One of the initial goals of this thesis was to describe how a potential manufactured surface inspired by collembola cuticle would behave in relation to corrosion. It is fundamental knowledge that increased surface area effects the corrosion rate and a surface structure similar to the collembolans would lead to a larger surface are in total, and hence probably affect and increase the corrosion rate. During a widely literature study throughout the semester, *not a single* article contained any information of this theme. If modification of surface structure to obtain a corrosive resistant behavior due to super-hydrophobicity is to be manufactured, the corrosion behavior of such a surface itself must be further investigated.

4. Theory

To understand and explain the wetting properties of the collembola basic wetting theory is presented. The general understanding is that a non-smooth surface contributes to hydrophobic properties. To survey the structures of collembola cuticle a dual Focused Ion Beam was utilized, and the principles behind the FIB is explained.

4.1 Wetting and super-hydrophobicity

The terms hydrophilic, hydrophobic and super-hydrophobic is frequently used in papers, but the meaning of the word hydrophobic has not been resolved before further modifications. Gao et al. (1) addresses this issue, and stresses that the words hydrophobic, hydrophilic and all of their derivatives should only be used as qualitative adjectives. The term super-hydrophobic is used with great variation(47), as an illustrating example see Figure 5. The gray shaded area in Figure 5e represents the sealed air, while the other air pockets are in open state.

In general the degree of hydrophobicity is determined my measured contact angle, θ. This is the angle between the liquid-gas interface and the liquid-solid interface when a drop rest on solid surface. In this master thesis the term hydrophilic will be used for surfaces with θ>90°, and super-hydrophobic for surfaces with θ>150°.

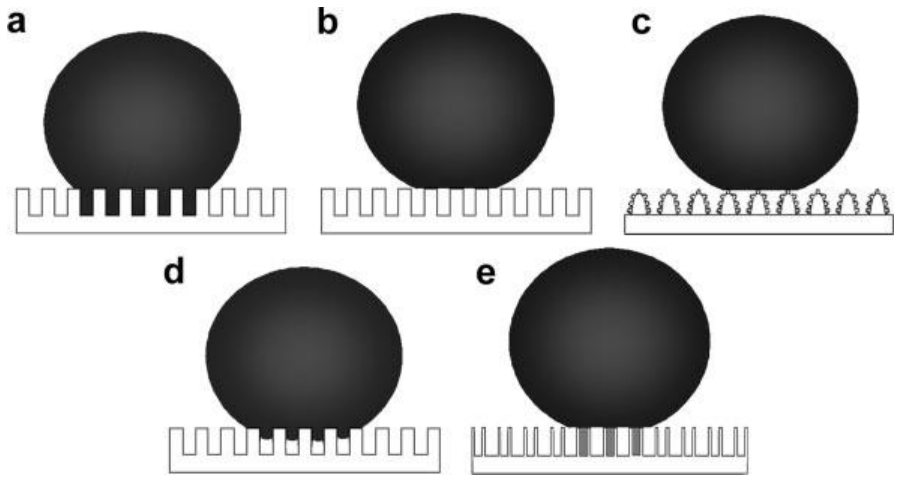

Figure 5 - Different states of super-hydrophobic surfaces: a) Wenzel state b) Cassie-Baxter state c) Lotus state d) Transition super-hydrophobic state between Wenzel and Cassie state e) Gecko state (47)

The contact angle (θ) is formed at the end of the drop, which is called the contact line. A small enough drop will be spherical, larger ones will be flattened due to gravity(48). The size of the contact angle is a result of the balance between three forces that acts along the interface of the three-phase contact line. Thomas Young described in words the equation now known as "Young's law"(3):

$$F_{sv} = F_{sl} + F_{lv}cos\theta \qquad [1]$$

Where *F* is interfacial free energies, *vg* = solid-vapour, *sl*= solid-liquid and *lv*= liquid-vapour. In the determination vapour, all gasses including air are valid, and air and gas is as frequently used as vapour in equation [1]. Figure 6 illustrates the force derivation of Young's equation. The surface tension of the solid-vapour interface equals the sum of surface tension of solid-liquid interface and the horizontal component of the surface tension of the liquid-vapour interface(49).

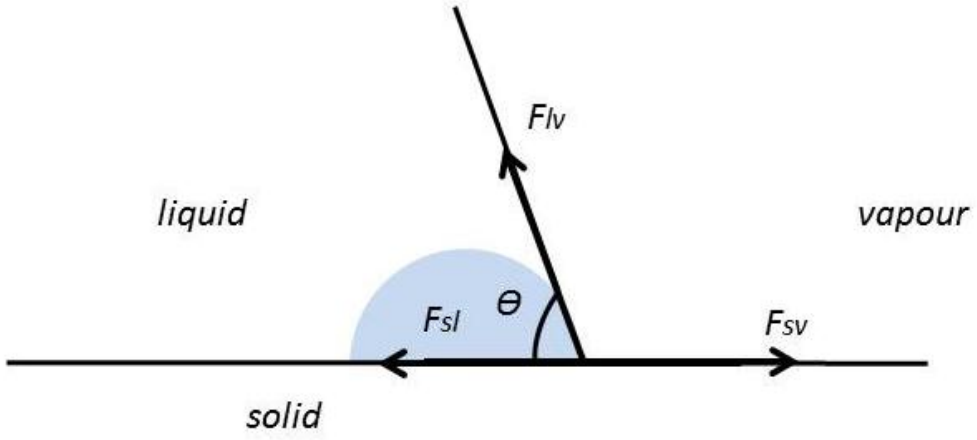

Figure 6 - Force derivation of Young's law.

Depending on the size of the contact angle, the wetting properties of the system can be described. In general the following definition is applicable for the contact angle(50):

- *θ < 10°: Super-hydrophilic*
- *θ < 90°: Hydrophilic*
- *θ > 90°: Hydrophobic*
- *θ > 150°: Super-hydrophobic*

Liquid will spread on surfaces when $F_{sv} - F_{sl} \geq F_{lv}$ ($cos\theta \geq 1, \theta = 0$), form contact angle of 90° when $F_{sv} = F_{sl}$ ($cos\theta = 0$) and form contact angle higher than 90° when $F_{sv} < F_{sl}$ ($cos\theta < 0$). F= [force/length] (8).

Young's law is an idealized state, which unfortunately rarely take place in real materials(10). In reality most materials show two stable contact angles and several metastable contact angles, which lead to difficulties of establishing the equilibrium contact angle.

When a drop is moving, it displays an advancing contact angle, θ_a, on the front half of the contact line and a receding contact angle, θ_r, on the back half of the contact line, see Figure 7(10). A growing drop will exhibit an advancing contact angle along the complete contact line(7). The difference between the advancing and the receding contact angle is the contact angle hysteresis, $\Delta\theta$, where $\Delta\theta$<5° is sometimes regarded as an additional criteria for super-hydrophobicity(51). Contact angle hysteresis is a measurement of energy dissipation during the flow of a droplet along a solid surface and an estimate of how easily the drop moves along the surface. A drop moving along a surface causes areas that are wetted or de-wetted, and to move this way the drop must change its shape. An energy barrier against wetting and de-wetting together with the changing of droplet shape will cause the hysteresis(52).

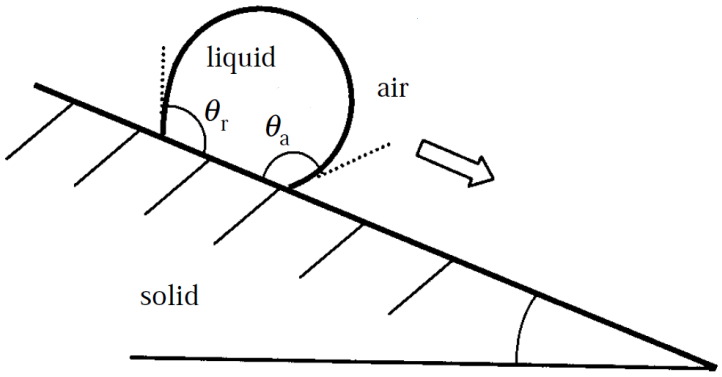

Figure 7 - Schematics of a droplet moving along an inclined surface(53)

4.1.2 Surface roughness

Surface roughness is a characterization of the surface topography(54). To describe the real surface should parameters that describe the variation of height and how these heights vary in the surface plane be included. The mean plane surface is called the nominal surface, see Figure 8.

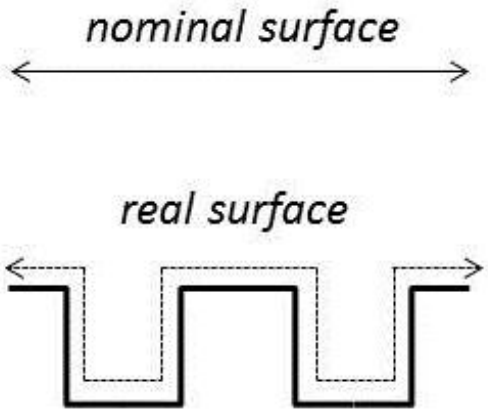

Figure 8 - Illustration of real and nominal surface

As the collembola display a surface with roughness, the effect of such roughness must be understood to explain the super-hydrophobicity of the animal. Young's law is still applied at the contact line, but the roughness results in an apparent contact angle, called θ'. To describe the effect of surface- roughness and structure at the contact angle, two well-known theories are utilized; the theories of Wenzel and Cassie and Baxter. The latter will be referred to as Cassie-Baxter.

4.1.3 Wenzel's theories

Wenzel emphasized the fact that a measured roughened unit area has a larger surface area compared to a smooth area within the same measured unit area, would lead to a greater intensity of surface energy for the roughened area(5). Wenzel points out that an increase of surface area due to roughness will not have any effect upon the specific surface energy values, only the intensity.

A process involved in any wetting of a solid by a liquid includes three interfacial boundary surfaces; solid-liquid, solid-vapour and liquid-vapour(5). As each interface has its own specific surface energy content, wetting results in a net decrease- or increase in total surface energy. Wenzel explains the difference of net energy decrease between smooth and rough surface as the following: A drop of water resting on a horizontal solid surface will display a different specific energy content of the solid interface for the wetted area under the drop, than the dry area around it. If the wetted area has the lower specific energy (either value may be greater), the tendency is the drop spreading spontaneously, and on its way to reach equilibrium both the wetted area under the drop and the free liquid surface over it will therefore increase. Increased wetted area underneath the drop releases energy and increased free liquid surface involves a consumption of energy. The difference is the net energy decrease, which determines how quickly the wetting takes place making it a measure of the wetting characteristic for the solid. The free liquid area at the upper surface of a drop is the same, regardless of surface structure. The amount of wetted surface underneath a drop is however larger if the surface is rough compared to smooth. The net energy decrease will be greater for a rough surface than a smooth, and if the smooth and roughened surface in question is water-repellent, the rough one will be displayed as the most hydrophobic of the two.

To describe the roughness' effect on wettability of a surface, Wenzel introduced a roughness factor, r_f(5). The roughness factor is equal to the ratio between the actual surface area and the geometric area of the solid-liquid interface:

$$r_f = roughness\ factor = \frac{actual\ surface}{geometric\ surface} \qquad [2]$$

If a rough surface of r_f=2, surface tension x and liquid-solid interfacial tension y, will display the same wetting properties as a smooth surface of r_f=1, surface tension 2x and liquid-solid interfacial tension 2y(5). Wenzel's point is illustrated in Figure 9. Line *mn* is a segment of the periphery of the wetted area, and Figure 9a) represent an ideally smooth area where *abcd* is the measured unit area which precisely will be the specific energy of the interface.

S_1 and S_2 is the force vector before and after wetting respectively acting on a unit length ab of the periphery, where their vector sum defines the solid-liquid tension, noted as A by Wenzel. A, or F_{sl} is given by the equation:

$$A = F_{sl} = F_{lv}cos\theta \qquad [3]$$

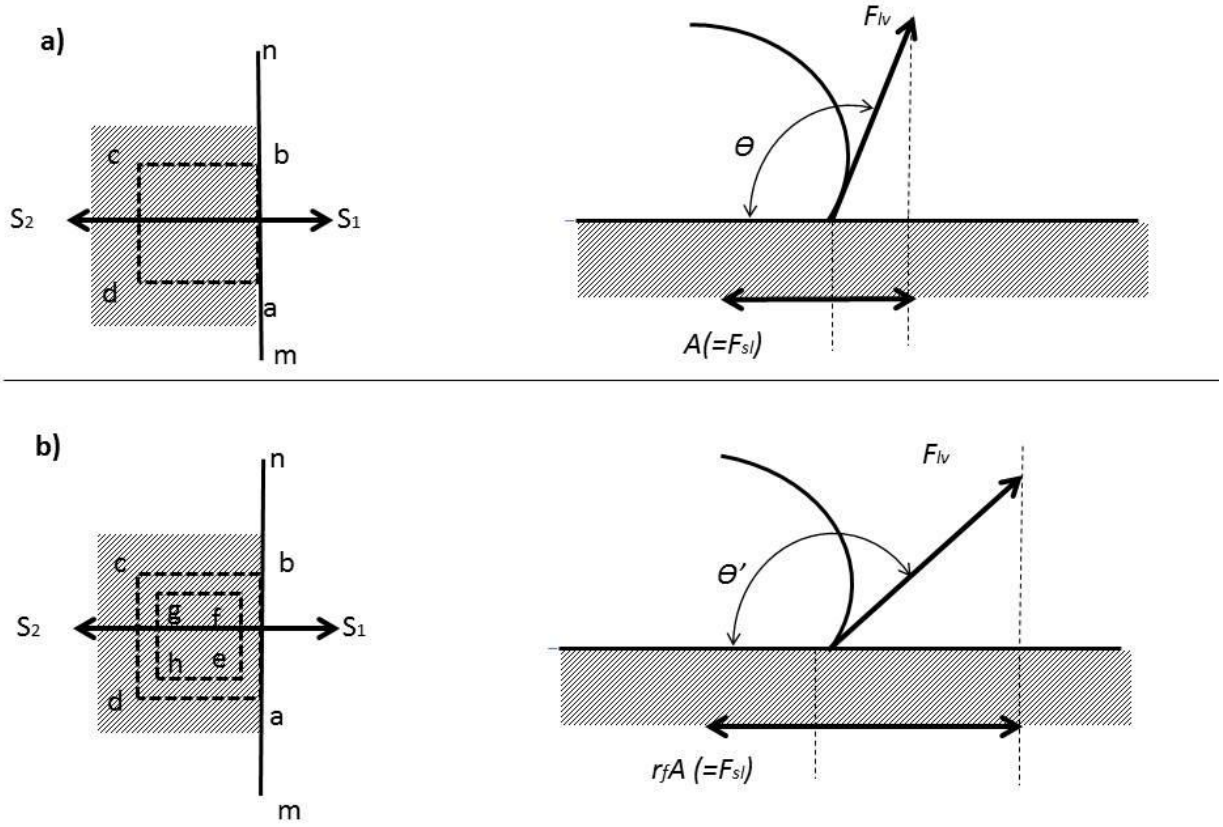

Figure 9 - Vector relations of surface forces for a) Smooth surface, b) Roughened surface, adapted from (5)

As for Figure 9b) the solid surface is concentrated in a smaller area, *efgh*, meaning the forces acting along solid-liquid and solid-vapour is magnified by the roughness factor, r_f, the surface-liquid tension will remain the same.

This meaning a larger contact angle, θ', must therefore act to balance the increased resistance which the solid surface now resisting to wetting process. Θ' can be expressed by modifying Young's equation (Equation [1])(8)), now known as Wenzel's equation:

$$cos\theta' = r_f cos\theta \quad [4]$$

Wenzel's model accounts for that a hydrophobic surface becomes more hydrophobic by an increase of r_f, and that a hydrophilic surface becomes more hydrophilic when r_f increase. By Equation [4] we see that roughness will reinforce the properties of either hydrophilicity or hydrophobicity, and push θ' towards 0° or 180°.

4.1.4 Cassie and Baxter's theories

Wenzel's research was centered on the effect of surface roughness, and Cassie and Baxter extended this analysis by examining porous surfaces and surfaces with asperities(6). In contrast with Wenzel, Cassie and Baxter's theory involves that the drop is resting on both surface and air, see Figure5a) and b) and varying the surface energy rather than the surface roughness. The part of the droplet resting on air pockets would behave as if in contact with air and the droplet fraction resting on asperities would behave as if contact with solid. For a droplet resting on a surface with asperities, f_1 is the total area of solid-liquid interface and f_2 is the total area of liquid-vapour interface. When fluid spreads over this unit area f_1 is destroyed leading the energy f_1F_{SV} is gained, and the energy f_1F_{LS} is extended when forming the solid-liquid interface over the very same area unit. The energy f_2F_{LA} is also extended when forming the air-water surfaces. This gives the net energy E_D as:

$$E_D = f_1(F_{LS} - F_{SV}) + f_2F_{LV} \quad [5]$$

If θ_1 represent the contact angle of the solid-liquid interface and θ_2 the contact angle of the liquid-air interface, a third contact angle Θ_c may be expressed of a binary composite surface with the two area fractions f_1 and f_2 (8):

$$cos\theta_c = f_1 cos\theta_1 + f_2 cos\theta_2 \quad [6]$$

Where:

$$f_1 + f_2 = 1 \quad [7]$$

The reader should be noted that there is disagreements on Equation 7 (55). If the asperities on the surface itself displays roughness or the asperities have different heights, Equation [7] should be reformulated to:

$$f_1 + f_2 \geq 1 \qquad [8]$$

As this section describes the theories of Cassie-Baxter, Equation [7] will be used as this was the definition used by the scientist themselves. Wenzel's and Cassie-Baxter's equations can be combined to express asperities with a certain roughness(50), this combination being the more general case:

$$cos(\theta) = rfcos\theta_h + f - 1 \qquad [9]$$

Where:

$$f = f_1\,, \qquad f_2 = 1 - f \qquad [10]$$

The Cassie-Baxter and Wenzel states are not permanent during wetting of a surface. The Wenzel state can develop into Cassie-Baxter state with an increase of roughness. Depending on surface geometry metastable states can occur. What seem natural for a system is to be in a state that is energetic favorable, but sometimes this is not the actual behavior. An energy barrier is causing the state to remain where it is, even if it is not energetic favorable. If the energy barrier is reached, the system will change states, and probably stay in its new state as a transition back to initiative state requires breaking an even higher energy barrier(18). A metastable Cassie-Baxter state can thus transform into a stable Wenzel state, which means there have been significant energy dissipation and is hence an irreversible transition(50). A transition between Cassie-Baxter to Wenzel state requires a certain pressure, e.g. from a hard rain fall. If a surface is to change its state, the parameters r_f, f_1 and f_2 must change, and in most cases this is rare behavior for a surface. If the same surface is measured and calculated with respect to Cassie-Baxter and Wenzel state, the equation that gives the lowest contact angle can be regarded as most appropriate, and based on the lowest contact angle a determination of which state the system is in can be determined.

The parameters deciding whether the system is in a Cassie-Baxter or a Wenzel state are r_f, f_1 and f_2.

4.1.5 The criticism against Wenzel and Cassie-Baxter

Both Wenzel and Cassie and Baxter made assumptions for their theories; Wenzel estimated that liquid would be in full contact with solid surface, and Cassie-Baxter's theories are based on contact between liquid drops and porous solids. The latter meaning the droplet will follow both theories on liquid-air and liquid-solid interface. Their theories have limitations due to their treatment of contact angles as a surface phenomenon, where later experiments have proved it to be a contact line phenomenon(8, 9).

In 2007 Gao and McCarthy published the paper "How Wenzel and Cassie Where Wrong"(8), where they express concern on the extent of the usage of their models, and argues for their lack of applicability, a quotation from their paper illustrates their concern: :" *…Wenzel and Cassie equations have become part of surface science education and are concepts that most of today's surface scientist believe and take for granted"*(8).

In 1953 Bartell and Shepard (9) published a paper challenging Wenzel's formula on roughened surfaces, Equation [4]. Their experimental part was based on Wenzel's modifications of Young's law; one should expect that if the contact angle on a smooth surface was greater than 90° roughening the surface would increase the observed contact angle. At the same time a contact angle for a smooth surface less than 90° roughening the surface would lead to a decrease of the observed contact angle. Bartell and Shepard applied Wenzel's calculations in their research with smooth and roughened surfaces and experienced the same contact angles for droplets on the two surfaces, leading to a conclusion of lack of applicability of Wenzel's equation.

For their calculations Bartell and Shepard used advancing and receding contact angles for smooth paraffin surfaces together with roughness factor r_f. For advancing angles the deviations ranges between 13°-40° were found between calculated and observed values. They had used three different systems in their experiment(9) and every systems had contact angles on smooth surface of >90°. In accordance to Wenzel's theory an increased contact angle should be displayed as the surface was roughened. What they experienced was however not in compliance with Wenzel's equation. Bartell and Shepard argues that

unless the roughness are of such magnitude that it increases the amount of surface located within the range of effectiveness of the forces producing the equilibrium at solid-liquid-vapour interface, an increase of surface area due to roughening would have no direct effect on this equilibrium.

In 2003 Extrand (7) raised questions on the reliability of Cassie-Baxter's Equation [6], and proved it to fail predicting the contact angle. He prepared surfaces that contained chemically heterogeneous islands, and compared them with smooth surfaces. The surfaces with the islands exhibit contact angles identical to surfaces without islands when the islands were in the interior of the contact line. Extrand explains the miscalculations by questioning the error could be Cassie-Baxter's model representing it as it is the interfacial contact area between the liquid and the solid controlling apparent contact angle, rather than a three-phase structure at the contact line. As an illustrating example, he achieved results of expected apparent contact angle being measured to 6°, but should according to Cassie-Baxter be 33°.

Gao and McCarthy's research gave results analogues to those of Bartell and Extrand(8). Three types of two-component surfaces were prepared that contained "spots" in a surrounding surface: a hydrophobic spot in a hydrophobic surface, a rough spot in a smooth surface and a smooth spot in a rough surface. Then water contact angles were measured within the spots, and with spots limited to within the contact line of a sessile drop. Both spot diameter and contact line diameter were varied. Their results supports the theories of contact angle behavior, that is advancing- and receding contact angle and hysteresis, is determined by interactions of the liquid and the solid at the three phase contact line alone. This means the interface area within the contact perimeter is irrelevant, and proves the contact line, and not the contact area is important in determination of wettability. This meaning Wenzel's and Cassie's equations are only valid to the extent that the structure of the contact area reflects the ground-state energy of contact lines and the transition between them.

The theories from Wenzel and Cassie-Baxter are most widely used, but it is important to know of their limitations and the critique towards them. Though their theories does not

account for local defects on a surface(56), for most systems they can be used to calculate wetting behavior.

4.1.6 Collembolan overhang effects on wetting

Theories on wetting and hydrophobicity have been introduced, but how does the overhang described in section 2 affect the collembolans resistance to wetting? To describe theories on behavior of droplets on the overhang Young's Equation [1] and Young-Laplace Equation [12] are used. The latter was deduced independently by Young and Laplace in 1805, and is now known as the Young-Laplace equation(57). It should be noted that the model presented for collembolan overhang is a 2D model, and based on circular shaped granules, see illustrative red lines in Figure 10 and 11.

$$\Delta P = F_{lv}\left(\frac{1}{R_1}+\frac{1}{R_2}\right) \qquad [11]$$

Here ΔP is the pressure difference across the interface, F_{lv} is the surface tension and R_1 and R_2 are the radii of curvature of the interface in principal direction 1 and 2 respectively. When a droplet hits the collembola cuticle, see Figure 10, a certain force, F, is required for the three-phase to move further down the solid interface. By implications of Young's law (see Figure 6 and Equation [1]) the following is implied(18):
For an ideal situation:

$$\begin{gathered}\text{When } \theta = \theta_0\text{, the forces are balanced and the triple line is steady}\\ \text{When } \theta > \theta_0\text{, the triple line is advancing} \qquad [12]\\ \text{When } \theta < \theta_0\text{, the triple line is receding}\end{gathered}$$

Here θ_0 is a static, metastable angle. In reality there is no existence of θ_0, when in equilibrium θ can only take values between θ_a and θ_r(52). The real situations are described in Equation [14]:

$$\begin{gathered}\text{When } \theta = \{\theta_r, \theta_a\}\text{, the triple line is steady}\\ \text{When } \theta \geq \theta_a\text{, the triple line is advancing} \qquad [13]\\ \text{When } \theta \leq \theta_r\text{, the triple line is receding}\end{gathered}$$

Simplifications of the Young-Laplace Equation [12] have been made; it is reasonable to assume the same pressure difference is across the whole interface, leading to constant mean curvature of the interface. For the pressure difference from impact and immersion this assumption is almost correct, but not for pressure difference from gravitation. The gravity effect of small droplets are however believed to be ignored(58). By using a 2D model, Equation [12] is simplified by $R_2 \rightarrow \infty$ and only R_1 is describing the curvature of the droplet.

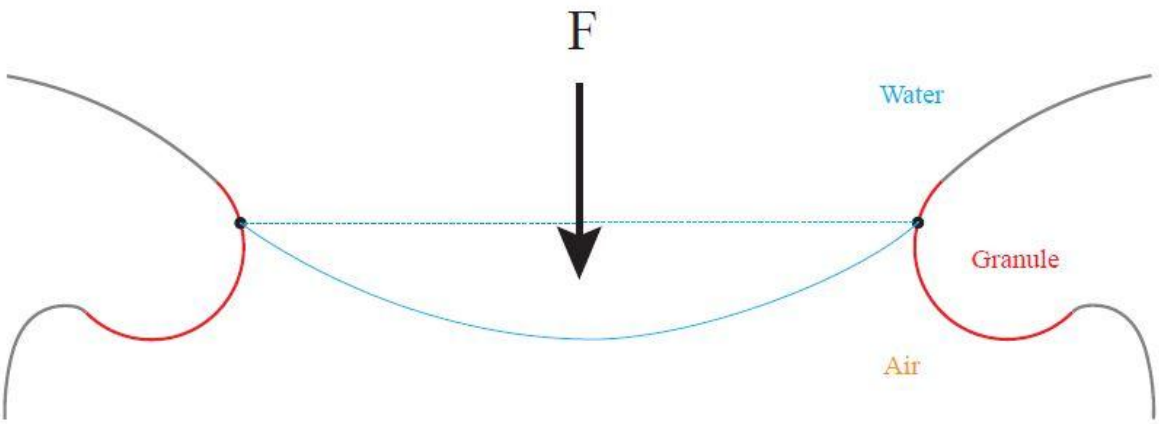

Figure 10 - Droplet between two granules(18)

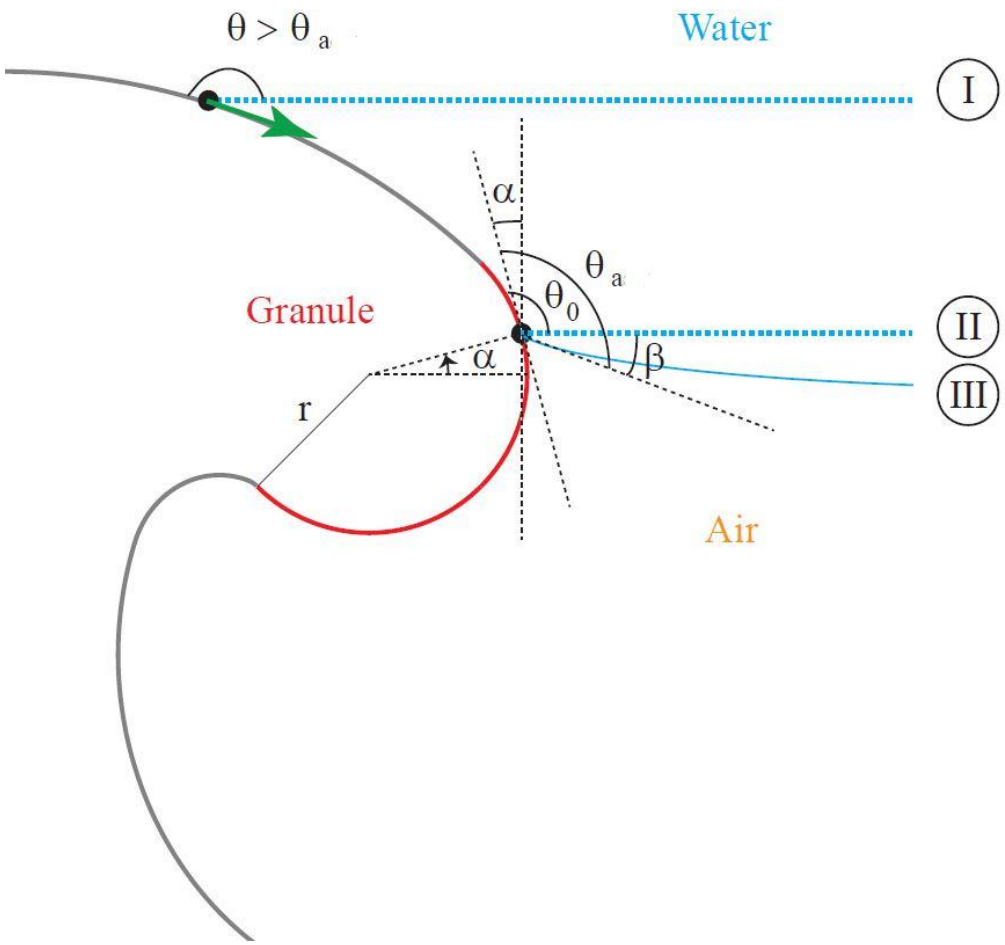

Figure 11 - Granule of Collembola (18)

In Figure 11 *r* is the radius of the assumed circular granule, *α* is the angle between three-phase point at a certain point and a horizontal radius, *β* is the angle between a horizontal line between two granules when $\theta = \theta_a$, θ is the contact angle and θ_0 is an angle between θ_a and θ_r.

At point I in Figure 11 the water touch the granule, and the triple line will slide spontaneously along the overhang, as $\theta > \theta a$, implied by Young's Equation [1](18). At point II the triple line settles as $\theta = \theta_0$, also implied by Equation [1]. From Equation [12] further advancing of the triple line requires $\theta \geq \theta_a$ to again be achieved. At point II, the curvature of the granule results in an utterly increased pressure to make the triple line advance. For collapse of contact line and completely wetting of surface, the last point on the contact line

must let go of the granule(59). The magnitude of such pressure is not further discussed in this thesis.

If granule and ridge structures can be thoroughly presented by FIB processing and SEM imaging, there are geometrical measurements of great interest with respect to the properties of the collembolans and these are presented in Figure 12. If these measurements can be established a surface structure similar to the collembolans may be mimicked.

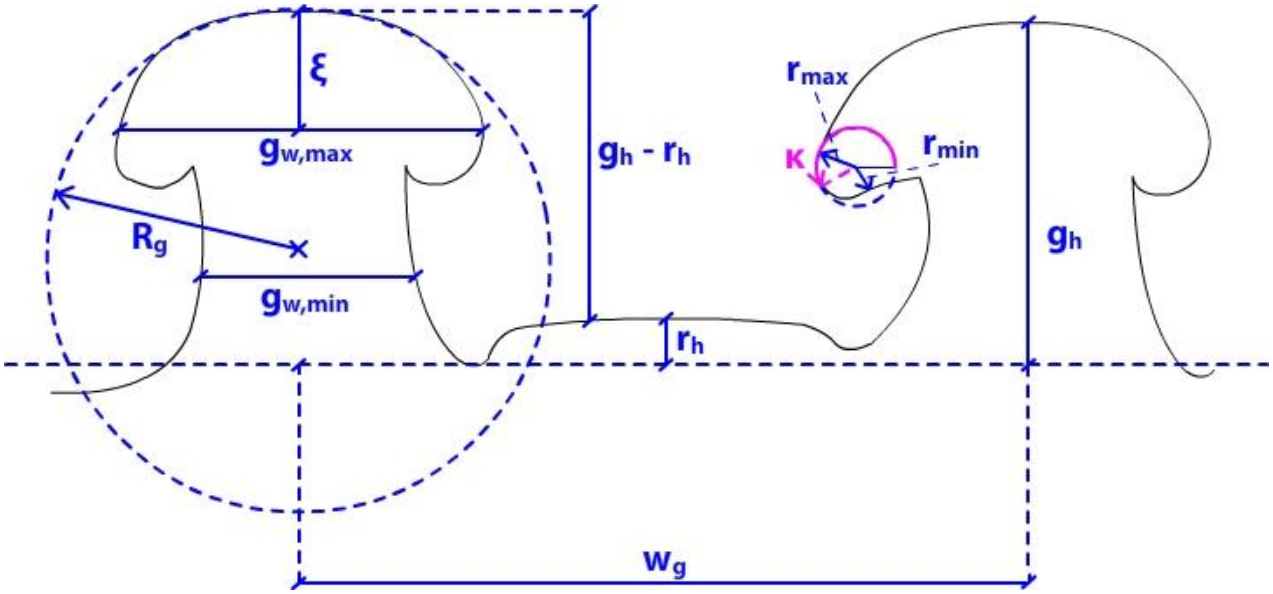

Figure 12 - Valuable measurements of the colembola

The ridge in Figure 12 is exaggerated to illustrate its appearance. The parameters presents as follow: R_g is the radius of a circle shaped after the arc length presented by the overhang, $g_{w,min}$ is the smallest width of the granule (the stem of the mushroom), $g_{w,max}$ is the broadest part of the granule, ξ is the cord of the granule at its broadest, w_g is the width between the center of two granules, r_h is the height of the ridge and g_h is the height of the granule from top to bottom of the mushroom. Assuming the overhang is not perfectly circular shaped, r_{max} is the largest radius of the overhang and r_{min} the smallest. The pink angle κ is the angle within a unit circle, between the beginnings of the perfectly circular overhang, to the point where the perfect circle turns to a non-perfect circle. Here 0° is at the beginning of the perfect circle.

The above parameters have several applications if contact angles of collembolans are to be calculated. To calculate r_f at Wenzel state, equation [2], all parameters in Figure 12 is necessary. When r_f is established the contact angle for a system at Wenzel state can be computed. To calculate f_1 and f_2 for a system at a Cassie-Baxter state (equation [6]), the values of ξ, $g_{w,max}$, κ, r_{max}, r_{min}, R_g and w_g is required. When f_1 and f_2 is established the contact angle in Cassie-Baxter state can be computed(60). The model illustrated in Figure 11 requires the knowledge of hydrostatic pressure ΔP to determine when a transition from Cassie-Baxter to Wenzel state occurs, see Equation [11]. To calculate ΔP, the parameters κ, g_h, w_g and g_{max} must must be known(18).

When the cuticle of a collembola is wetted, the system is in a metastable Cassie-Baxter state. The overhang represents the energy barrier described in section 4.1.5, and to transit into a Wenzel state this barrier must be overcome. If ΔP is high enough to transit the metastable Cassie-Baxter into Wenzel state, the system is likely to remain at Wenzel state, as the energy barrier for a return to Cassie-Baxter state is higher than the first barrier(18).

4.2 Dual Focused Ion Beam (FIB)

A focused ion beam (FIB) with integrated Scanning Electron Microscopy (SEM) was utilized for the experimental part of this thesis. Compared with modern FIB's the development have been enormous, the 1973 FIB had a minimum beam spot diameter of 3.5 μm. When the FIB was commercialized in the 1980s, it was mainly a tool for the semiconductor industry (19), as it is still is being used for today, but it is also used in material science and increasingly in biologically science(23).

The instrument consists of a vacuum chamber, a liquid metal ion source (LMIS), an ion column, a SEM column, a sample stage, detectors, gas delivery system and a computer to run and control the system(20). The combination of electron and ion column is beneficial; the user may locate and investigate features at high magnification without harming the sample and control processes executed by the ion-beam with the electron-beam simultaneously as the ion-beam is processing(61). Biological samples are particularly vulnerable to damage from the ion beam(24).

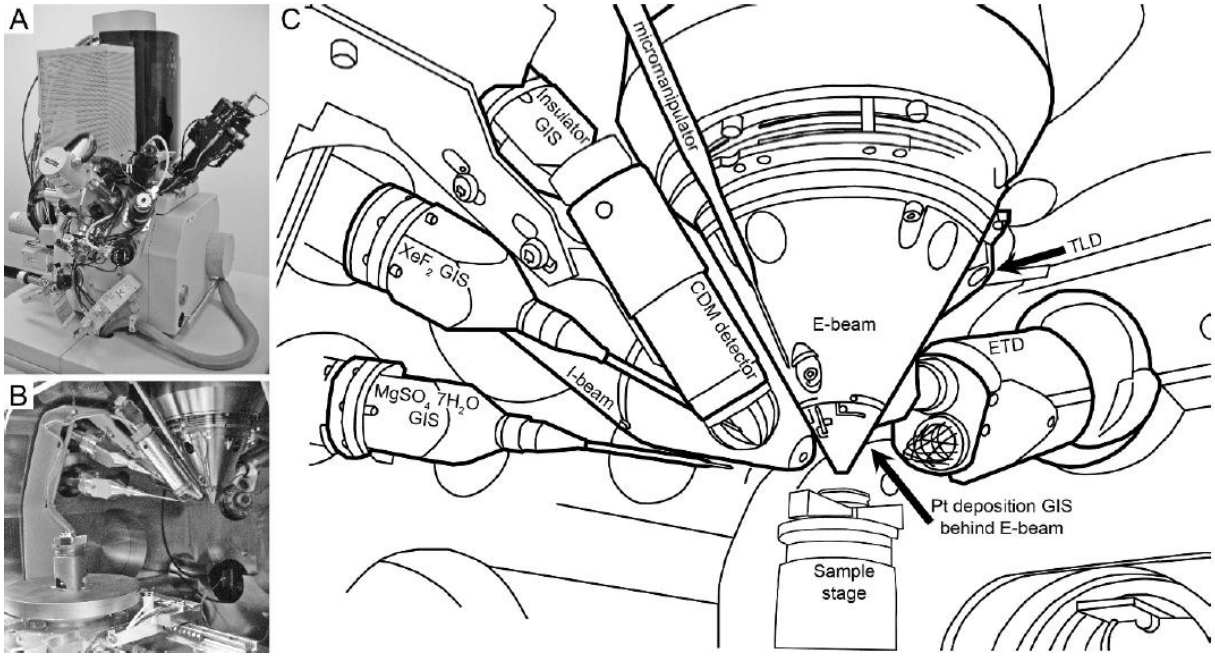

Figure 13 - FIB-EM instrument. A) Photograph of FEI Company's DualBeamTM Helios 600 NanoLabTM. B) Sample chamber photograph with E-beam, GIS nozzles, CDM detector, and sample stage. C) Schematic diagram (61)

4.2.1 The vacuum system

The typical vacuum system in a FIB has three vacuum regions; one for the source and ion column, one for the sample and detectors and one for sample exchange(20). Its purpose is to avoid contamination of the source and to prevent electrical discharges in the high voltage ion column. Without proper vacuum there would be collision between the beam source and molecules or gas atoms.

4.2.2 Sample stage

The sample stage is orientated in a 5-axis system, x,y,z, rotation along the z-axis and tilting along an axis in the x-y plane(20). All five axis stage motions may be motorized for automatic positioning. It is required that the stage must be very stable and not subjected to heating due to the mechanical action necessary for stage movement. Thermal stability prevents specimen drift during FIB milling or deposition.

4.2.3 Detectors

There are two types of detectors that are used to collect secondary electrons for imaging, a multi-channel plate or an electron multiplier(20). The FIB used during these experiments is equipped with an Everhart-Thornley electron multiplier detector (EDT), and the multi-channel plate will therefore not be further explained. The detector is placed at an angle of 45° to the beam, and consists of a charged cage(19). The cage can be charged positive or negative to attract ions, secondary- or backscattered electrons. Most of the charged elements are accelerated into the scintillator which causes it to scintillate. The number of photons generated per electron or ion is typically 100 for a scintillator of 10 kV.

4.2.4 The liquid metal ion source

The liquid metal ion source (LMIS) can provide a beam of ions of approximately 5nm in diameter(20). The most common LMIS in commercial use, including the FEI Helios NanoLab Dual Beam FIB, is Gallium (Ga). In the process of Ga^+ emission the heated Ga flows and wets a tungsten needle with a tip radius of ≈2-5 μm. An electric field (10^{10} V/cm) is applied to the end of the wetted tip to make the liquid Ga form a point source in order of 2-5 nm in the shape of a Taylor cone[2]. As a result of the electrostatic and surface tension force the conical shape form a balance that is set up due to the utilized electric field. When the force balance

[2] A Taylor cone is the cone observed in electrospraying (here ion spraying) before the jet and plume is formed

is achieved, the tip of the cone is small enough for the extraction voltage to pull Ga from the tungsten tip and efficiently ionize it by the field evaporation of the Ga-metal at the end of the Taylor cone. A flow of Ga to the cone continuously replaces the evaporated ions.

4.2.5 Ion column

When the Ga^+ ions are extracted from the (LMIS), they are accelerated trough a potential down the ion column(20). The ion column has a condenser lens which is the probe former lens and an objective lens which is used to focus the ion beam at the sample surface. Beam currents can be adjusted from a few pA to as high as 20-30 nA.

4.2.6 SEM column

The common source for electrons, including in this study, is a tungsten filament(19). This filament is heated by a large current, resulting in a emission of a spectrum consisting of radiation accompanied by a number of loose electrons that have gained sufficient energy to overcome the work function of the metal and escape. These electrons are accelerated away from the tip by a set of electrostatic fields, and then reduced to a relatively clean beam by an aperture below the source. As electrons are much lighter than ions, the lenses utilized are magnetic rather than electrostatic.

4.2.7 Gas delivery system

The gas delivery system can be used together with the ion beam to produce site specific deposition of metals or insulators, or to provide enhanced etching capabilities(20). Metals are deposited by ion beam assisted chemical vapor deposition from an organometallic gas. A controlled amount of gas is inserted through a needle and into the chamber. The gas molecules are adsorbed on the surface near the gas outlet, but decompose only where the ion beam strikes. The adsorption and decomposition is repeated, and as an end result there is a buildup of material in the ion scanned region.

The samples used in this master thesis are of a biological material and thus especially sensitive to the ion beam at high currents(62), leading to the dual FIB being more suitable than a basic FIB instrument. See Figure 14 for example of sample damaged by ion beam.

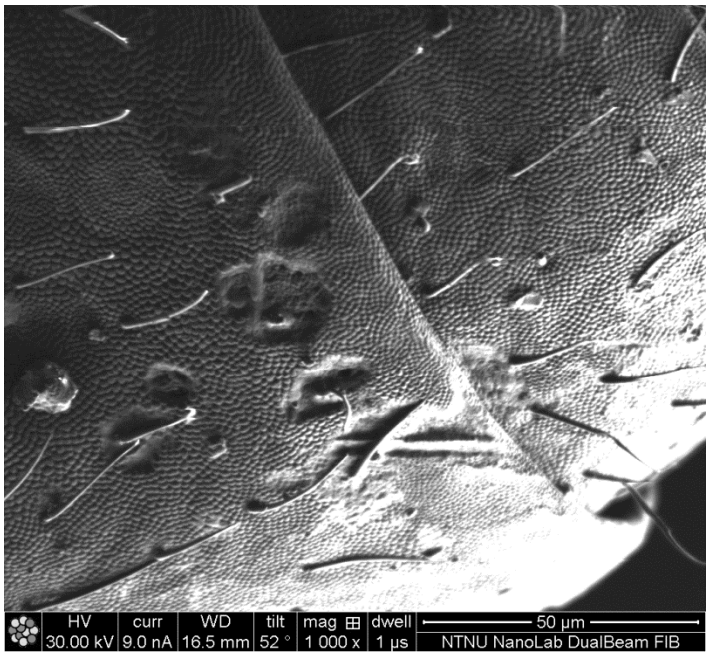

Figure 14 Surface exposed to high current during removal of hair

4.2.8 Measurements of SEM images

When initially starting the FIB the chamber is ventilated and the sample is placed in the grid(63). After re-vacuuming the chamber, the stage is carefully placed at its working distance, approximately 4.1 mm underneath the conductor. Before any operating can take place, one must locate the eucentric point. This is where the electron beam and the ion beam converge(64), and when it is situated the stage is tilted from 0° to 52°. Finding the eucentric point on a collembolan cuticle was more challenging than on a flat metal sample due to the curvature of the cuticle.

Images taken by SEM or FIB can manually or by suitable software be measured after procedures. Adjustments of these measurements due to tilted stage and the angle between the ion and electron beam, see Figure 15, are then necessary to get the correct measurements. When the SEM is imaging the surface of a milled cross section perpendicular to the surface plane, the images seen by operator is l', but the real image will be $l^{(cs)}$. Equivalently the real surface structure on the cuticle, noted as $s^{(s)}$, will be displayed as s'. See equations on Figure 15 for calculations of real measurements.

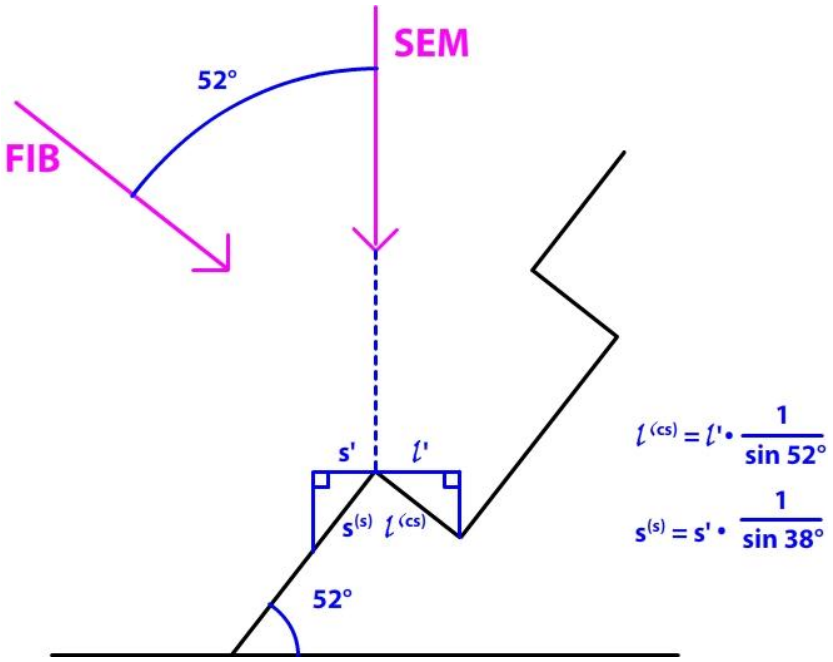

Figure 15 - Visible and real surface in FIB

4.2.9 Charging problems

A non-conducting area of a sample will accumulate a net positive charge as a result of the impinging Ga^+ ions(20).The net positive charge will hinder the escape of secondary electrons (SE) released from the surface, and they will not be detected. The charging artifact can be observed as a dark contrast in the image.

Charging can cause drifting in the displayed image(65). The consequence of this is reduced accuracy and quality of FIB milling, imaging and chemical vapor deposition. To avoid charging problems one can coat the sample(66). Coatings frequently used are Au, Pt, Cr, C and Pd. Lowering the current intensity will also reduce the charging problems(20), but this will affect the quality of the image. Switching to mode of Backscattered electrons (BSE) can also have a positive effect of imaging because BSE have much higher energy than SE and is hence less affected by disturbance from charging.

4.2.10 Biological samples in dual FIB

As mention in section 1, biological samples are increasingly studied in FIB, even if biological material are very sensitive to etching which traditionally have led to serious limitations on the several FIB applications. Even so, ion and electron sources can reveal images of biological structures that are not possible to achieve in any other way(67). All samples that

are exposed to Ga-ions may suffer from uncontrolled Ga^+ implantation that could cause deformations or changes in compositional contrast, which may lower quality of imaging. In general there is lack of information on how biological samples behaves towards FIB milling and imaging(23), leading a lot of try, fail and try again, before suitable parameters for the experimental part was established in this thesis.

When preparing a biological sample for dual FIB, it is generally required to wash and dry it in advance(24). Biological samples do not conduct electricity, and it is then necessary to place coating on the specimen in the form of thin, electrically conducting layer. This is done with a sputter coater.

To monitor and observe structural features of a biological specimen, the usage of secondary electron (SE) imaging is the majorly used method(24). To see the true situation of a biological sample, the backscattered (BSE) image should be preferred when it contains more information than just morphological information. BSE are elastically scattered electrons, which are electrons with kinetic energy conserved after an incident, of high energy.

A disadvantage by using BSE on biological samples is that the electrons may exit some distance from the entry point of the beam electron(24). This meaning a flat sample structure is much more beneficial, and this is rarely the case of a biological sample in its original form. Cutting out suitable tissue samples can solve the problems of curvature.

5. Experimental methodology

The FIB utilized for the experimental part of this thesis was the model FEI Helios NanoLab Dual Beam FIB. The purpose of using the FIB in this master thesis was to make 3D models of the collembola's granules and take pictures of their profile to confirm the overhang. To be able to image the overhang, it was necessary to process the cuticle by milling cross sections with the FIB perpendicular to the surface. The SEM was than enabled to image features not visible when untreated by FIB. To make 3D models of the overhang hundreds of slices were milled by the FIB at the area of interest, and both the SEM and FIB would take an image for each slice for later assembly of these images to a 3D model.

5.1 Collembolans used in the experiments

For the collembolans examined in this study see Figure 16. During contact angle measurements of the specie Cryptopygus clavatus, it was discovered that depending on the season, summer or winter, the animal exhibit different wetting properties. To see if Cryptopygus clavatus displayed different features between summer and winter a sample of the animal from both seasons were investigated in the FIB. The animals were provided by H. P. Leinaas, Department of Biology, University of Oslo. All of the species displayed different surface structure and different amount of hair on their cuticle. The latter proved to cause charging problems during FIB examination.

Sample number	Species
1	Anurophorus septentrionalis
2	Xenilla maritima
3	Folsomia quadrioculata
4	Archisotoma besselsi
5	Desoria olivaca
6	Anurophorus laricis
7	Cryptopygus clavatus, summer adapted
8	Cryptopygus clavatus , winter adapted

Figure 16 - Sample numbers and species overview

5.2 Sample preparation

The sample preparation was executed by co-supervisor Håkon Gundersen. All samples were killed with chloroform vapor and immediately dried with a freeze-dry method. Two blocks of brass were chilled in liquid nitrogen. The samples were placed in a recess on one of the blocks and the other was placed on top; the samples were enclosed in this way to minimize condensation on the sample. The brass blocks, with the samples, were then placed in a vacuum chamber at 5 mBar for approximately 20 hours. The brass blocks were much larger than the samples, ensuring that the temperature increase caused by adding the samples was negligible. The long period in vacuum meant that the block and samples had regained an ambient temperature at the end of the process. The dried samples were mounted on SEM stubs with carbon tape or silver glue. The dried samples were coated with carbon and subsequently with platinum. An SEM Turbo Carbon Coater from Agar Scientific was used, with the samples mounted on a tilted, rotating stage. Typical settings for the carbon coating was t = 2 x 8 seconds, with E = 4.8 kV. An Edwards Sputter coater S150B was used to coat the samples with platinum. Typical settings for the platinum coater were 1 minute with a current of 20 mA.

In addition to the samples prepared for FIB, another set had been prepared for contact angle measurements by Håkon Gundersen. These samples were killed by chloroform and within an hour they were tested with sessile drop method. The result from this test was used to compare with FIB results.

5.3 Considerations due to geometry and surface morphology

Using the FIB to study collembolan cuticles raises special problems. The sample is an animal with rounded geometry, which made it challenging to locate the eucentric point. If the animal's "backs" were chosen as the object of study, this became easier as this area is somewhat flatter.

The hair on its surface proved to cause problems with charging. This affected the imaging and accuracy during milling. Some samples had less hair than others and suitable areas were easier to detect. If hairless areas could not be located, the hair was removed by the ion beam. This was done at high magnitude at 0.26nA, and only after platinum deposition to protect the surface from ion beam.

Figure 17 shows sample 2 before and after etching of hair. This was done during practice, therefore there is no platinum deposit at the surface.

When inserting the platinum needle, this came up on the right side of the sample, see Figure 18. The round shape of the samples acquired that chosen area for further examination should thus be at the "back" of the collembolan, somewhat to the right due to the platinum depositing needle's position, and avoid areas near features or cuticle making "valleys" or "bumps". These valleys and bumps could trap or block the platinum deposition.

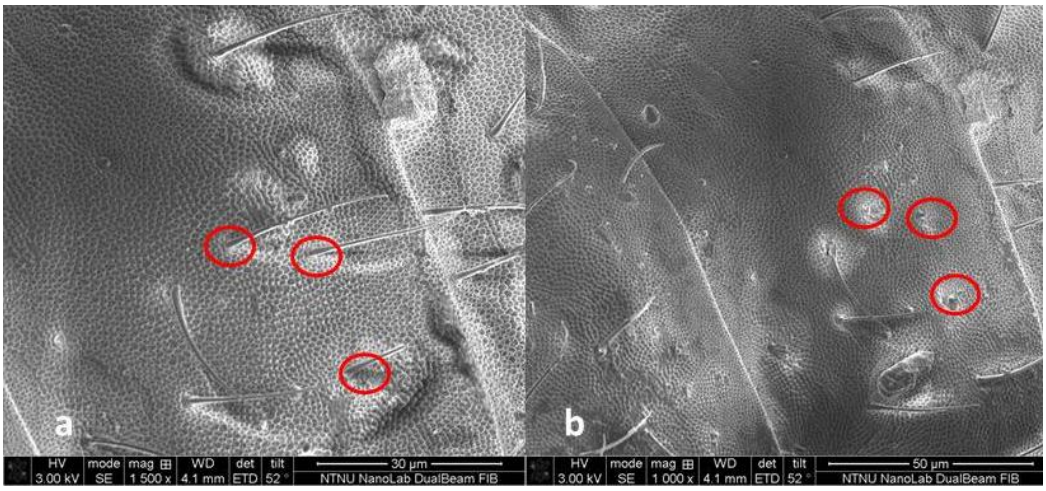

Figure 17 - Folsomia quadrioculata a) Before etching of hair b) After etching of hair

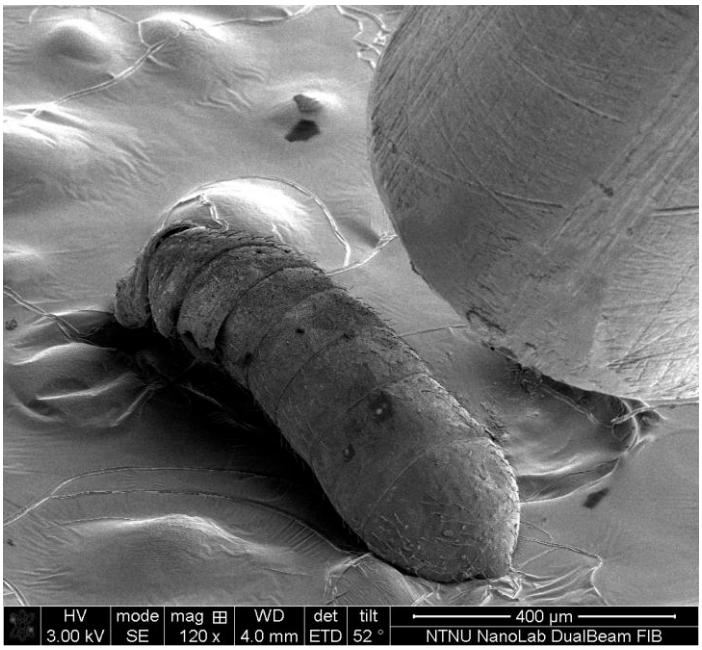

Figure 18 - Needle before deposition of platinum

5.4 Preparation inside FIB

The deposition of platinum was done in two stages. The site was elected based on feature structure and the factors described earlier. The area of the site varied 2.77-15µm in the x-direction and 1.58-7 µm in the y-direction. The purpose of platinum deposition was to protect the sample from the ion beam and to ensure that surface topography were preserved during milling(62). After platinum deposition some samples experienced problems with charging, this was solved by lowering the current or using BSE.

Parameters that need introduction will be explained. The "Dwell time" is simply the time the beam spends on a single pixel each time it passes the area in question(68). Relative Interaction Diameter (Rel. Int. Diam) is used to affect the step size of the beam.

Initially a 0.3 µm thick layer was deposit by the electron beam at 3.0 kV and 0.34-0.69 nA. Dwell time was always set at 1.0 µs, Rel. Int. Diam 0 %, and scan direction from bottom to top. This relatively thin layer compared with the end result was to protect the sample from damages from further platinum deposition of the ion beam. Experience obtained during these studies showed that for these samples it was more suitable to locate the eucentric point after this deposition, and then tilt the stage to 52° for further utilizing of ion beam.

Platinum deposition by the ion beam took about 25 % of the time the electron beam deposition, which made this beneficial. A rectangular cross section was chosen in software and placed above the existing layer. The z-direction was now 0.7 µm, resulting in a complete layer of 1.0 µm of platinum. It is important to be aware of that by typing "0.5 µm" in z-direction you only have an estimate of the amount that will be deposited, in practice the thickness of the deposited layer may differ. Suitable current for deposition with the ion beam showed to be 0.26-0.44 nA, and voltage was at 30.0 kV. The scan direction was bottom to top, dwell time 1.0 µs and Rel. Int. diam. 0%. See Figure 19 for illustration of platinum deposition.

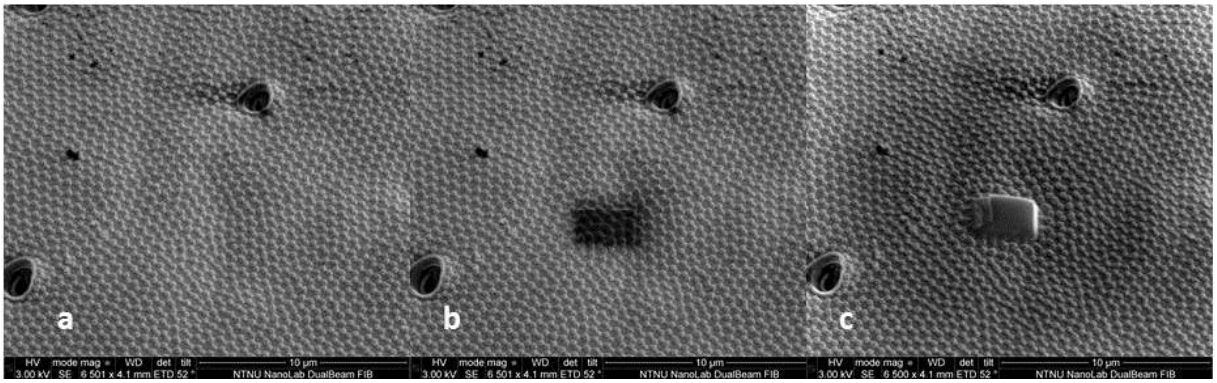

Figure 19 - a) Bare surface b) After 0.3µm deposit with electron beam c) After 0.7 µm platinum deposit with ion beam

5.5 Milling of cross-sections

To view the profile of the granules a cross-section was milled. This was a stair formed feature that enables the SEM to image the features of interest. The milling was done in an area that overlapped the platinum layer, and the milling was conducted with following parameters: current; 0.44 nA, voltage; 30.0 kV, scan direction; Bottom to top, Dwell Time; 1.0 µs and Rel.Int. Diam; 0 %. The x- and y-direction was adapted to the area of platinum layer, and z-direction was always at 0.7 µm.

When this milling was completed, the surface in z-direction was rough, and to even it a cross-section cleaning process was performed. The x- and z-coordinate were kept the same as for the cross-section, but the y-direction was smaller, down to 1.0 µm in this study. The current was lowered to 25-50% of the main current(68). Lower beam currents were less destructive, but took longer to mill. In this study the current was set to 46-90 pA. Dwell time was 1.0 µs and scan direction Bottom to top. See Figure 20 for illustration of cross section and cleaning cross section.

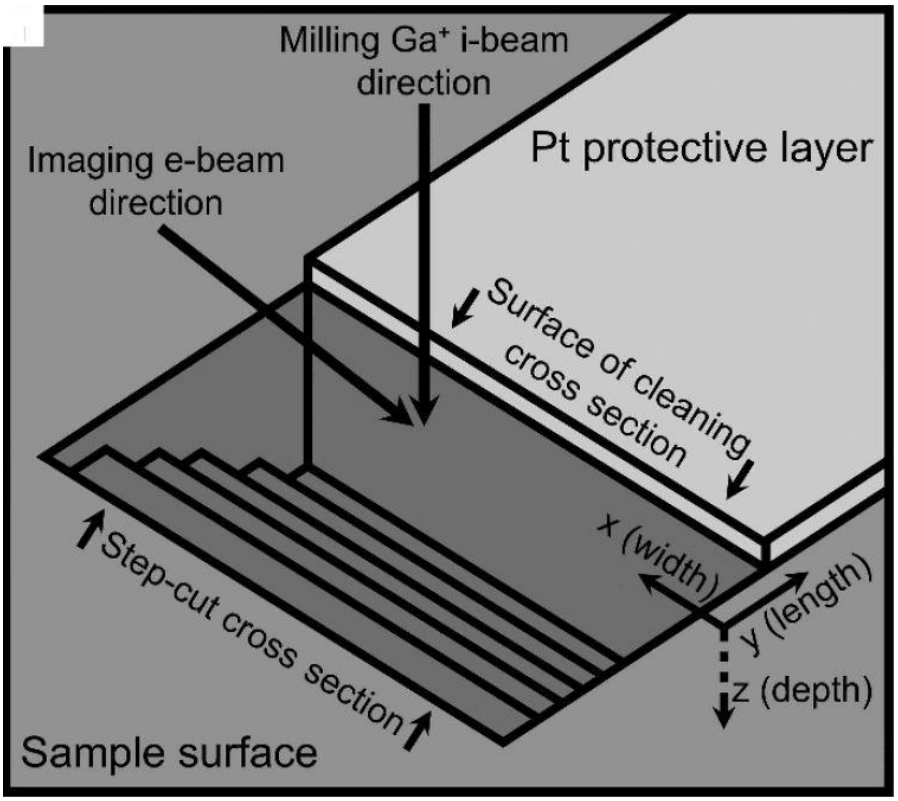

Figure 20 - Schematic representation of FIB nanotomography sample processing (61)

5.6 Slice and view

Slice and view (S&V) was an operation integrated in the FIB which automatically mills consecutive slices through a pre-selected three-dimensional feature while both the SEM and FIB takes one picture after each slice(68). When the operation was complete one could review the images individually, as an animated sequence or modify the images in additional software. Initially in this study the goal was to create three-dimensional pictures of several of the species samples. During examination of the samples, most of them proved to have charging problems severe enough to disturb the process of S&V. This means unfortunately sample 1 and 4 were suitable for S&V.

The FEI software was Auto Slice & View Software. The samples used were prepared by the same method as described in section 5.2. Once the sample was placed in the FIB an area of the sample that is suitable for S&V was located.

The charging had to be at a minimum and the surface area selected had to be flat and large enough to fit the operational features that were applied. The granules on the cuticle of selected area had to be horizontal placed as shown in Figure 21, which gave a more relevant and usable result. If only diagonal granules were available, the stage was turned to a more appropriate position.

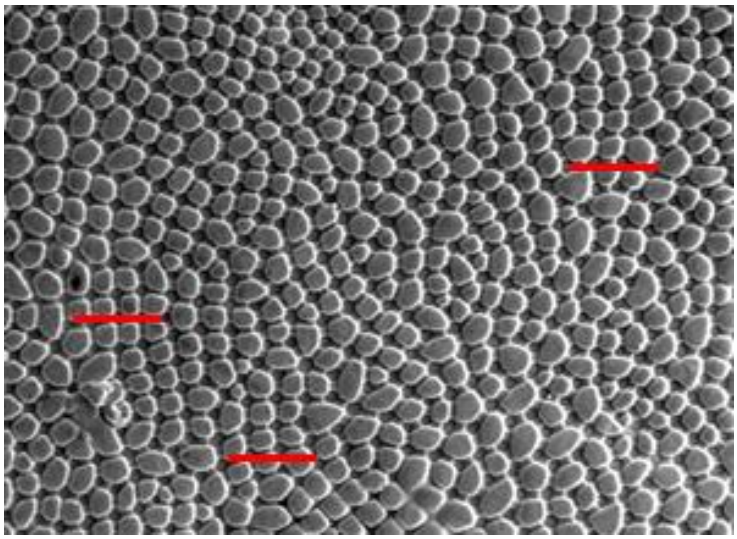

Figure 21 - Sample 5, suitable areas for S&V operation marked with red

The area selected for S&V was also protected in advance with a layer of platinum deposited by the electron beam before tilting the stage. The parameters was voltage; 3.0-5.0kV, current; 0.34- 0.69 nA, Scan Direction; Bottom to top, Dwell time; 1.0µs and Relative Integrated Diagram; 0%. The selected surface area varied between 1.62 -5.0 µm in x-axis and 1.69-4.0 µm in y-axis, depending on how many granules was to be examined. The depth of the platinum layer had to be thick, 1.0 µm in the z-direction. After the first layer were deposited the stage was tilted to 52°, and a second layer adjusted to the already existing square area of platinum were deposited by the ion beam. The parameters were voltage; 30 kV, current; 0.26-0.44 nA, Scan Direction; Bottom to top, Dwell time; 1.0 µs Relative Integrated Diagram; 0% and z-direction; 0.5 µm

In the S&V software the image resolution for both electron and ion beam were set to 1024x884 and Dwell time were 1.0 µs. To determine the number of slices the SEM window in software was adapted so the features of interest were properly displayed, and the width was measured. By dividing this width with the resolution the outcome denomination was index nm/voxel, where voxel is a volume pixel. By adjusting this to the slide thickness the suitable number of slices was obtained.

To get ultrahigh resolution electron images of the sample during S&V, Mode 2 was selected. In this mode the immersion lens was switched on, and the standard detector was the TLD in Secondary Electron operation(68). Mode 2 cannot be used with magnetic samples(63).

The ion beam currant should not be higher 440 pA. As the collembolan were sensitive to the ion beam, selected ion beam current was set to 90 pA. Figure 22 shows sample 1 destroyed by high currant. The next step in the process was to deposit a fiducial pad height and mill a rough cut. The fiducial pad height is a protecting pad of platinum deposited by the ion beam, where the fiducial cross was milled. It was important that this layer were thick enough to make a flat and even square, completely covering the features of the collembolans cuticle. The height of these features varied, depending on the species and the size of the animal, and to be sure that the granules were covered, the fiducial pad height was set to 1.5-2.0 µm. The fiducial cross defines the width and position of the sample, and during the S&V process an image recognition system uses the fiducial to align the sample after stage movement and beam current changes as well as monitoring and correct for drift during milling(68). During the procedure of milling a rough cut, the system milled a cross section to allow the electron beam to image the face of the features selected. When these operations was done the S&V could be conducted, which would take several hours depending on the size of the area selected.

Figure 22 – Sample 1 destroyed by high current

As soon as the first images were displayed considerations regarding the parameters was done. This included contrast, focus and the x- and y stigmator, the latter being most difficult to adjust during S&V. If the pictures was adjusted with one of mentioned parameters early in the S&V process, the pictures already taken was discarded, but this did not ruin the end result as the number of pictures were 270-450.

6. Results

Figure 23-30 displays the surface structure of samples investigated in this thesis. No indications of structural deformation or changes in compositional contrast due to Ga^+ implantation were observed. The granule geometry of sample 2, 4 and 5 is clearly a hexagonally pattern. Sample 4 have features that looks like secondary granules, but these are simply a thickening of primary granules. This is however the only sample not displaying ridges between the granules. Sample 2 have in reality secondary granules, but for some reason they are gone. Sample 1 and 6-8 seem to have a rhombic pattern of granules, and sample 3 displays both rhombic and hexagonally patterns. The reader should be noted that the images in Figure 23-30 illustrates geometrical patterns at a certain area of the animal, and structural design may vary on the same animal depending on location on the collembola, as described in section 2.

As sample 7 and 8 were of the same species and showed different wetting properties depending on whether it was summer or winter, one could assume they would display some differences in surface structure, but by the looks of Figure 29 and 30 this is not visible.

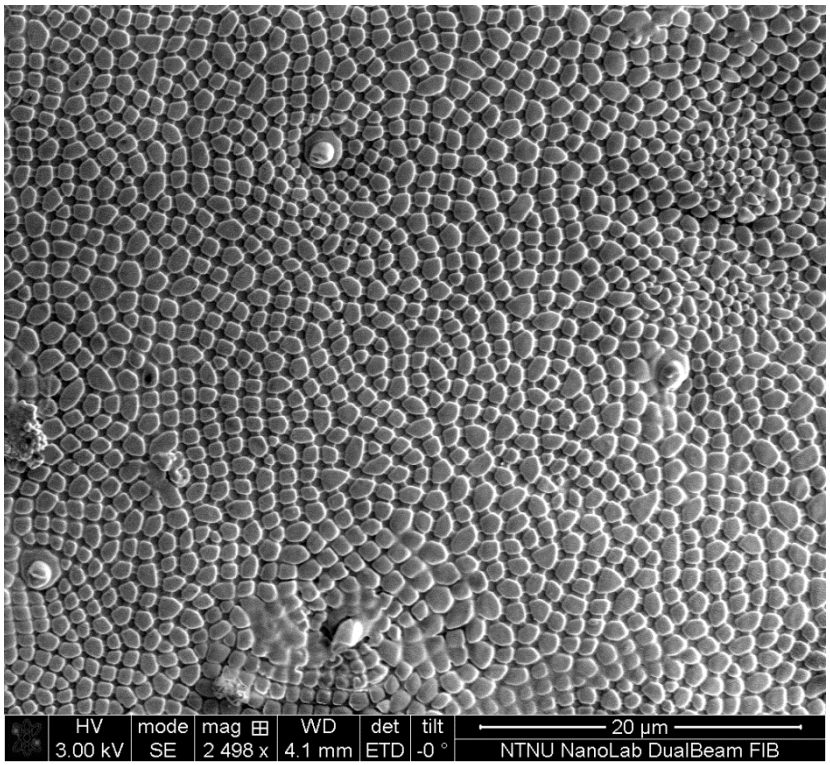

Figure 23 - Surface structure of sample 1

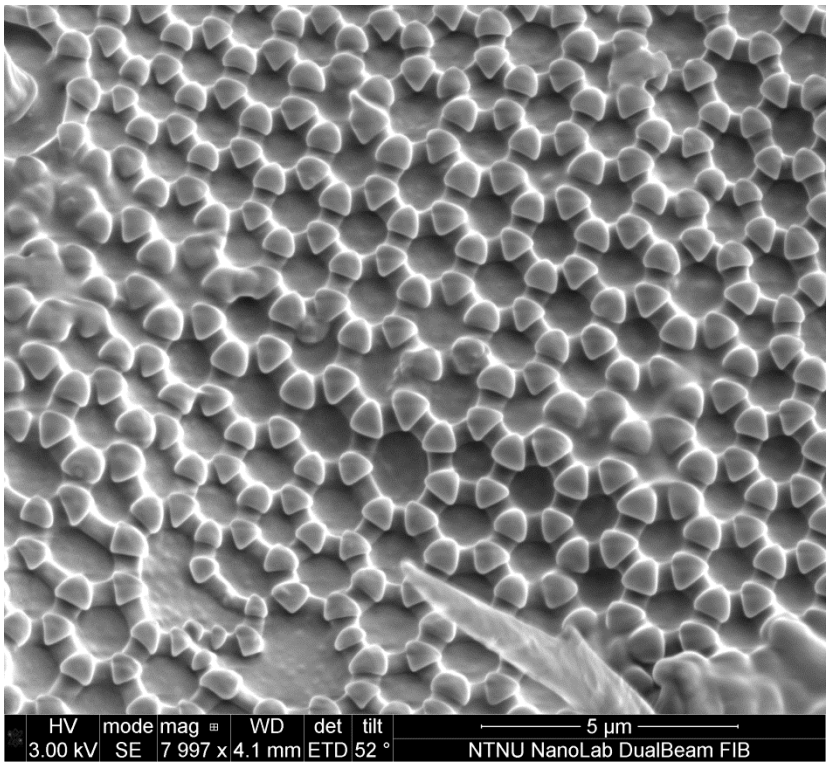

Figure 24 - Surface structure of sample 2

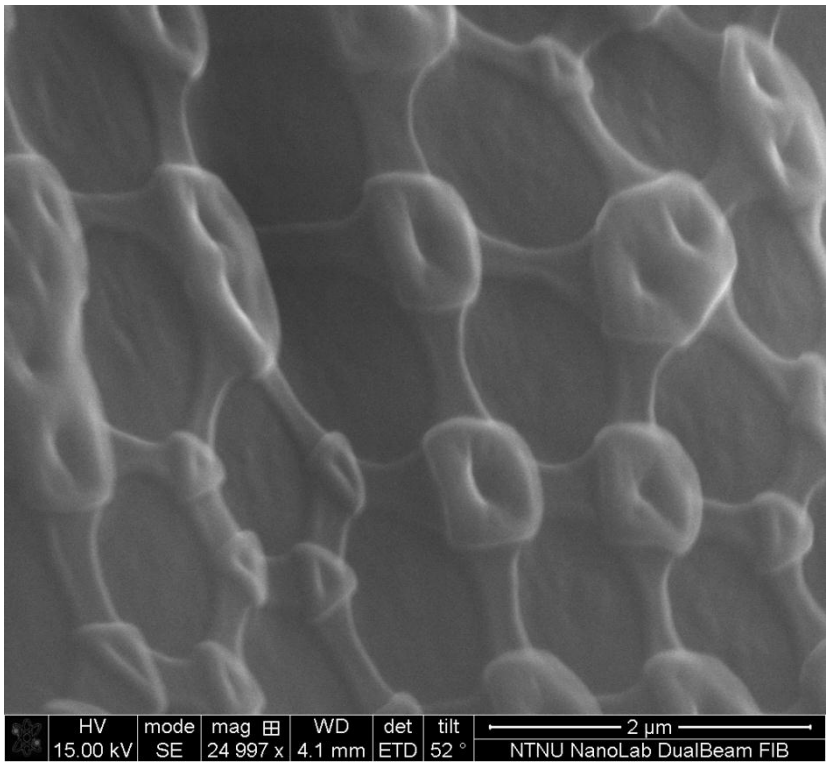

Figure 25 - Surface structure of sample 3

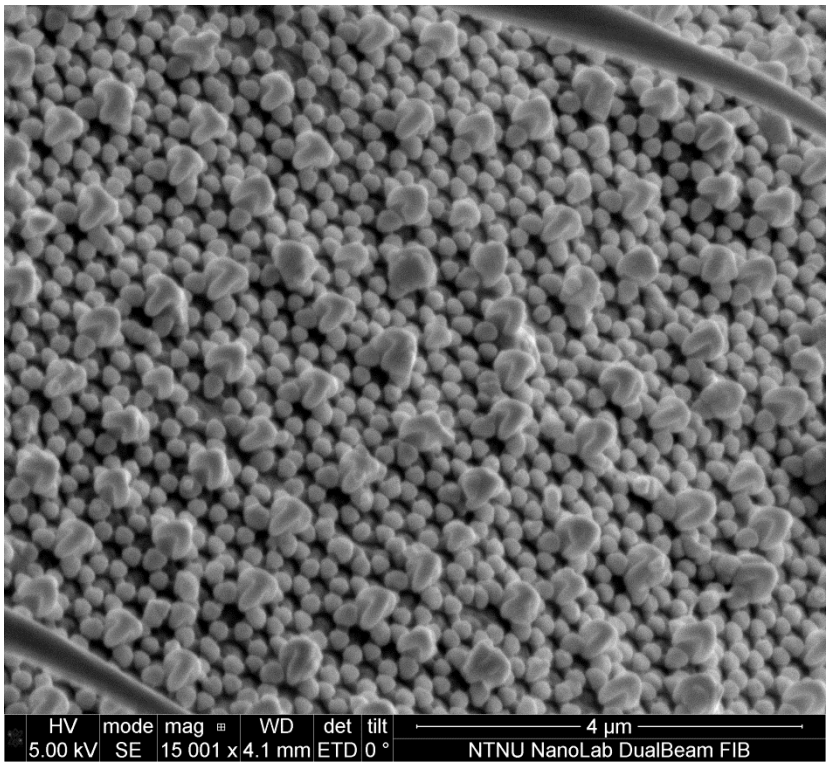

Figure 26 - Surface structure of sample 4

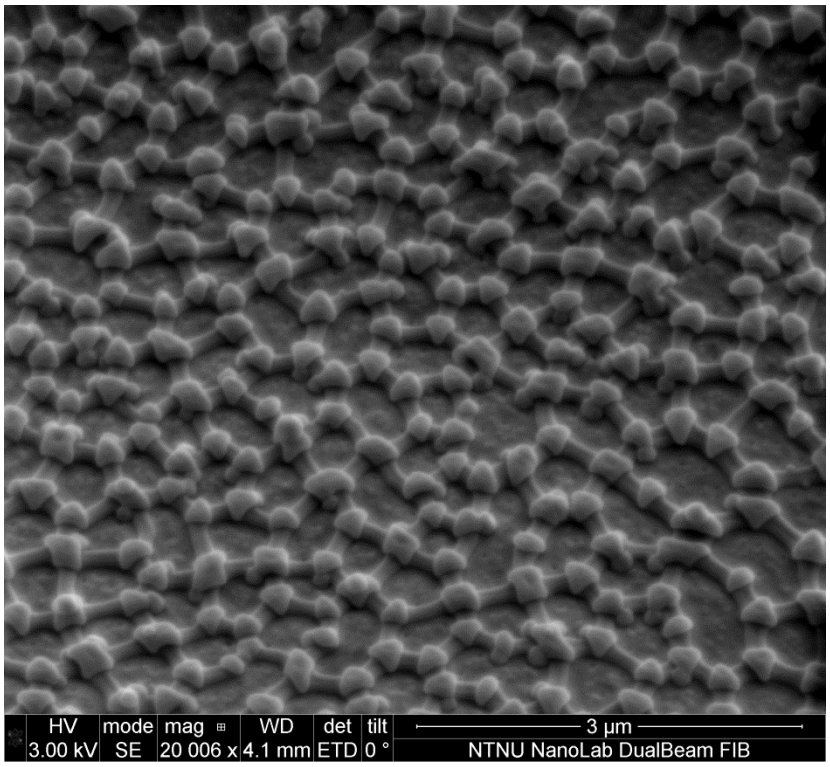

Figure 27 - Surface structure of sample 5

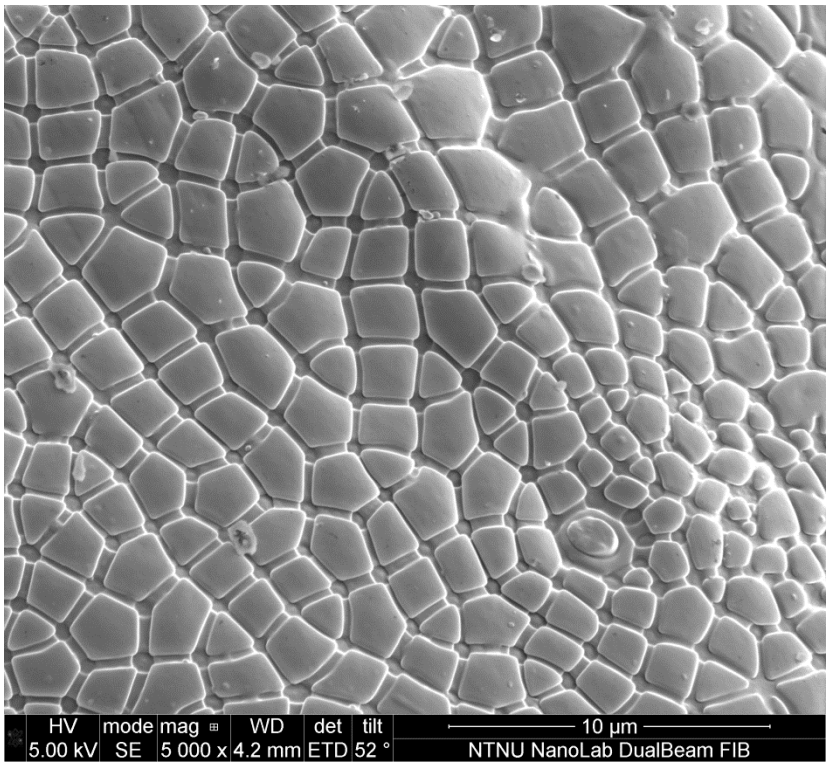

Figure 28 - Surface structure of sample 6

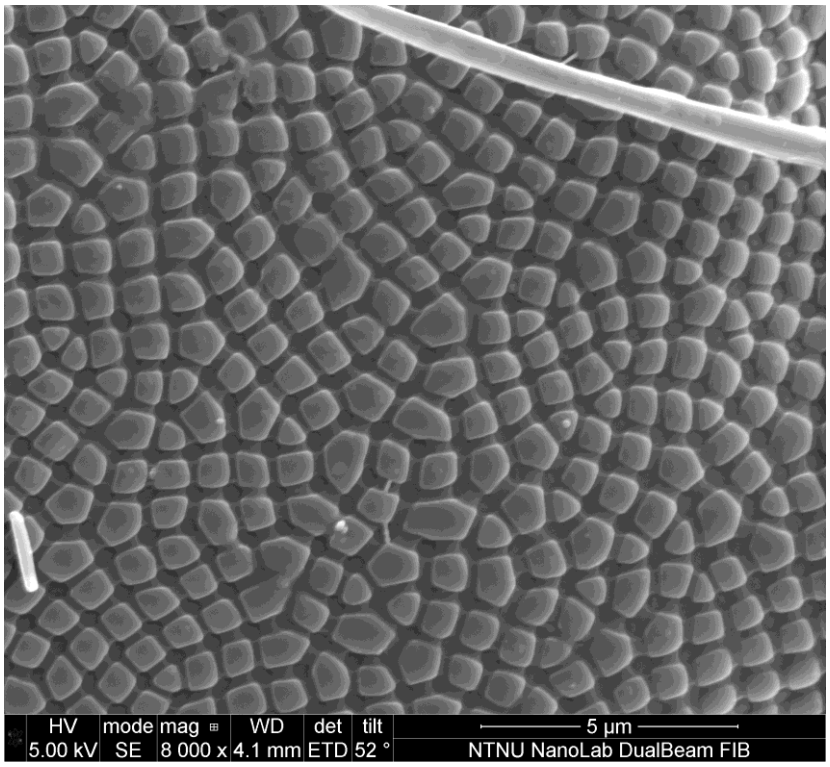

Figure 29 - Surface structure of sample 7

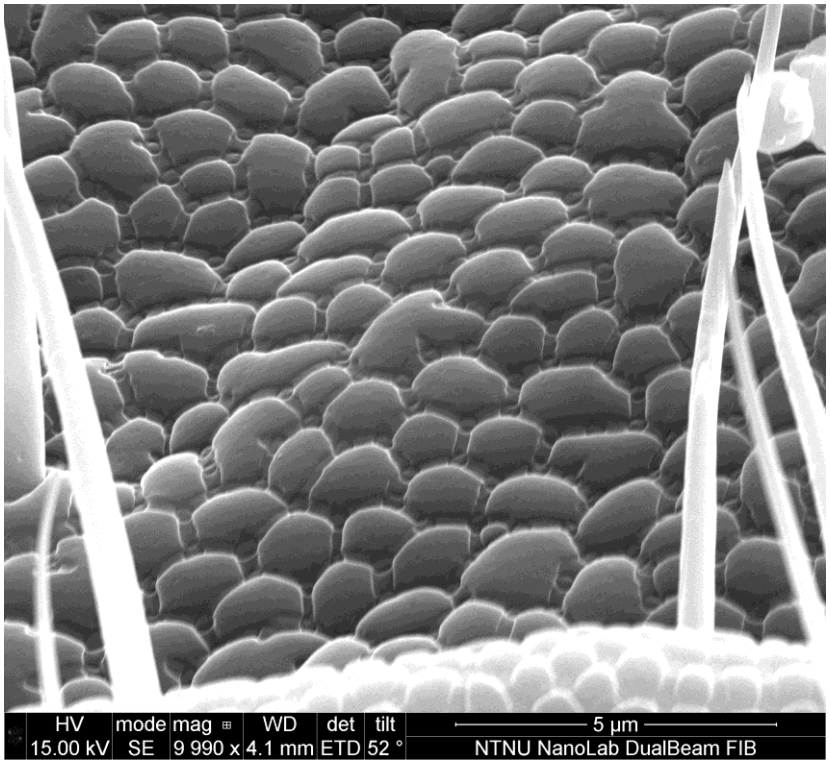

Figure 30 - Surface structure sample 8

Figure 31-38 displays cross section of sample 1-8, respectively. Figure 31, sample 1, displays several granule profiles, where overhang is visible on some. It appears that the overhang structure of sample 1 is uniform all over the sample, and that the features in Figure 31 are representative for every granule on the collembola.

Figure 32, sample 2, is the image with highest magnification, and the overhang is clearly visible. The overhang does not seem to be perfectly circular, cf. section 4.1.6, rather sharpened. This image illustrates well why the granule with overhang is referred to as a "mushroom". The image of sample 2 is chosen because it has an interesting appearance, and it is very well possible that it represents the general granule shape. Figure 7A and 8A in appendix shows two other granule cross sections of sample 2, and it looks like they display a similar feature.

In Figure 33(sample 3), 36 (sample 6), 37 (sample 7) and 38 (sample 8) there is no overhang visible, only the contour of the granules. Sample 3 displays what looks like more randomly spread granules, but when these are compared to the surface structure in Figure 25, it is likely that this appearance is due to rhombic and hexagonally placement of granules with well-defined ridges between them. Sample 6 did not display significant ridges, as seen in Figure 28, but granule closely placed next to its neighbor granule. The cross sections of sample 6-8, Figure 36-38, shows granules very representative for the species. There is a variation of $g_{w,max}$, but in general the size is quite uniform

In Figure 34, sample 4, the cross section image is taken from S&V session where scale bar is not included. The image was measured manually and is an approximately value. By studying the 270 images from S&V it is clear that Figure 34 represent the structure for this sample. What stand out for this species are the thickened primary granules which have a different appearance. Some of the thickened granules looked like magnified ordinary granules, but the majority was shaped like an elevated mushroom stem with two granules displaying an overhang.

Figure 35, sample 5 displays two granule profiles, and what is likely to be the profile of the ridges. As for sample 2 and 4, the granules form a hexagonally pattern on the cuticle, see Figure 24, 26 and 27, and this is probably the reason for only two overhangs visible. It seems to be a connection between the distances between granules in hexagonally patterns and the amount of overhang profile imaged at a cross section. The closer the granules are placed together, i.e. shorter ridges, the more likely it is to see several overhangs in the same cross section.

Figure 37 and 38 display a cross section of the summer and winter adapted specie Cryptopygus clavatus, and these images reveal no significant difference of the structures of sample 7 and 8. The granules look very much the same, regardless of season. As what proved to be a trend for the flatter surface structured samples, the profile of the granules are displayed as an even line with thick pancake shaped profiles. This was a hairy species of collembola, see Figure 22A-24A in appendix, and it would have been interesting to investigate if the density of hair varied between summer and winter, and whether the amount of hair results in different wetting properties. When studying sample 8 in the SEM it was discovered that the sample was almost drowned in silver glue, and an image of the animal in its entirety was not achievable, hence no image to compare the surfaces of sample 7 and 8 with respect to hair.

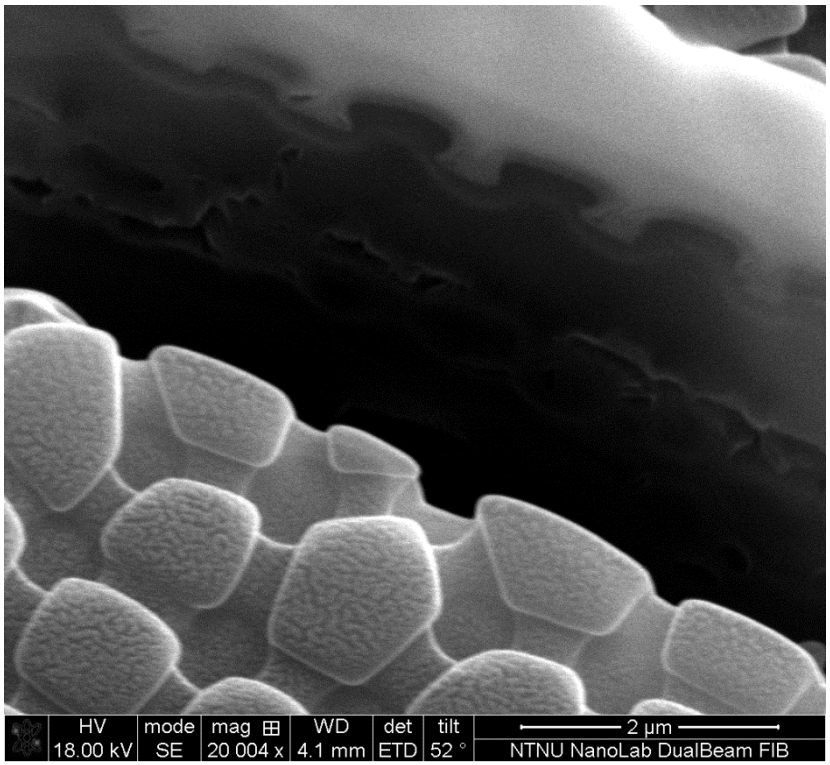

Figure 31 - Cross section of sample 1

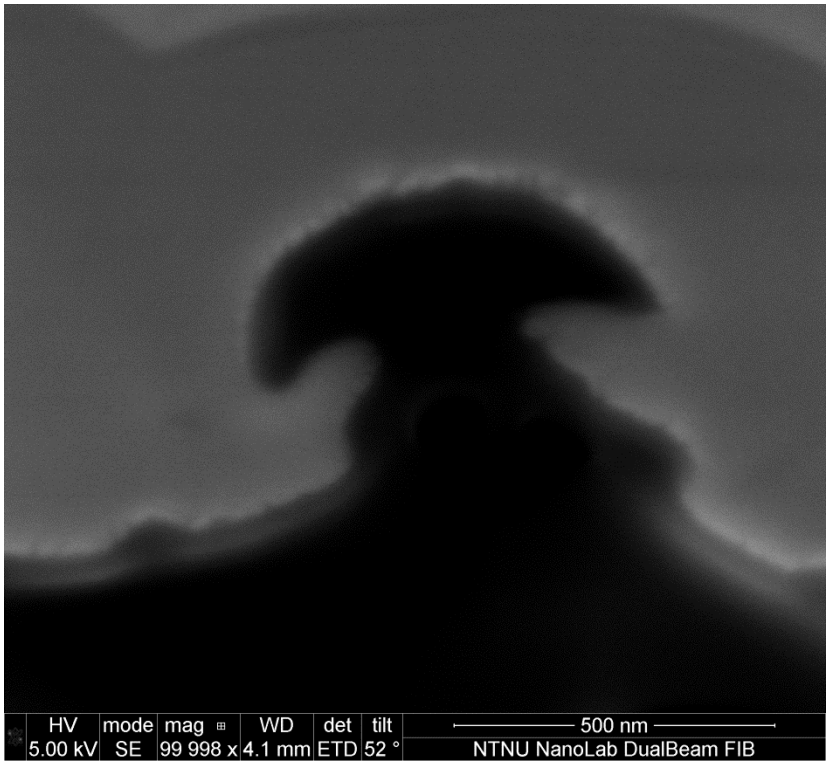

Figure 32 - Cross section of sample 2

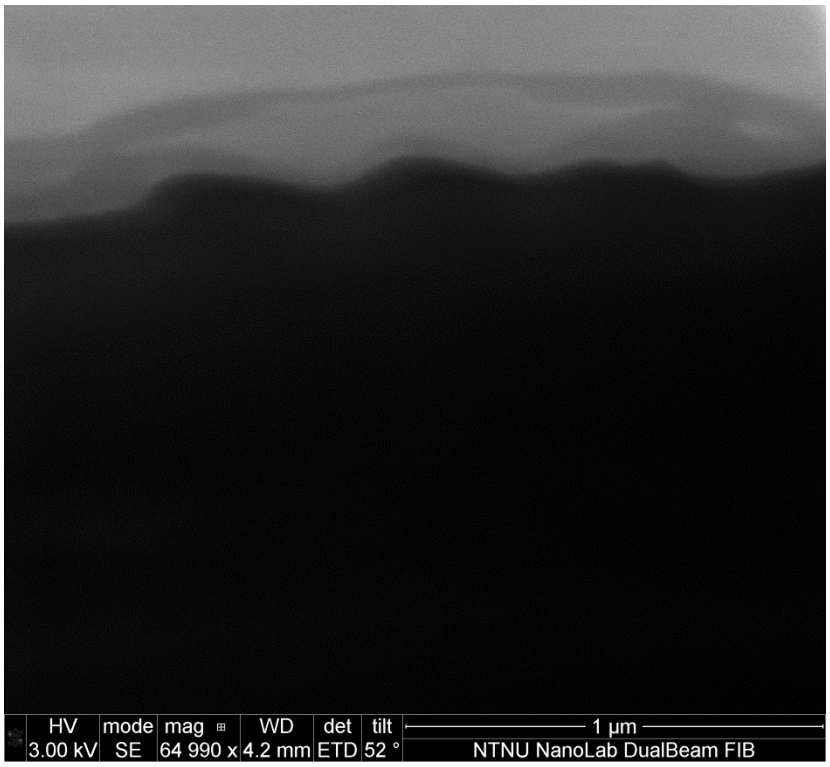

Figure 33 - Cross section of sample 3

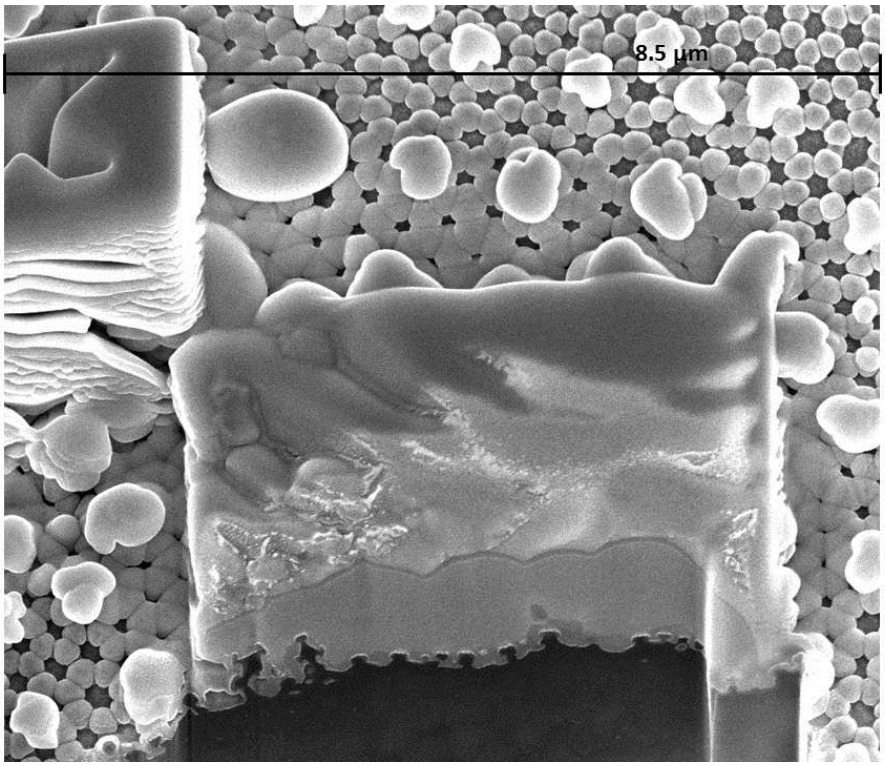

Figure 34 - Cross section of sample 4

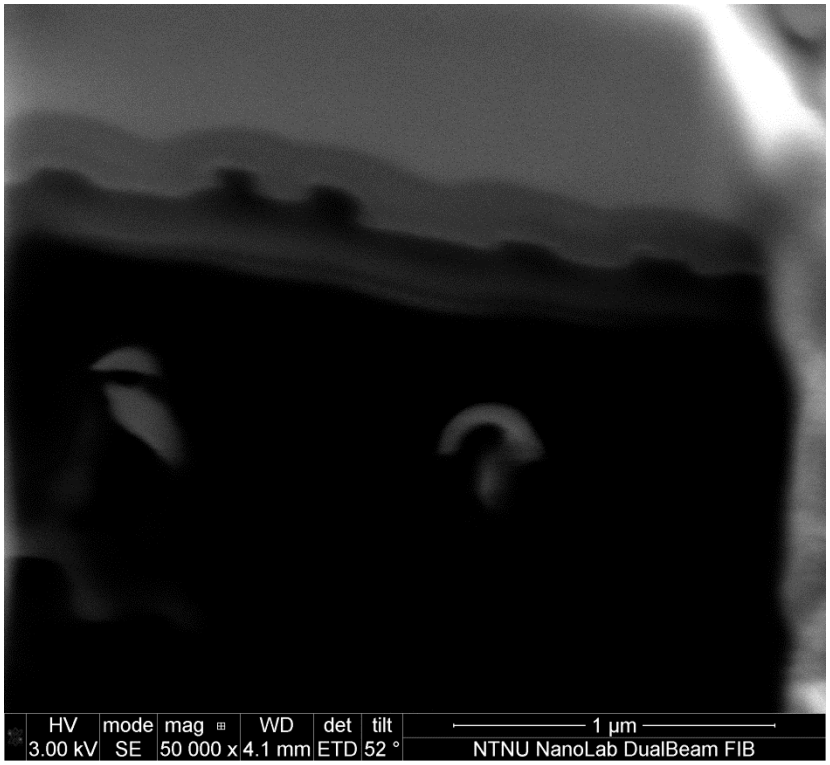

Figure 35 - Cross section of sample 5

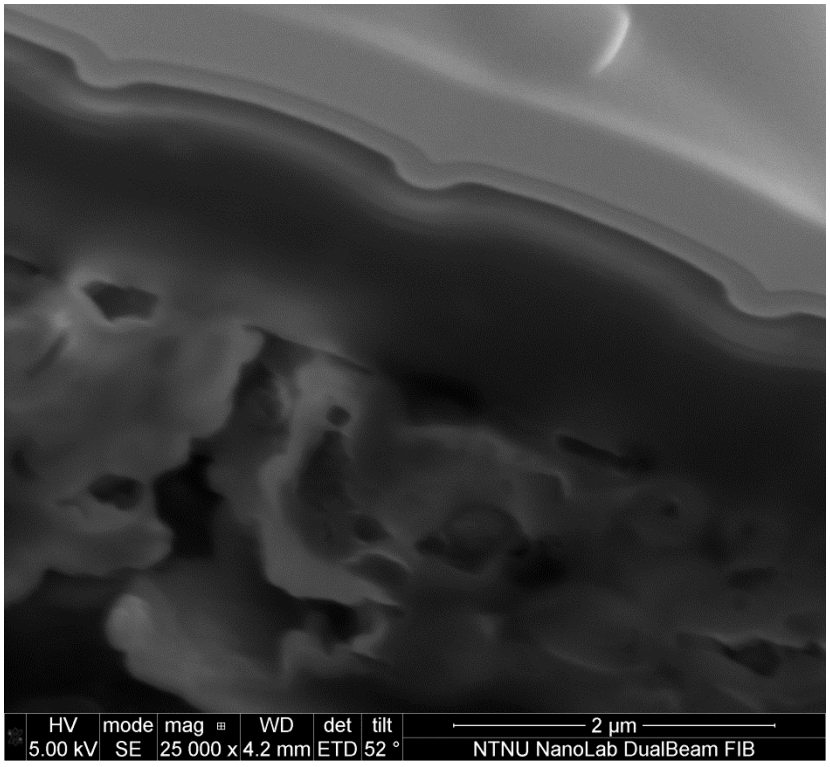

Figure 36 - Cross section of sample 6

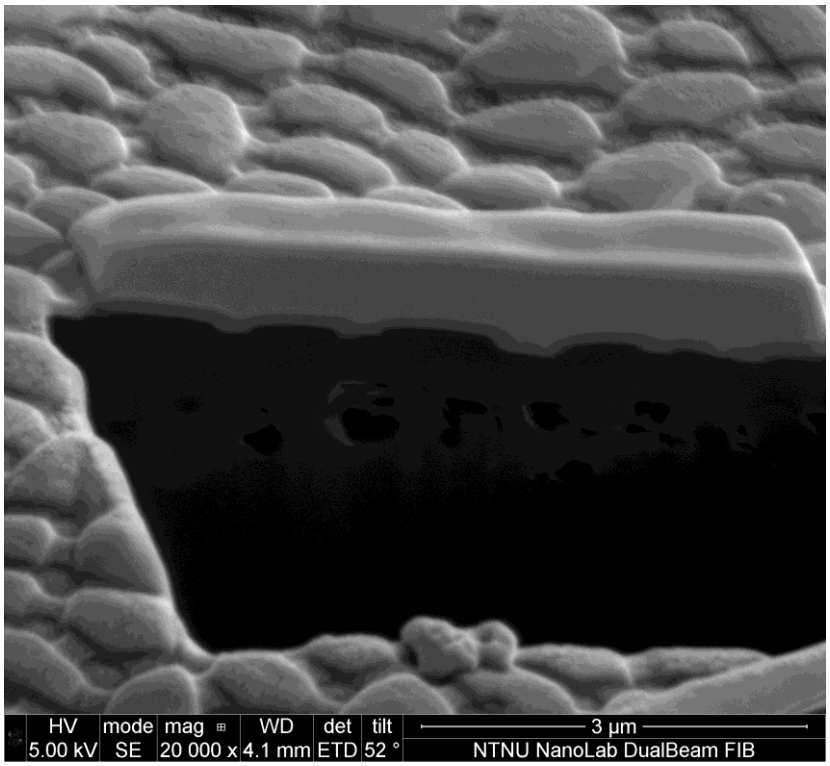

Figure 37 - Cross section of sample 7

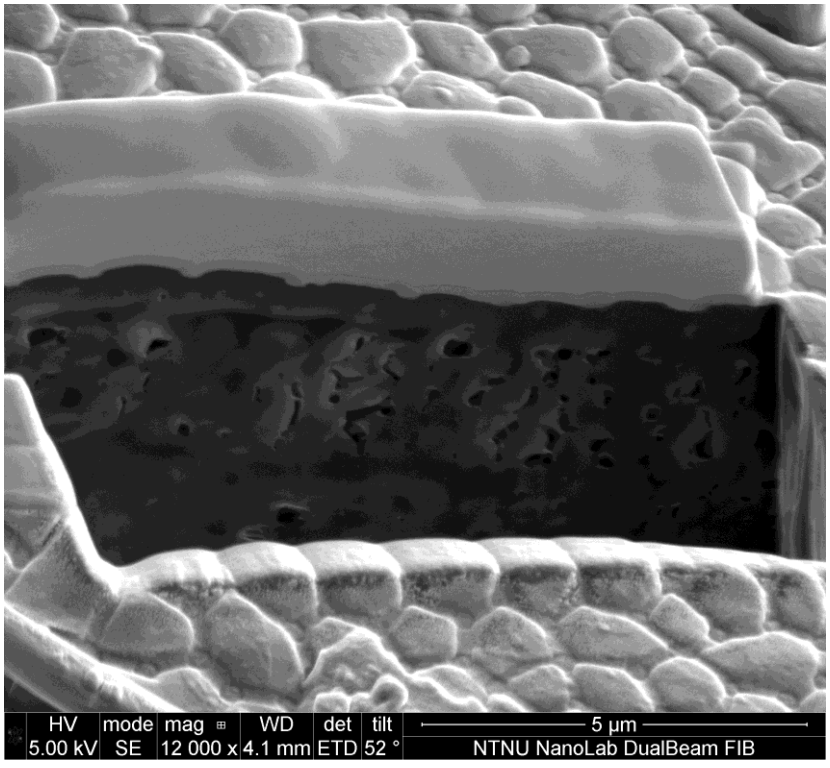

Figure 38 - Cross section of sample 8

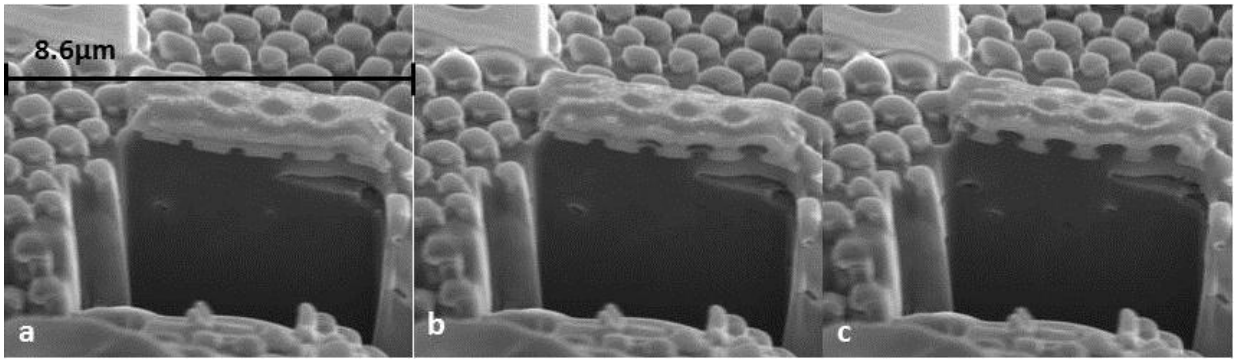

Figure 39 – Sample 1, emerging granules during S&V

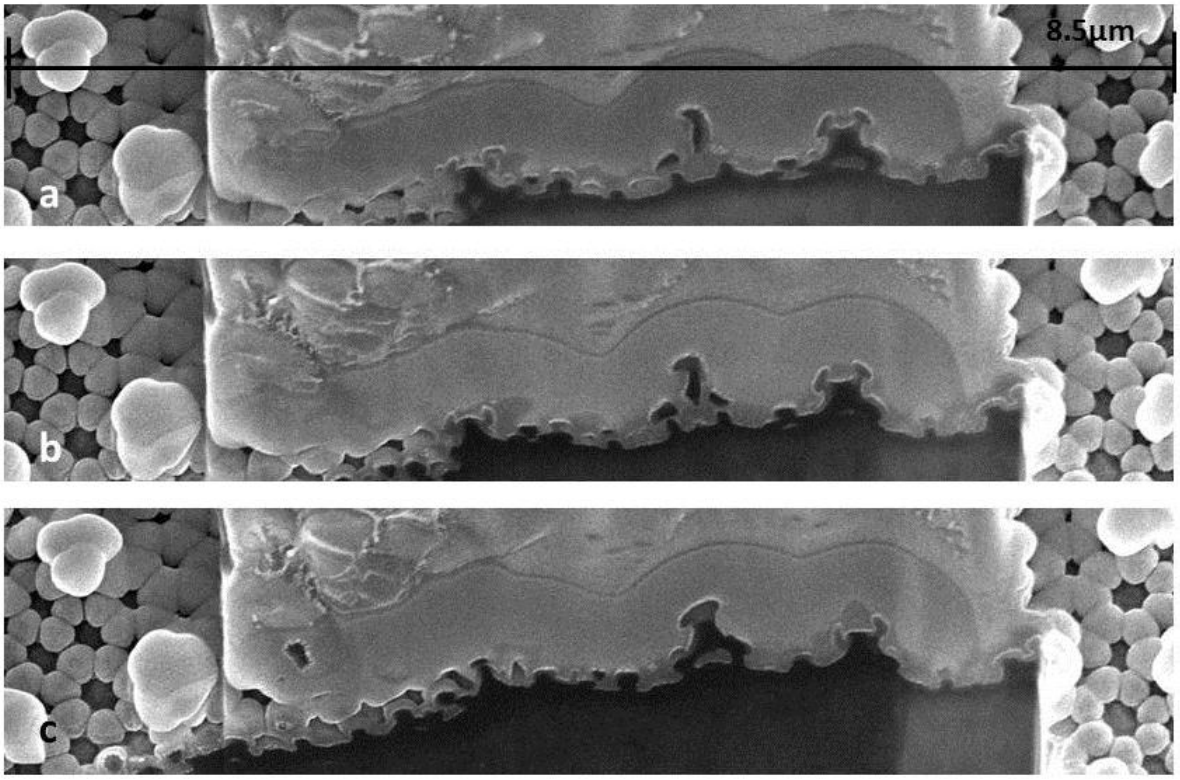

Figure 40 - Sample 4, emerging granules during S&V

As mentioned, during the review of the 270 images taken during S&V of sample 4, it was noticed that several of the thickened primary granules displayed a pair of twin mushrooms shapes granules, thus two granules that originates from the "stem". On Figure 26 of sample 4 these are the popcorn-like features, also seen as the whitest granules in Figure 40. These granules have a remarkable similarity of the film figure "Shrek", see Figure 41, and will from now on be referred to as "The Shrek" structure or "The Shrek" granule in this thesis.

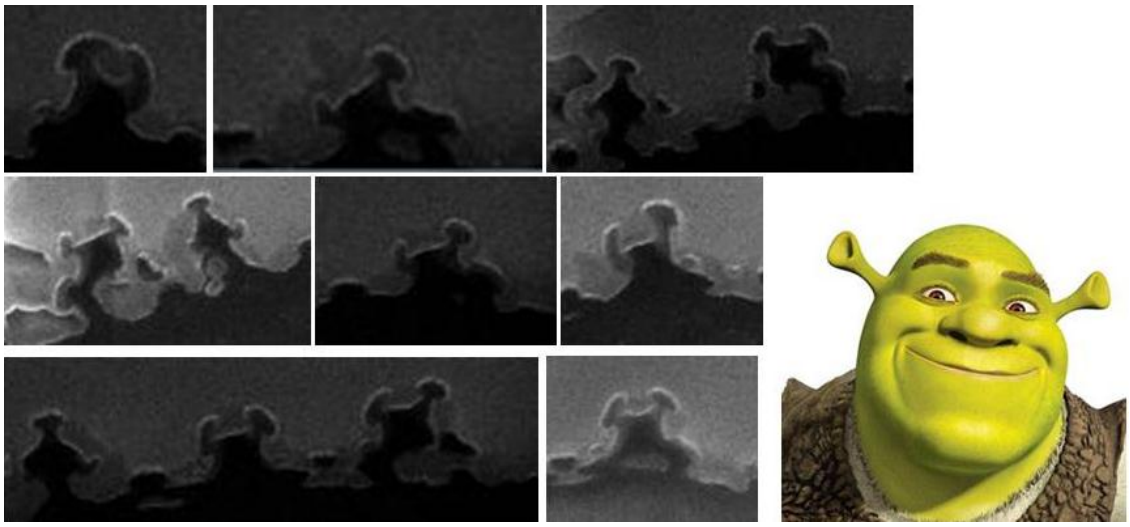

Figure 41 - The Shrek formed granules on sample 4

It is likely those two smaller granules instead of one large result in higher resistance to wetting as the total mechanisms of granule overhang are increased.

Figure 42-45 displays sample 1 and 4 after modifications in software of images from S&V. Scale bar is not available in the software, and the manually measurements from SEM is not transmittable. Disturbing features on the images is a result of noise, interfering changes in images that not represents the area of interest.

Sample 1 in Figure 42 and 43 clearly shows the ridges between the granules, and it look like the ridges also have an overhang. Based on Figure 43 the overhang does not seem to be circular. From Figure 31 the granule profile looked more oval shaped that what is displayed in Figure 42 and 43. Figure 44 and 45 displays sample 4 and its hexagonally structure is easily seen. The Shrek structure is however not preserved. Ridges with overhang are not as obvious as for sample 1, and the overhang appears to be more circular. The 3D images look similar to the surface structure of the sample imaged by SEM.

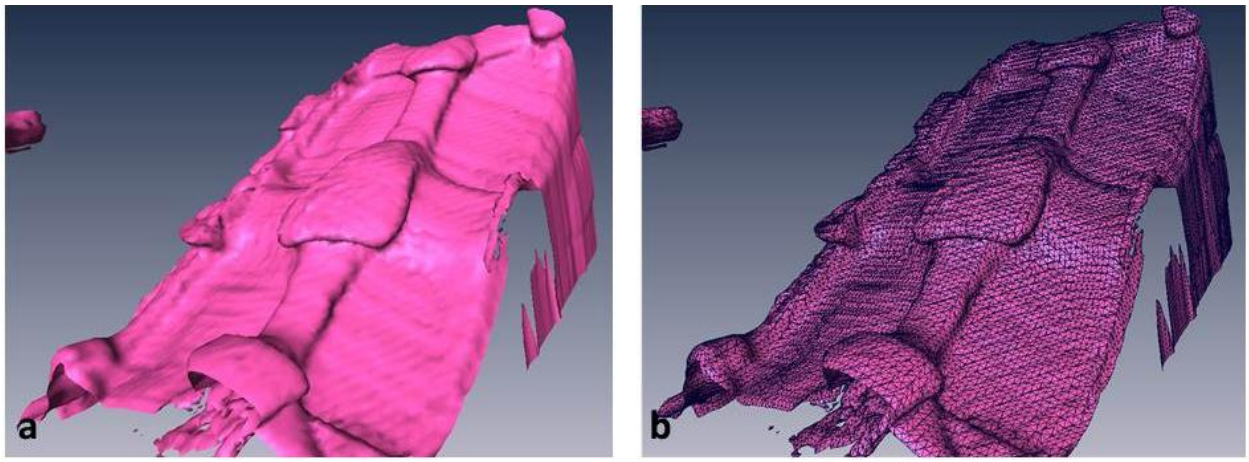

Figure 42 - Sample 1 3D model, a) Unmeshed surface, b) Meshed surface

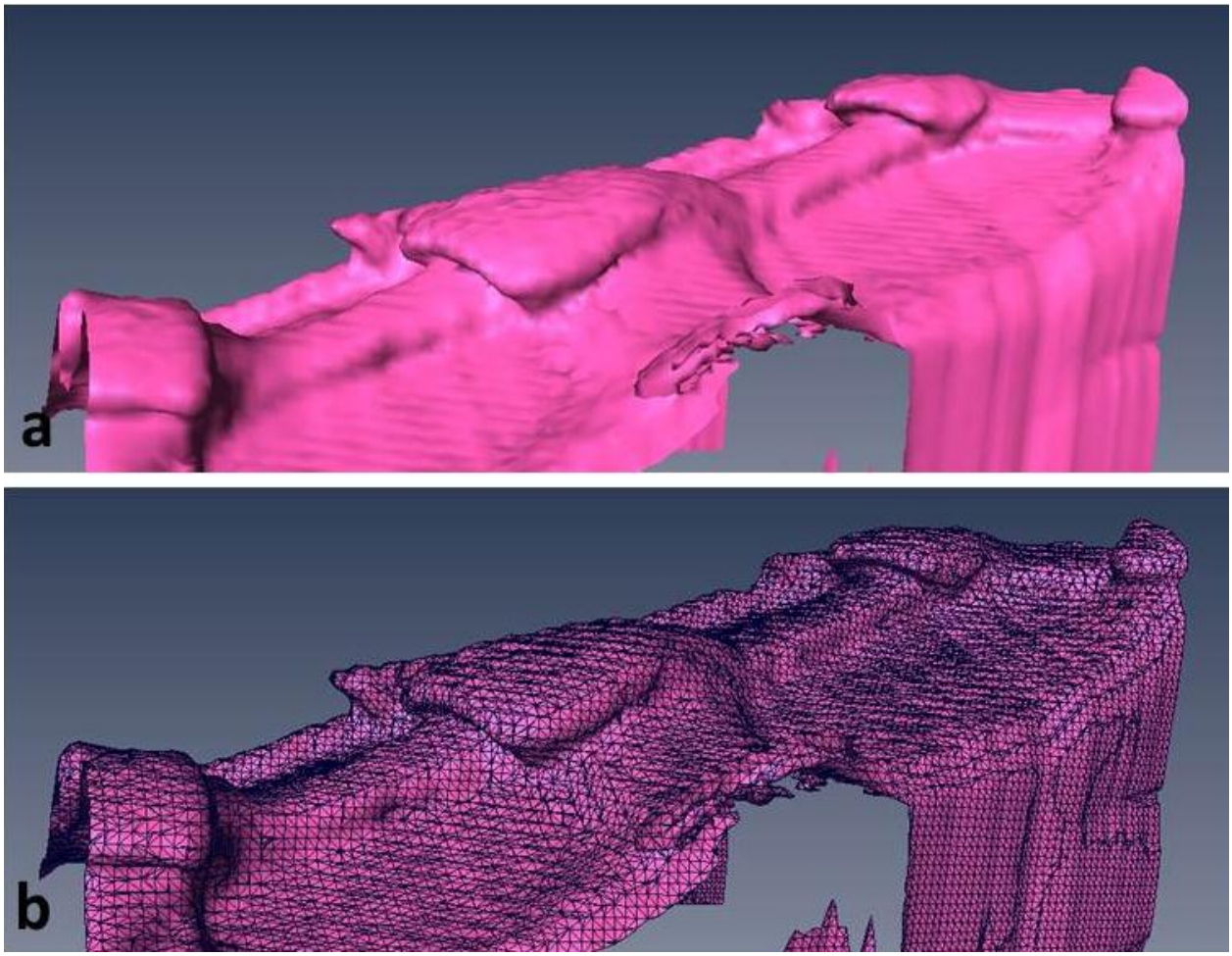

Figure 43 - Sample 1 3D model from the side, a) Unmeshed surface, b) Meshed surface

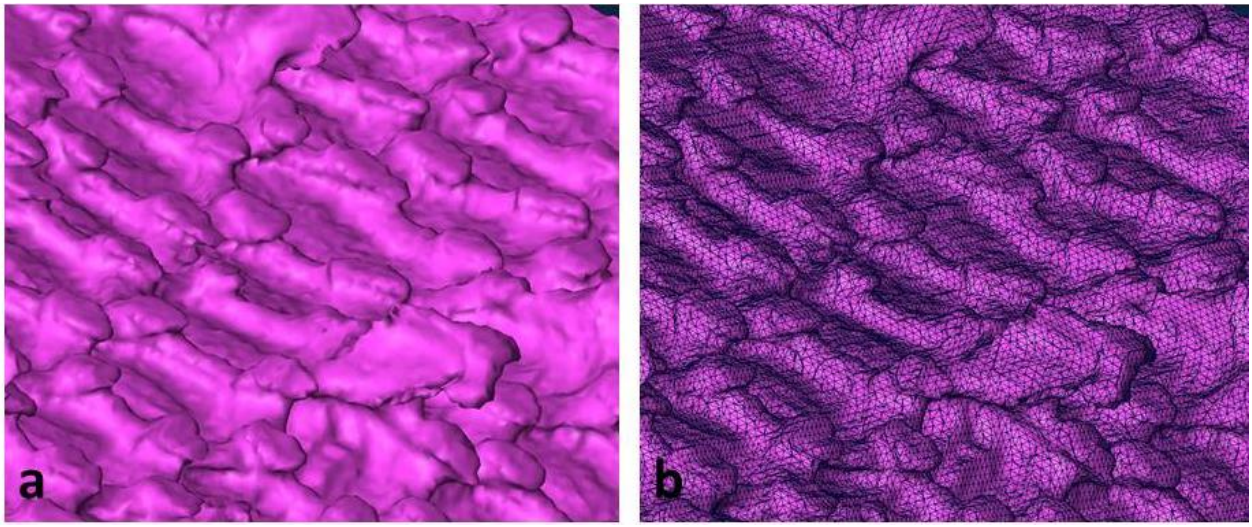

Figure 44 - Sample 4, 3D model, a) Unmeshed surface, b) Meshed surface

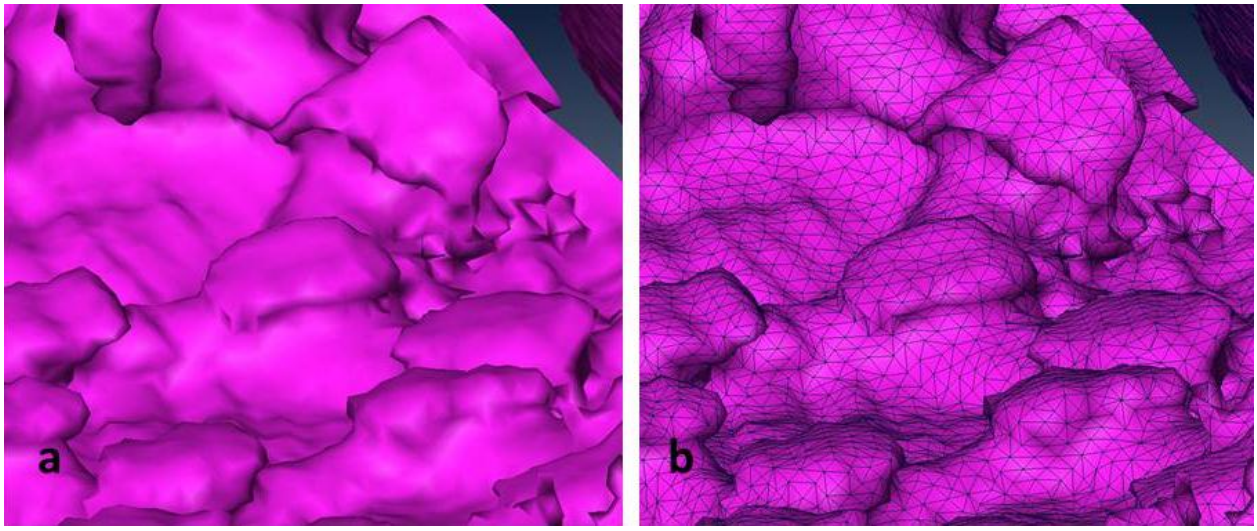

Figure 45 - Sample 4, 3D model closer up, a) Unmeshed surface, b) Meshed surface

Measurements of advancing and receding contact angle together with calculations on hysteresis of sample 1-8 are presented in Figure 46. Sample 6 should have a negative $\Delta\theta$ according to measurements, but as this make no sense, $\Delta\theta$ is set to ≈0. Measurement error is probably the reason for negative hysteresis.

	1	2	3	4	5	6	7	8
θ_a	168°±1°	159°±1°	171°±3°	170°±2°	164°±1°	157°±2°	141°±3°	166°±2°
θ_r	165°±2°	132°±2°	166°±2°	165°±3°	163°±2°	161°±4°	118°±11°	166°±2°
$\Delta\theta$	3°	26°	5°	5°	2°	≈0°	22°	0°

Figure 46 - Measurements of receding and advancing contact angles for sample 1-8

Quantitative measurements of the granules and ridges were conducted as seen in Figure 47. Depending on image quality and what they displayed the values in Figure 47 was measured and re-calculated as described in section 4.2.8. Measurements were taken from images with different scale bar, and results from images with smaller scale bar are likely to be more conservative. To illustrate which values are from which scale bar, a colour code is utilized, see Figure 48. Sample 4 had thickened primary granules with a very different appearance than the smaller primary granules. 4* column gives values of an ordinary thickened primary granule and 4** is values of the Shrek-granule.

	Sample number									
	1	2	3	4	4*	4**	5	6	7	8
ξ	107.8	186	-	-	104	-	-	-	-	-
$g_{w,max}$	871.7	628	390	91	279	100	206	2205	627.2	1500
$g_{w,min}$	623.75	243	-	-	165	55	108	-	-	-
g_h	372.3	473	65.86	132.5	398.5	-	168.8	-	136	190
R_g	-	273	-	-	-	-	-	-	-	-
r_h	142.1	-	-	-	-	-	-	-	890	-
w_g	1281	998.1	353	182	-	289	296	-	588.5	1450
r_{max}	-	46.1	-	-	-	-	-	-	-	-
r_{min}	-	13.7	-	-	-	-	-	-	-	-
κ	-	525°	-	-	-	-	-	-	-	-

Figure 47 - Measurements of granules and ridges [nm]

Colour codes for measurement					
500 nm	1000 nm	2000 nm	6400 nm	8500 nm	Measured by FIB software

Figure 48 - Color codes for scale bars used during measurements

In addition to measurements in Figure 47, the ridges width of sample 7 was measured to 196 nm. It is important to be aware that the measurement of a sample is taken from the same granule. The $g_{w,max}$ of one species may greatly vary from granule to granule, see Figure 49a and b. The value of g_h in Figure 49 a is not adjusted to the tilt and should be ignored, the $g_{w,max}$ values are however the real value.

The granules in Figure 49 display a $g_{w,max}$ difference of 429.6 nm. For further comparison of measurements of the same sample, see Figure 25A and 26A in appendix.

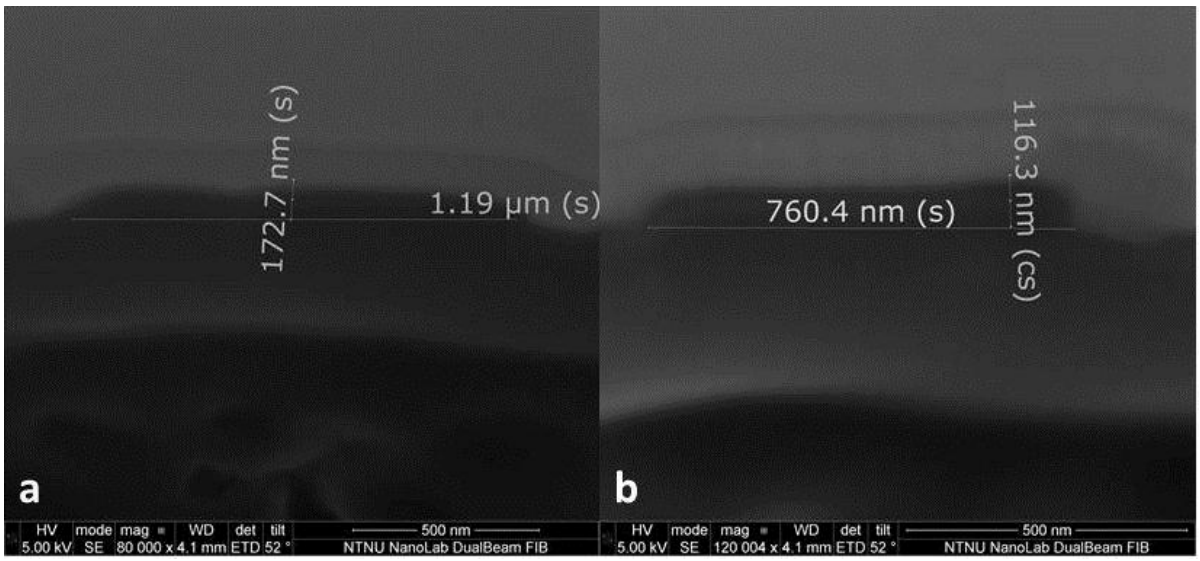

Figure 49 - Different values of $g_{w,max}$ of sample 8

Figure 50 - Great variation of granule size, illustrated by sample 8

7. Discussion

Regardless of any overhang, all the collembolans display a roughened surface which is a great contributor to resistance against wettability, see Figure 23-30. The asperities and roughness represented by granules and ridges prevent liquid from touching the cuticle due to tension at the interface.

As the effect of an overhang of these granules is included in the wetting the hydrophobicity should utterly be increased. The force required to move the triple line in Figure 11 after it is settled must be strong enough for θ to become higher than θ_a. This model is however based on simplifications and assumptions; 2D model, perfect circular granules and the same pressure difference across the whole interface. There is no 2D shaped living animal, and thus the model should be further developed. The errors caused by this simplification are not known, but it is reasonable that including the radius of a droplet in both the principal directions 1 and 2 will lead to another pressure difference and curvature of the interface. Figure 31-32, 34-36 and 40-45 displays profiles of the overhang and they are not circular, neither is the overhang of the ridges in figure 42 and 43. The consequence of assumption of circular overhang with respect to reliability of theories described in section 4.1.6 is also unknown, but it is probably not very complicated to adapt the theory to a more sharpen overhang. From Figure 42-45 it also may look like different species displays different geometry of the overhang, and a model that easily can be customizes to the species of interest would be beneficial.

In Figure 31, 34 and 35 several granule profiles are displayed, and only some granules on each image show an overhang. This is probably because of the placing of the rough cut. If the cut is made at the beginning of a granule it is less likely that the overhang shape will be displayed. The granules that shows overhang on these images would also have been easier to study visually at a higher magnification, as in Figure 32, where the overhang is magnified by almost 100000. Most of the samples became unclear at such magnification, and that is why the rest of the images are presented within the rage of 12000-65000 times magnified. The reason for unclear images could come from charging problems, physical placement of the overhang or not locating the right settings of the SEM. By more experience and training the latter should be improved.

Sample 3 and 6-8 did not display an overhang; see Figure 33 and 36-38. The granules could have suffered from damages during preparation, platinum deposition, FIB milling destroying the overhang, but most likely the overhang is not there from the beginning. If this assumption is confirmed by a further survey, an evaluation if roughened surface alone causes the wetting properties, or if other factors as hair and surface chemistry are involved.

The overhang of sample 1's granules and ridges is very clear in Figure 42 and 43, and the overhang does not look circular. It is difficult to estimate an angle value of the overhang based on images alone, the angle between the top of a ridge to the smooth cuticle could be ≈20° or less. Based on theories for circular granules, this overhang further contributes to the super-hydrophobic surface. Figure 44 and 45 shows of the granules overhang of sample 4, the ridges is not presented as clearly, but they look as to display an overhang as well.

If the platinum deposition on sample 1 and 4 had been thicker, it is likely the results from S&V and the modified images had more realistic. The images of sample 4, see Figure 44-45, is somewhat uneven compared to what the granules look like in cross section images. The granules and ridges on the left side in Figure 42 are not very visible because the platinum layer was too thin and the features were destroyed. It is also possible that other parameters in software would utterly have reduced the noise, and a more realistic imaging. Initially in this study there were concerns regarding requirements of re-deposition of platinum after each slice to protect the sample, but this proved not to be necessary.

The parameters in Figure 12 are necessary to measure for calculation of wetting properties given that the granule has an overhang. As the granules without an overhang look less geometrically complex, it is likely to assume is would be easier to calculate r_f, f_1 and f_2 for utilization of Wenzel and Cassie-Baxter's equations of samples without overhang. The reliability of the measurements in Figure 47 is depending on the scale bar of the image the measurements were taken from, and images of higher magnification are favorable when regarded as more conservative. None of the images could be used to gather all the parameter in Figure 12, and if such measurements are to be used to design a super-hydrophobic surface, more accurate footage must be available to collect required information.

By definition of the contact angle >150°, all samples exhibit super-hydrophobic properties according to contact angle measurements in Figure 39, except from sample 2 which displays a receding contact angle, θ_r=132°±2° and sample 7 which displayed a receding contact angle, θ_r =118°±11° and an advancing contact angle θ_a =141°±3° . This is still within the definition of hydrophobic (Θ>90°). These two samples were also the only ones displaying contact angle hysteresis larger than 5°; sample 2 showed $\Delta\theta$=26°, and sample 7 showed $\Delta\theta$= 22°

Sample 6 did neither appear to have overhang of granules, but by contact angle measurements both advancing and receding contact angle are by definition super-hydrophobic; Θ_a= 157°±2° and Θ_r= 161°±4°. The hysteresis of sample 6 is however negative, probably due to measurement errors. As an assumption this was then set to ≈0°. Measurement errors must be taken into consideration when evaluating every value in Figure 46.

Sample 3 proved to have highest advancing and receding contact angle: Θ_a=171°±3° and Θ_r=166° ±2 °. Sample 7 displayed the lowest advancing and receding contact angle and largest hysteresis: Θ_a =141°±3°, Θ_r=118°±11° and ΔΘ= 22°. None of these samples show any overhang, and thus there is no clear link between the overhang and super-hydrophobic properties. The random connection between overhang and hydrophobic properties are presented in Figure 51. The advancing- and receding contact angle is descending from left to right, and the values of contact angle hysteresis are ascending from the left. The blue sample numbers are samples without overhang, and the red numbers are samples with an overhang. The cells with a diagonal line and two sample numbers are illustrating two samples displayed the same values.

Red sample numbers corresponds to samples with overhang Blue sample numbers corresponds to samples without overhang								
Largest Θ_a	3	4	1	8	5	2	6	7
Largest Θ_r	8 / 3	1 / 4	5	6	2	7	-	-
Smallest $\Delta\Theta$	6	8 / 5	1	3 / 4	7	2	-	-

Figure 51 - Rating the values of advancing and receding contact angle and contact angle hysteresis.

By just a glans at Figure 51, it is clear that hydrophobicity is not depending on the overhang. Samples displaying the most hydrophobic properties are all without an overhang, but by a comparison with sample 4 the difference between their advancing and receding contact angle is 1° only, and $\Delta\theta$ is the same. There is no sample that stands out as absolutely most super-hydrophobic. Sample 4 that showed the most characteristic shape of a mushroom, is however outside the definition of super-hydrophobic with a receding contact angle of 132°±2°, and displays the largest contact angle hysteresis of $\Delta\theta$=26°. The notion that the overhang is leading to super-hydrophobic properties must hence be evaluated. However, it is possible that the transition from a metastable Cassie-Baxter state to a Wenzel state required a higher pressure for the samples with overhang because of the granule shape.

When investigating sample 7 and 8, the specie that adapted whether it was summer or winter, showed great differences of contact angle and contact angle measurements, and the winter adapted animal clearly displayed the most hydrophobic properties. Sample 7 was not even within the definition of super-hydrophobic as it displayed θ_a =141°±3° and θ_r =118°±11°. The difference of receding contact angle between the two samples was in total 48°, disregarding measurement error considerations, and the contact angle hysteresis difference was 20°. From the theoretical perspective one could assume these relatively large differences in wetting properties was due to different surface structure, but this was rejected after examination by FIB and SEM. Without labeling the images from the two samples, they cannot be told apart. By the $g_{w,max}$ values from Figure 47 and 25A in appendix it may look like the granules of sample 8 are larger, but this is believed to be a coincidence.

If the surface structure and granule shapes are apparently identical for samples displaying very different wetting properties, this strongly indicates other factors than surface geometry is contributing to hydrophobicity. They may have different chemical composition of their surface structure or different hair density, but this was not investigated.

.

8. Conclusion

The collembolans property of resistance to wetting is highly valuable for industrial applications. Mimicked biological features of hydrophobic plants are already used in different industries, but collembolan cuticle is assumed more sustainable and mechanically stable due to the incorporated bristles and the alignment of granules and ridges.

To examine and inspect the geometrical features of the collembolans a dual FIB was utilized. Biological features and structures can be displayed by FIB in ways no other method can provide. The collembolans were fragile to the ion beam, but parameters could be adapted so the samples were not damaged. To protect biological samples from milling procedures, a thick protective layer of platinum must in advance be deposited at low currents. The electron beam causes less damage then the ion beam, and initially a ≈0.3 µm thick layer was deposited by electron beam at 0.34-0.69 nA. An additional platinum layer of approximately 0.7µm was subsequently deposited by the ion beam at 0.26- 0.44 nA. At sufficiently low current, milling is fully possible to conduct on biological samples without destroying them.

The rough cut made for the SEM to visualize the profile was milled at 440 pA, followed by a cleaning cut milled at 90 pA. For the slice and view procedure the ion beam current was set to 0.26 nA, and even after hundreds of slices the sample did not suffer from damages induced by ion beam. It was neither necessary to re-deposit platinum after each slice to protect from the ion beam. Charging related problems can be handled with a carbon and platinum coat on the animal, and by mounting them on stubs with silver glue. By using low current and/or back scattered electrons good imaging is achievable. Measurements of the geometrical features displayed on collembolan cuticle can be achieved by study the images presented after FIB procedure. These can be used for a manufactured, reconstructed sample.

The collembolans display their hydrophobic or super-hydrophobic properties due to a roughened cuticle as a combination of granules, ridges and possibly because of hair. Some species have an overhang on their granules, and this is likely to contribute to

hydrophobicity and maybe impede the metastable Cassie-Baxter state to transit to Wenzel state.

All samples showed an intricate and sophisticated pattern of granules on the cuticle, which make a roughened surface. This rough surface alone causes the forces in solid-vapour interface to be stronger than the forces in solid-liquid interface, resulting in a contact angle higher than 90°. Six out of eight samples showed low contact angle hysteresis ($\Delta\theta \leq 5°$), which is a property that results in droplets being able to easily move along the surface. Four out of eight samples proved to have an overhang on their granules, and two samples could be confirmed to have an overhang on their ridges. When the three-phase-point of solid-liquid-vapour settles on the granule or ridge, the contact angle equals the advancing contact angle and high pressure as a combination of gravity, impact and immersion is required for the three-phase-point to slide further down to wet the surface.

The model presented for calculations of wettability of collembolans takes into account that the granules displays overhang. This proved not to be the case as half of the samples had none, and the sample that showed the most super-hydrophobic properties was one of these. There are no indications pointing towards the presence of an overhang leading to either higher or lower hydrophobic properties. In a rating of highest advancing- and receding contact angle and lowest contact angle hysteresis, the granules with and without overhang is randomly scattered. Two very important conclusions can be made: All collembolans do not exhibit overhang on their granules, and the overhang is not the reason alone behind hydrophobic- and super-hydrophobic properties. Surface chemistry composition and/or hair and bristles may be additional factors that lead to the resistance to wetting for collembolans. This could not have been discovered without the operations done in FIB.

9. Further work

By further investigation and research of suitable SEM and FIB parameters, better images at higher magnifications is likely to be achieved. This also applies for the software used to modify images from S&V session. Higher quality imaging can be used to improve geometrical measurements of the granules and ridges.

To understand mechanisms and consequences of an overhang on granules and ridges a more adapted model should be developed to account for non-circular granule- and ridge shape. This should also be a 3D model without simplifications of the pressure difference in Young-Laplace equation.

As the experimental part proved that additional factors besides an overhang must exist to cause the super-hydrophobic properties, these should be investigated.

If the collembolan's surface structure are to be copied for industrial applications, a thoroughly survey of corrosion properties of such a surface due to the enlarged surface area must be conducted.

10. References

1. Gao L, McCarthy TJ. Teflon is Hydrophilic. Comments on Definitions of Hydrophobic, Shear versus Tensile Hydrophobicity, and Wettability Characterization2008.
2. Hobæk TC, Leinan KG, Leinaas HP, Thaulow C. Surface Nanoengineering Inspired by Evolution. Bionanoscience. 2011;1(3):63-77.
3. Young T. An Essay on the Cohesion of Fluids. Phil Trans Soc Lond. 1805;95:65-87.
4. Laplace PS. Mécaniqe céleste. 1805;4(8).
5. Wenzel RN. Resistance of Solid Surfaces to Wetting. Industrial and Engineering Chemistry. 1936;28(8):988-94.
6. Cassie ABD, Baxter S. Wettability of porous surfaces. Trans Faraday Soc. 1944;40:546-51.
7. Extrand CW. Contact Angles and Hysteresis on Surface with Chemically Heterogeneous Islands. Langmuir. 2003;19(9):3793-6.
8. Gao L, McCarthy TJ. How Wenzel and Cassie Were Wrong. Langmuir. 2007;23(7):3762-5.
9. Bartell FE, Shepard JW. Surface Roughness as Related to Hysteresis of Contact Angles. II. The System Paraffin-3 Molar Calcium Chloride Solution-Air and Paraffin-Glycerol-Air. J Phys Chem 1953;57(4):455-8.
10. Pease DC. The significance of the contact angle in relation to the solid surface. J Phys Chem. 1944;49(2):107-10.
11. Helbig R, Nickerl J, Neinhuis C, Werner C. Smart Skin Patterns Protect Springtail. PLoS ONE. 2011;6(9):1-6.
12. Fürstner R, Barthlott W. Wetting and Self-Cleaning Properties of Artificial Superhydrophobic Surfaces. Langmuir. 2005;21(3):956-61.
13. Yabu H, Shimomura M. Single-Step Fabrication of Transparent Superhydrophobic Porous Polymer Films. Chem Mater 2005;17(21):5231-4.
14. Youngblood JP, McCarthy TJ. Ultrahydrophobic Polymer Surfaces Prepared by Simultaneous Ablation of Polypropylene and Sputtering of Poly(tetrafluoroethylene) Using Radio Frequency Plasma. Macromolecules. 1999;32(20):6800-6.
15. Han JT, Xu X, Cho K. Diverse Access to Artificial Superhydrophobic Surfaces Using Block Copolymers. Langmuir. 2005;21(15):6662-5.
16. Ming W, Wu D, Benthem Rv, With Gd. Superhydrophobic Films from Raspberry-like Particles. Nano Letters. 2005;5(11):2298-301.
17. Bormashenko E, Stein T, Whyman G, Bormashenko Y, Pogreb R. Wetting Properties of the Multiscaled Nanostructured Polymer and Metallic Superhydrophobic Surfaces. Langmuir. 2006;22(24):9982-5.
18. Sandnes R. Unpublished master thesis, NTNU 2012.
19. Yao N. Focused Ion Beam Basics and Application New York: Cambridge University Press 2007.
20. Lucille A. Giannuzzi FAS. Introduction to Focused Ion Beams: Instrumentation, Theory, Techniques, and Practice. New York: Springer; 2005.
21. Lewis SM, Osborn JS, Stuart PR. Demonstration of an Internal Structure within the Red Blood Cell by Ion Etching and Scanning Electron Microscopy. Nature. 1968;220:614-6.
22. Spector M. Ion beam etching in a scanning electron microscope: red blood cell etching. Micron. 1974;5(3):263-73.

23. Drobne D, Milani M, Lešer V, Tatti F. Surface damage induced by FIB milling and imaging of biological samples is controllable. Microscopy Research and Technique. 2007;70(10):895-903.
24. Milani M, Drobne D, Tatti F. How to study biological samples by FIB/SEM. Formatex 2007:787-94.
25. Lešer V, Drobne D, Pipan Ž, Milani M, Tatti F. Comparison of different preparation methods of biological samples for FIB milling and SEM investigation. Journal of Microscopy 2009;233(2):309-19.
26. Ishitani T, Hirose H, Tsuboi H. Focused-Ion-Beam Digging of Biological Specimens. J Electron Microsc. 1995;44(2):110-4.
27. Drobne D, Milani M, Zrimec A, Lešer V, Zrimec MB. Electron and ion imaging of gland cells using the FIB/SEM system. Journal of Microscopy. 2005;219(1):29-35.
28. Winter DAMD, Schneijdenberg CTWM, Lebbink MN, Lich B, Verkleij AJ, Druby MR, et al. Tomography of insulating biological and geological materials using focused ion beam (FIB) sectioning and low-kV BSE imaging. Journal of Microscopy. 2009;233(3):372-83.
29. Resh VH, Cardé RT. Encyclopedia of Insects. San Diego, California: Academic Press; 2003.
30. Rusek J. Biodiversity of Collembola and their functional role in the ecosystem. 1998;7(9):1207-19.
31. Leinaas HP. Personal communication, Biologist at the University of Oslo. 2012.
32. Rawlings AE, Bramble JP, Stainland SS. Innovation through imitation: biomimetic, bioinspired and biokleptic research2012.
33. Wagner P, Fürstner R, Barthlott W, Neinhuis C. Quantitative assessment to the structural basis of water repellency in natural and technical surfaces. Journal of Experimental Botany. 2003;54(385):1.
34. Marmur A. The Lotus Effect: Superhydrophobicity and Metastability. Langmuir. 2004;20(9):357-3519.
35. Guo Z, Liu W, Su B-L. Superhydrophobic surfaces: From natural to biomimetic to functional. Journal of Colloid and Interface Science. 2010;353(2):335-56.
36. Norheim HM. Petroleumsaktiviteter i Arktis. Arctic - Changing Realities Conference; Copenhagen2010.
37. Virk PS. Drag reduction fundamentals. AIChE 1975;21(4):625-56.
38. Wang Y, Bhushan B. Boundary slip and nanobubble study in micro/nanofluidics using atomic force microscopy. Soft Matter. 2010;6(1):29-66.
39. Liu MM, Wang S, Wei Z, Song Y, Jiang L. Bioinspired Design of a Superoleophobic and Low Adhesive Water/Solid Interface. Advanced Materials 2008;21(6).
40. Zhang L, Zhang Z, Wang P. Smart surfaces with switchable superoleophilicity and superoleophobicity in aqueous media: toward controllable oil/water separation. NGP Asia Materials. 2012;4(8).
41. Boduroglu S, Cetinkaya M, Dressick WJ, Singh A, Demirel MC. Controlling the Wettability and Adhesion of Nanostructructured Poly-(p-xylylene) Films. Langmuir. 2007;23(23):11391-5.
42. K. Autumn, Sitti M, Liang YA, Peattie AM, Hansen WR, Sponberg S, et al. Evidence for van der Waals adhesion in gecko setae. PNAS. 2002;99(19):12252-6.
43. www.acp.no. Active Cathodic Protection AS Visited May 2012.

44. Liu T, Chen S, Cheng S, Chang X, Yin Y. Super-hydrophobic surfaces improve corrosion resistance of copper in seawater. Electrochimica Acta. 2007;52(11):3709-13.
45. Zhu L, Jin Y. A novel method to fabricate water-soluble hydrophobic agent and super-hydrophobic film on pretreated metals. Applied Surface Science. 2007;253(7):3432-9.
46. Li G-Y, Li X-P, Wang H, Yang Z--Q, Yao J-Y, Ding G-F. Fabrication and characterization of superhydrophibic surface by electroplating regular rough micro-structures of metal nickel. Microelectronic Engineering. 2012;95:130-4.
47. Wang S, Jiang L. Definition of Superhydrophobic States. Advanced Materials. 2007;19(21):3423-.
48. Bikerman JJ. A Method of Measuring Contact Angles Ind Eng Chem Anal Ed. 1941;13(6):443-4.
49. Blokhuis EM, Shilkrot Y, Widom B. Young's law with gravity. Molecular Physics: An International Journal at the Interface Between Chemistry and Physics. 1995;86(4).
50. Bhushan B, Jung YC. Natural and biomimetic artificial surfaces for superhydrophobicity, self-cleaning, low adhesion, and drag reduction. Progressin in Material Science. 2010;109(8):1029-34.
51. Nosonovskya M, Bhushan B. Superhydrophobic surfaces and emerging applications: Non-adhesion, energy, green engineering. Current Opinion in Colloid & Interface Science. 2009;14(4):270-80.
52. Gao L, McCarthy TJ. Wetting 101°. Langmuir. 2009;25(24):14105-15.
53. Bhushan B, Nosonovsky M, Jung YC. Towards optimization of patterned superhydrophobic surfaces. Journal of the Royal Society Interface. 2006;4(15):643-8.
54. Stachowiak GW, Batchelor AW. Engineering Tribology. Boston: Elsevier; 2005.
55. Milne AJB, Amirfazli A. The Cassie equation: How it is meant to be used. Advances in Colloid and Interface Science. 2011;170(1-2):48-55.
56. McHale G. Cassie and Wenzel: Were They Really So Wrong? Langmuir. 2007;23(15):8200-5.
57. Pellicer J, García-Morales V, Hernández MJ. On the demonstration of the Young-Laplace equation in introductory physics courses. Physics Education. 2000;35(2):126-9.
58. Luo C, Xiang M, Liu X, Wang H. Transition from Cassie–Baxter to Wenzel States on microline-formed PDMS surfaces induced by evaporation or pressing of water droplets. Microfluids and nanofluids. 2011;10(4):831-42.
59. Forsberg P, Nikolajeff F, Karlsson M. Cassie–Wenzel and Wenzel–Cassie transitions on immersed superhydrophobic surfaces under hydrostatic pressure. Soft Matter. 2011;7(104-109).
60. Patankar NA. On the Modeling of Hydrophobic Contact Angles on Rough Surfaces. Langmuir. 2003;19(4):1249-53.
61. Schiffbauer JD, Xiao S. Novel application of focused ion beam electron microscopy (FIB-EM) in preparation and analysis of microfossil ultrastructures: A new view of complexity in early eukaryotic organisms. Palaios. 2009;24(9):616-26.
62. Stokes DJ, Morrissey F, Lich BH. A New Approach to Studying Biological and Soft Materials Using Focused Ion Beam Scanning Electron Microscopy (FIB SEM). J Phys: Conf Ser. 2006;26:50-3.
63. Heinze S. Theoretical part of FIB course, NTNU. 2012.

64. Schaffera M, Wagnera J, Schaffera B, Schmieda M, Mulders H. Automated three-dimensional X-ray analysis using a dual-beam FIB. Ultramicroscopy. 2006;107(8):587-97.
65. Stokes DJ, Vystavel T, Morrissey F. Focused ion beam (FIB) milling of electrically insulating specimens using simultaneous primary electron and ion beam irradiation. J Phys D: App Phys. 2007;40(3):874-7.
66. Kempshall BW, Giannuzzi LA, Prenitzer BI, Stevie FA, Da SX. Comparative evaluation of protective coatings and focused ion beam chemical vapor deposition processes. J Vac Sci and Technol B. 2002;20:286-90.
67. Li J, Stein D, McMullan C, Branton D, Aziz MJ, Golovchenko J. Ion-beam Sculpting at Nanometre Length Scales. Nature. 2011;412(6843):166-9.
68. Hayles M, Jiao C, Lieftink H, Reyntjens S, Wall D, Green JL, et al. Helios NanoLab 400/400S ML/600 System User's Guide. 2008.

Appendix

In this appendix supplemental images are presented. Challenges related to biological material in the FIB is illustrated by Figure 2A-4A. Figure 4A displays a typical incident during the experimental part. The same currents that had worked fine with other samples suddenly destroyed the surface. The specie represented on this image, Hypogastura viatica, was the only one showing secondary granules, visualized as the thicker granules. As the sample had great problems with charging, the sample and specie was not included in the thesis.

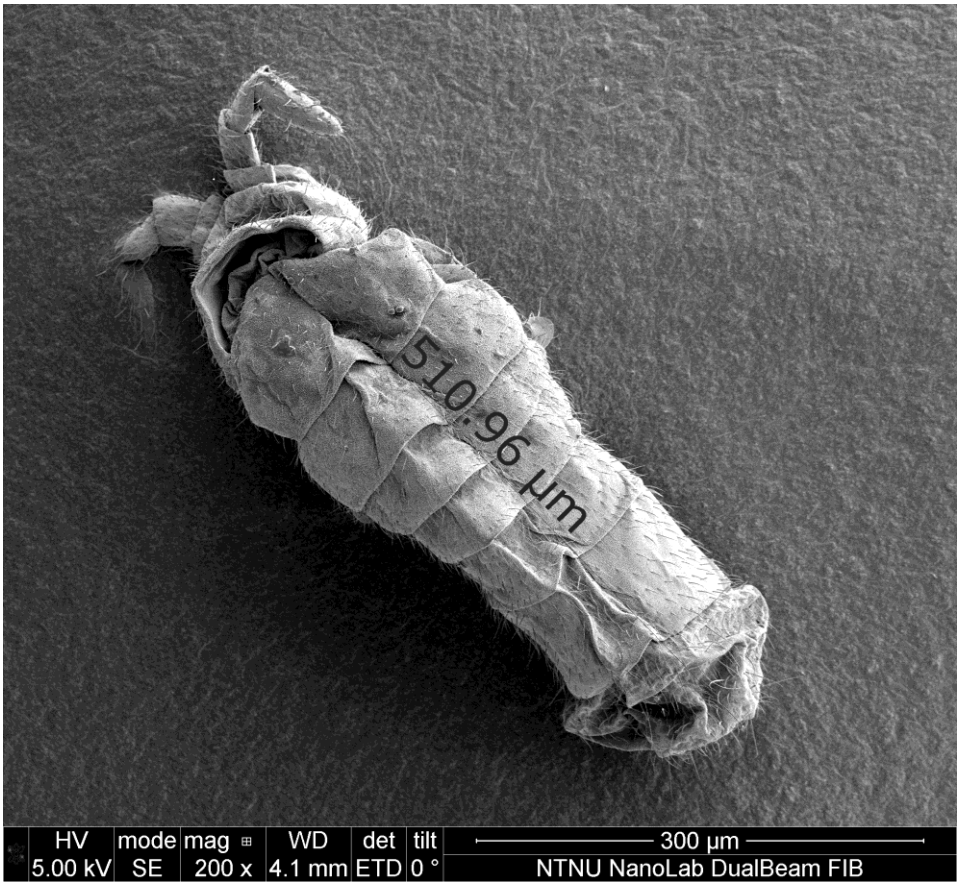

Figure 1A – Sample 4 with measurement of the collembola from head to end

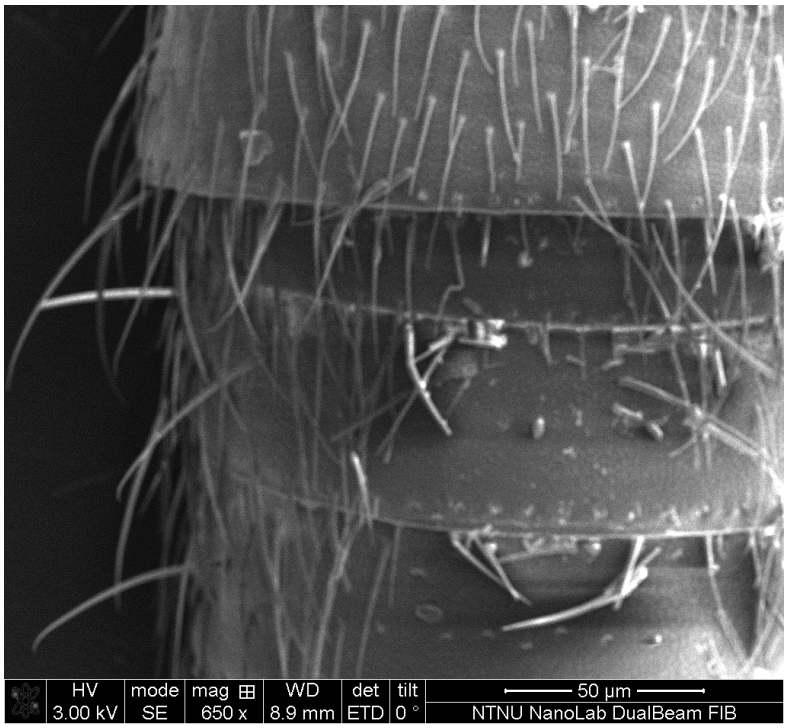

Figure 2A – Sample 3, Hairy cuticle proved to cause charging related problems

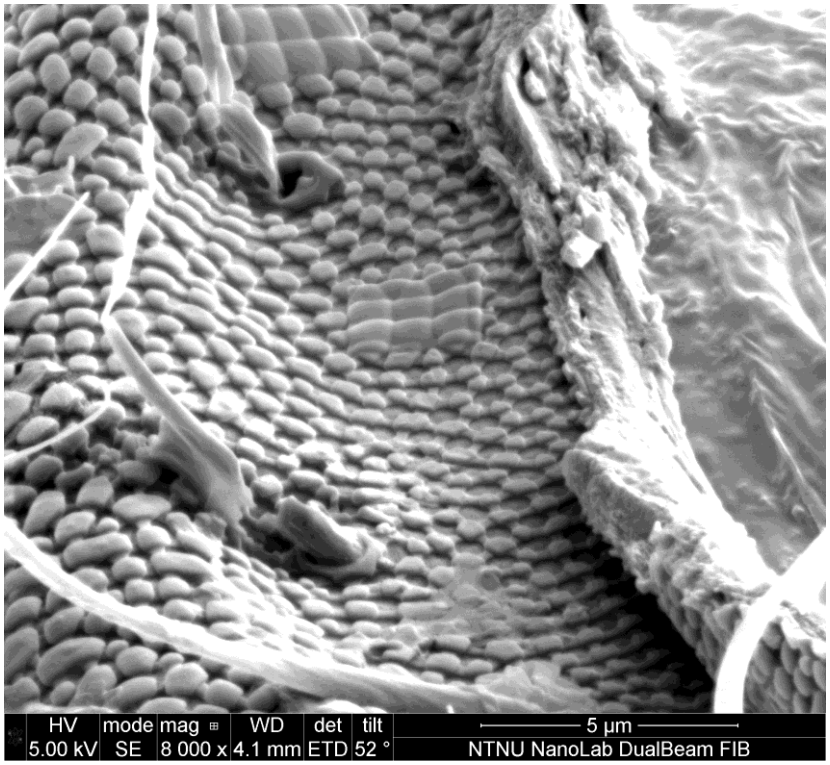

Figure 3A – Sample 1. The topography of some samples challenged the FIB procedures

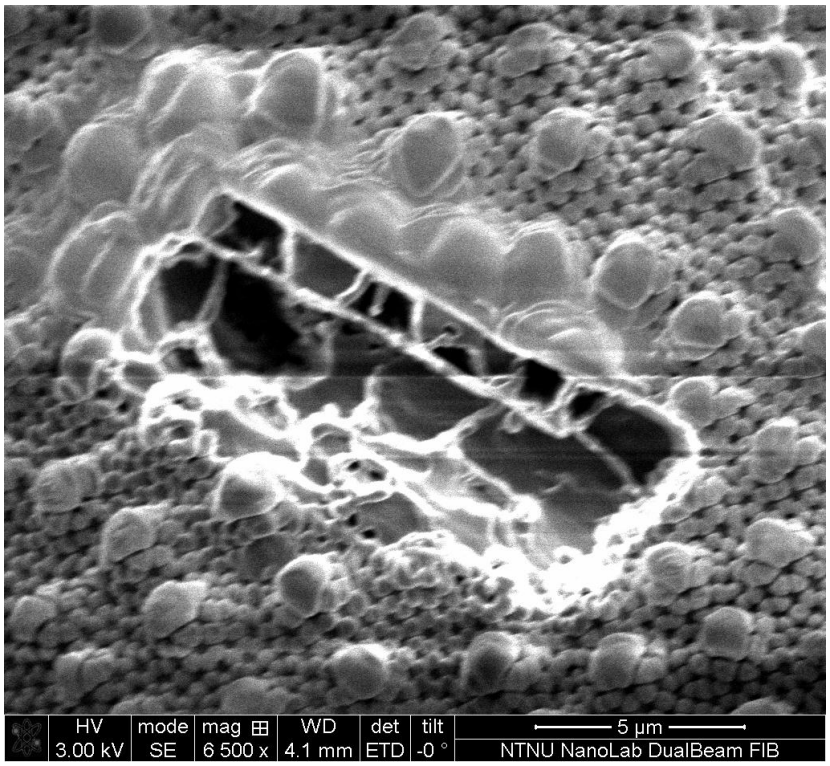

Figure 4A – Surface damages caused by FIB milling on *Hypogastura viatica*. This sample and species was not included in the thesis due to the charging problems.

Additional images of all the samples after cross section milling are presented in Figure 5A-15A. The images are either taken from a different view or from a different cross section area. Figure 16A-21A is from modified S&V images.

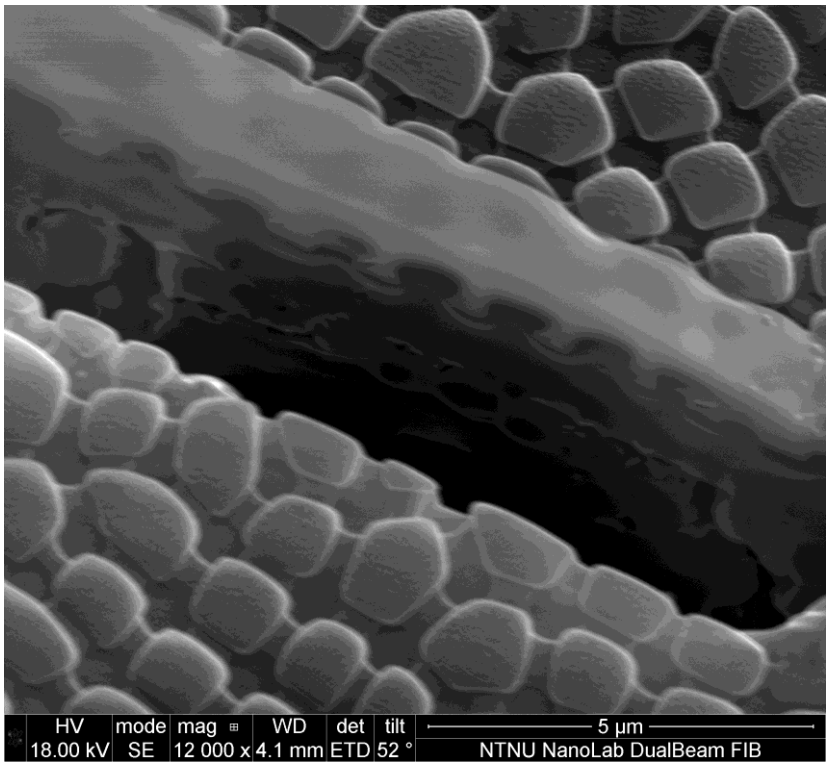

Figure 5A – Cross section of sample 1

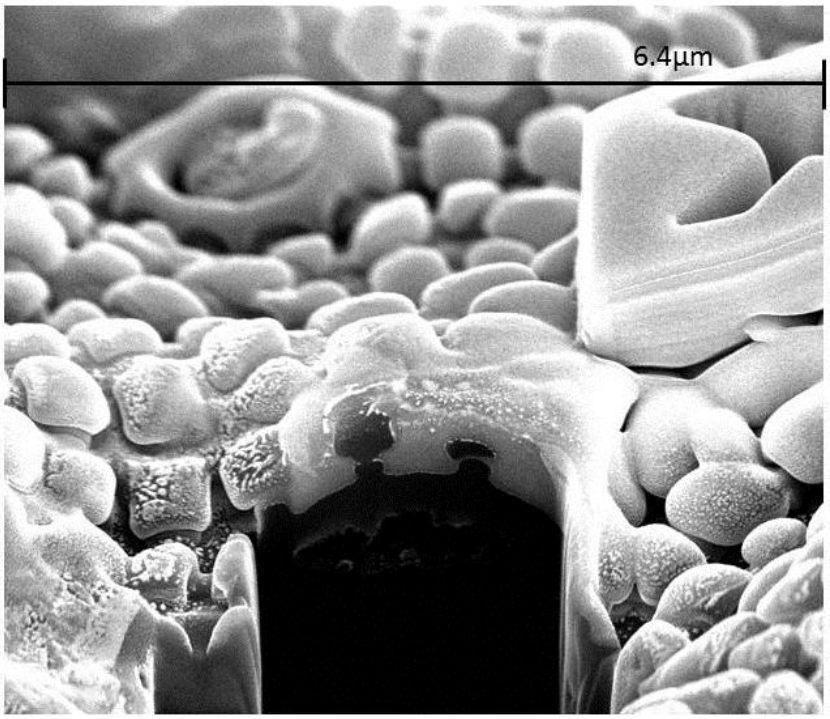

Figure 6A – Cross section of sample 1. Image is taken from S&V session where scale bar is not integrated. The measured value of image width is an approximately manually measured value. The left granule was destroyed during slicing due to too thin platinum layer.

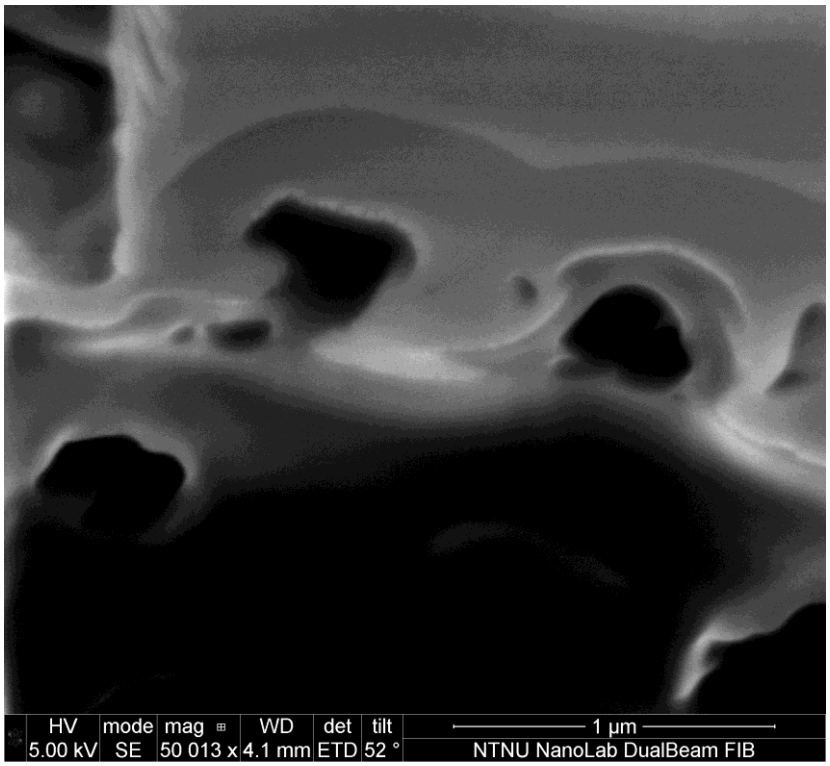

Figure 7A – Cross section of sample 2

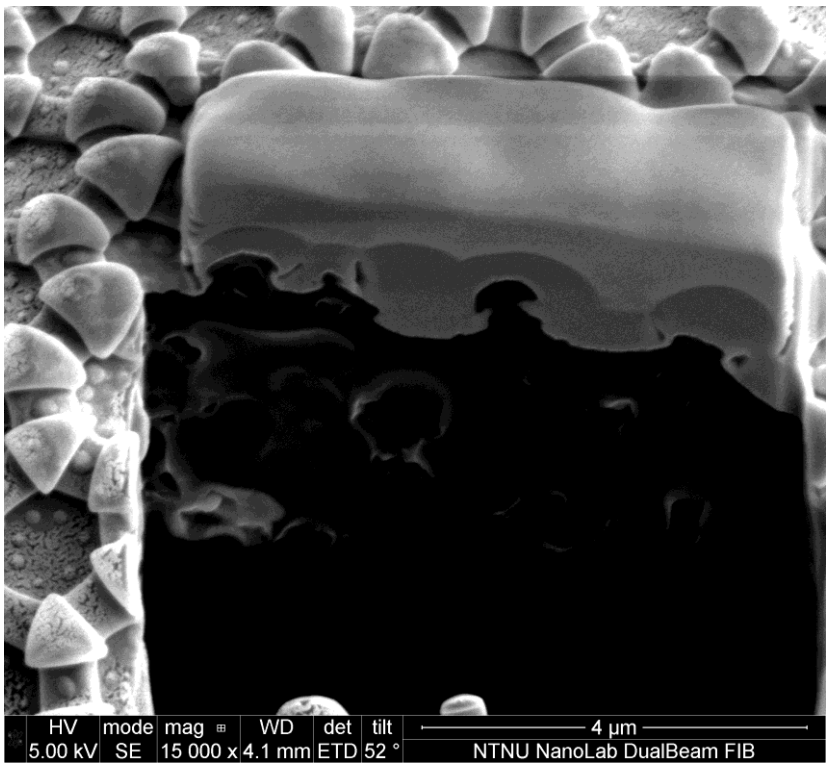

Figure 8A – Cross section of sample 2

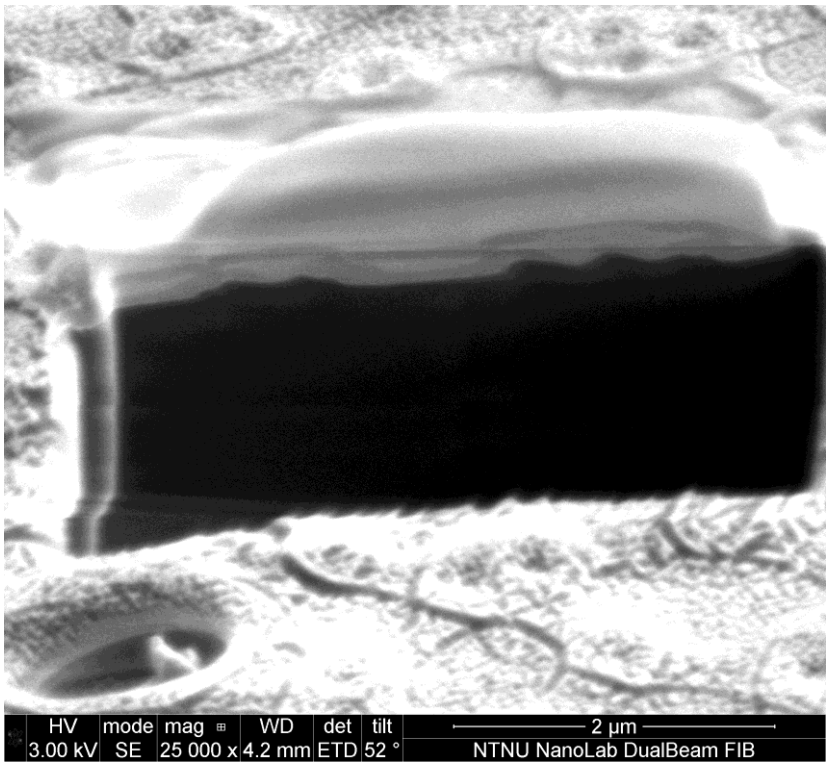

Figure 9A – Cross section of sample 3

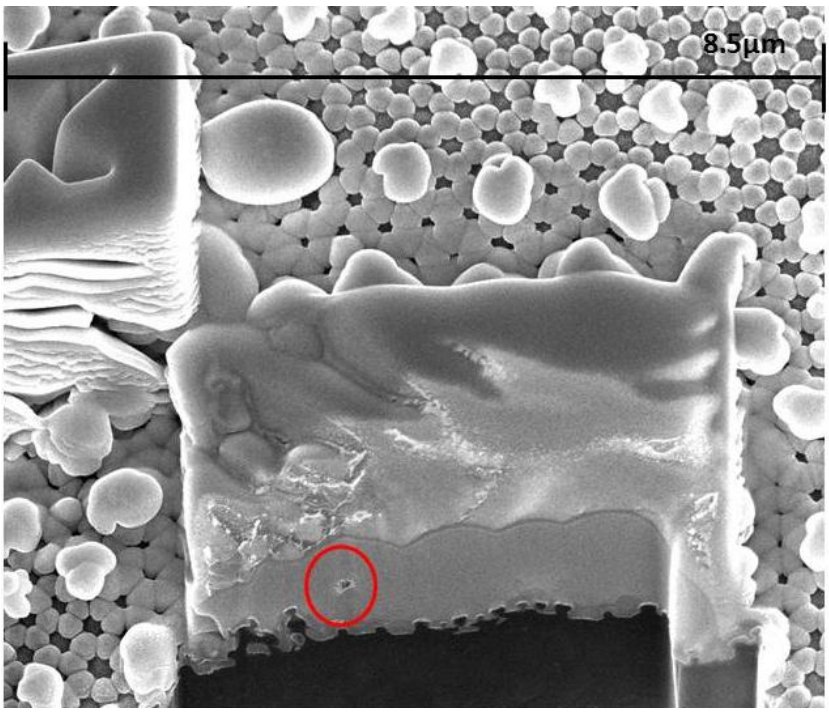

Figure 10A – Cross section of sample 4. . Image is taken from S&V session where scale bar is not integrated. The measured value of image width is an approximately manually measured value, the same as for Figure 11A. Notice how the marked granule emerges from Figure 10A to 11A.

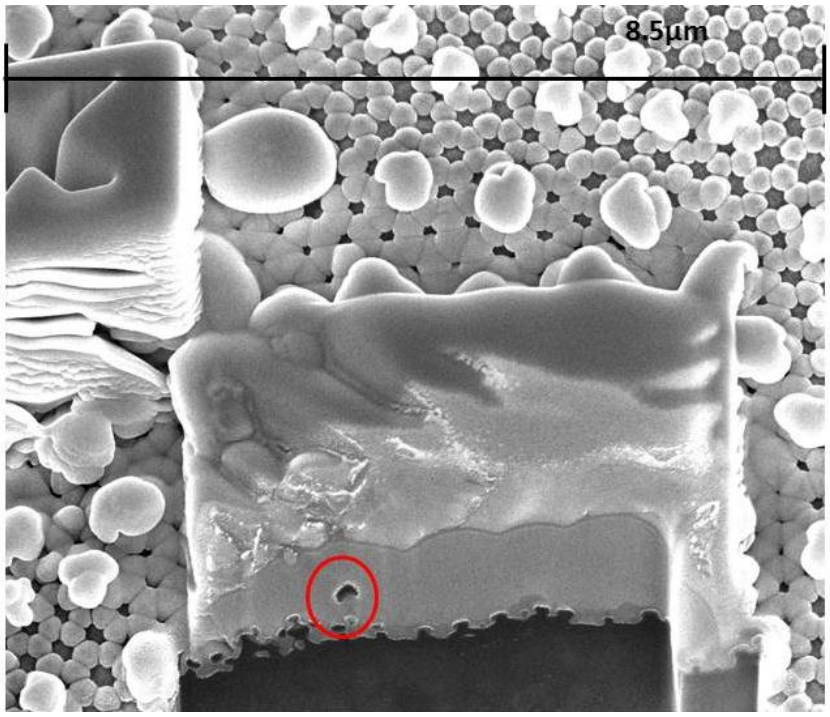

Figure 11A – Cross section of sample 4

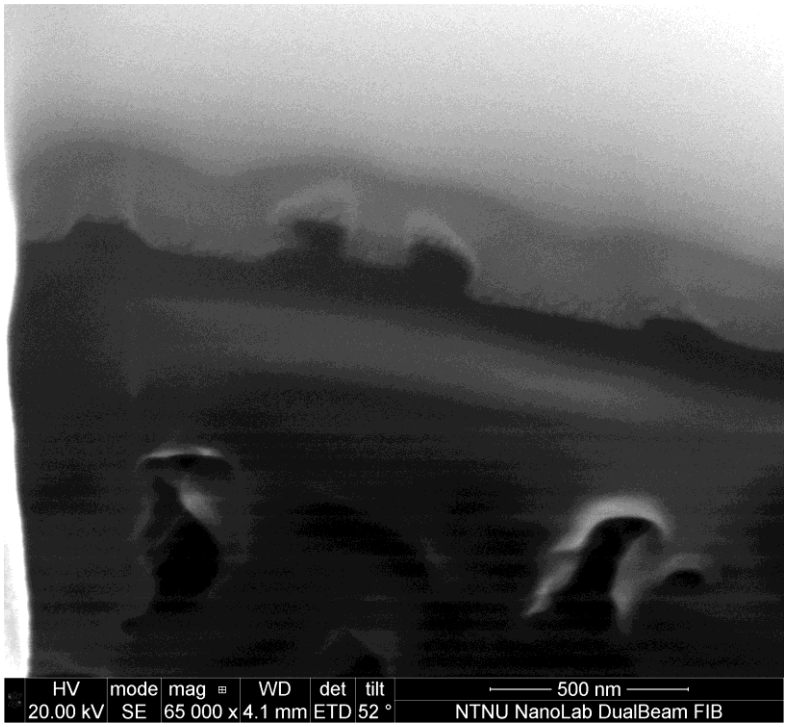

Figure 12A – Cross section of sample 5, high voltage (20kV) leads to a larger interaction volume and the SEM displays structure behind the feature of interest (here overhang). This makes the granule look somewhat transparent.

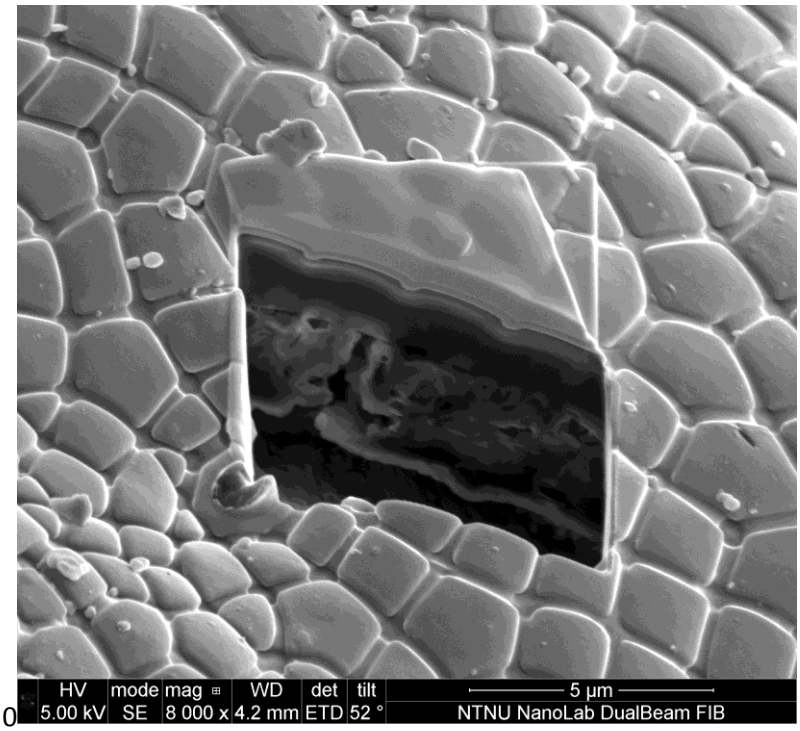

0

Figure 13A – Cross section of sample 6

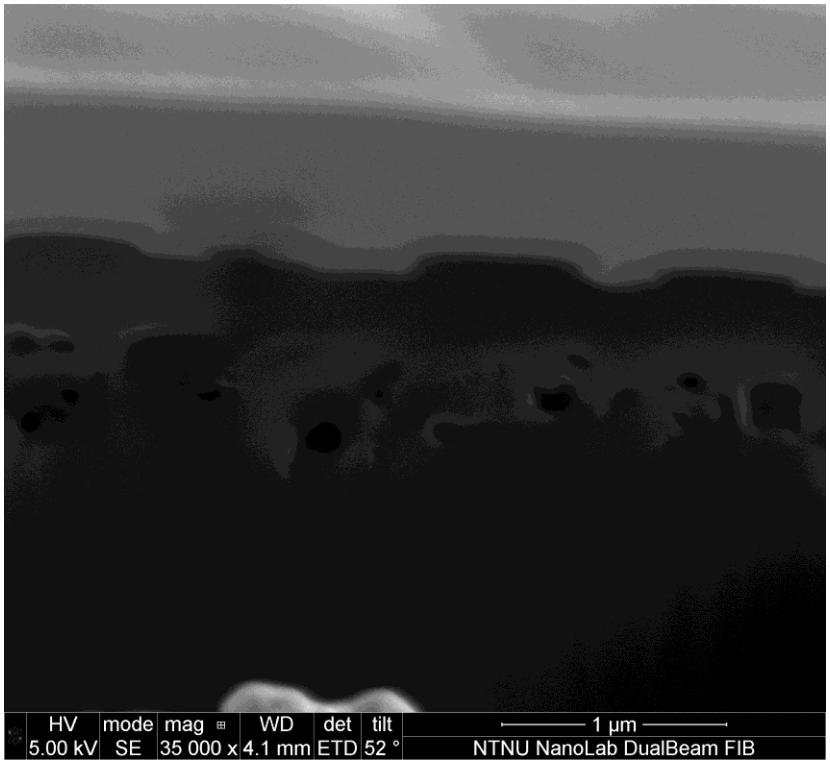

Figure 14A – Cross section of sample 7

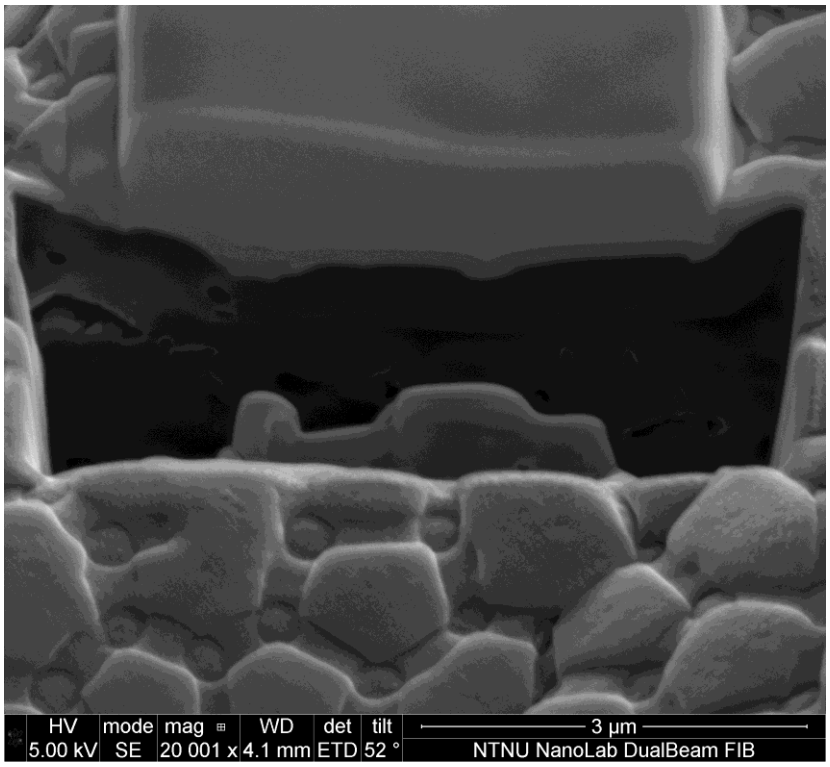

Figure 15A – Cross section of sample 8

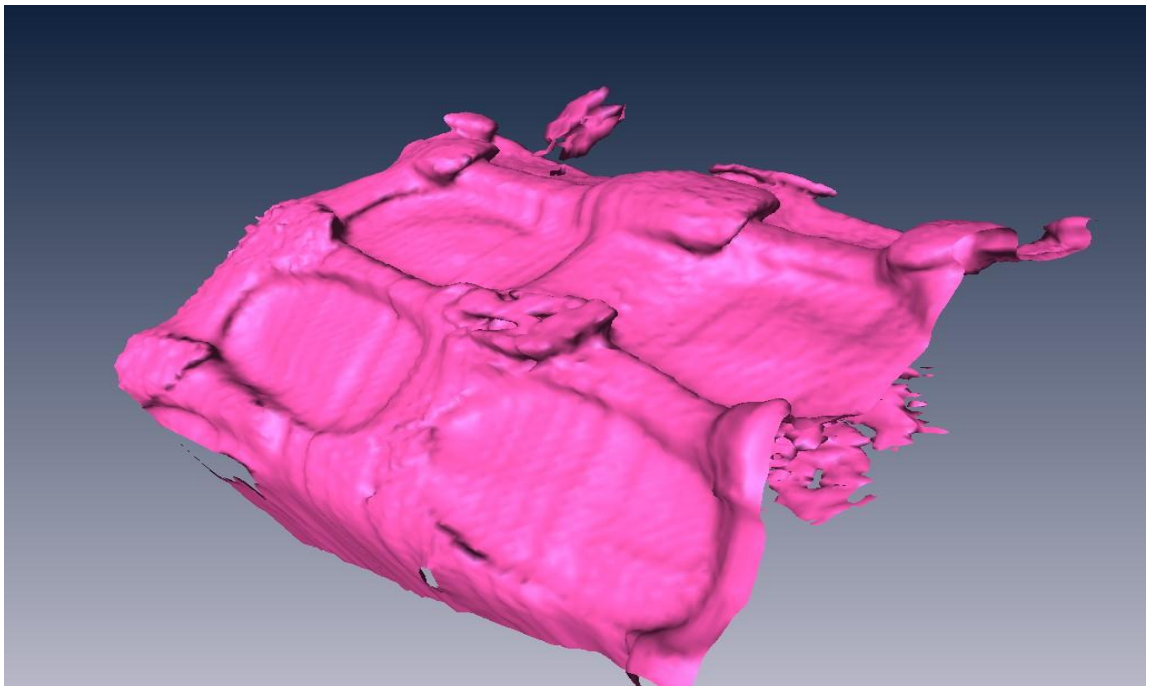

Figure 16A – 3D model of sample 1, Unmeshed surface. The destroyed granule in Figure 6A is here well displayed in the center of the image

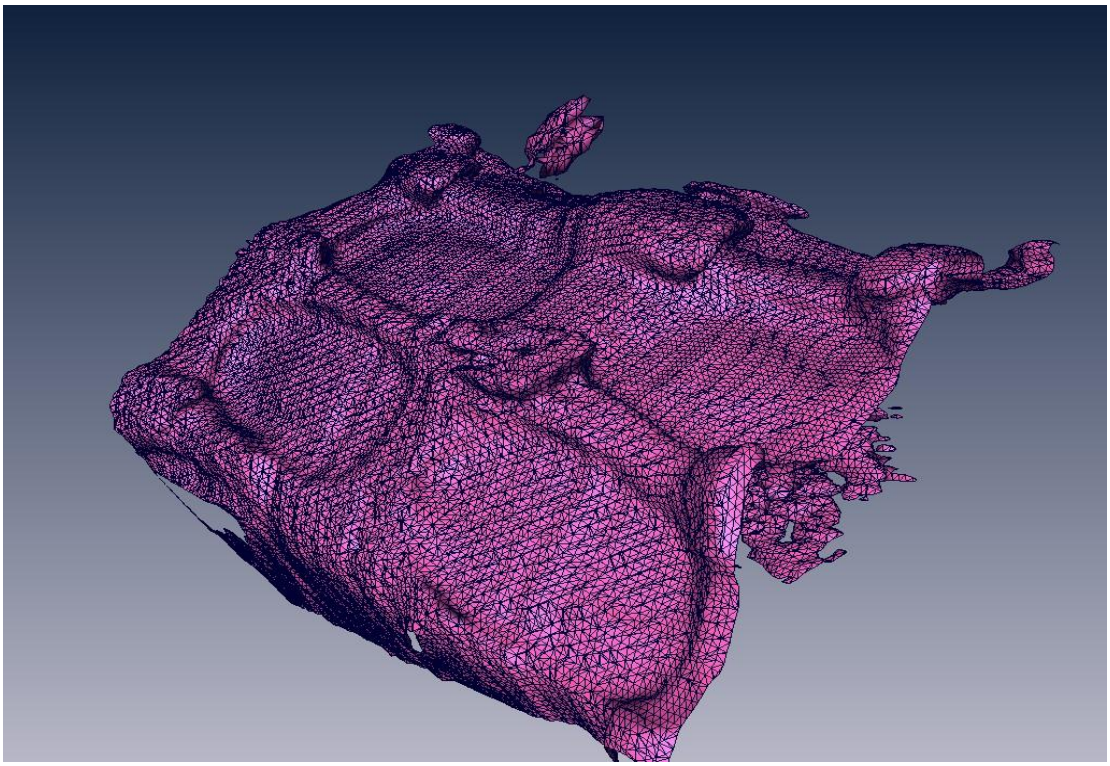

Figure 17A – 3D model of sample 1, meshed surface

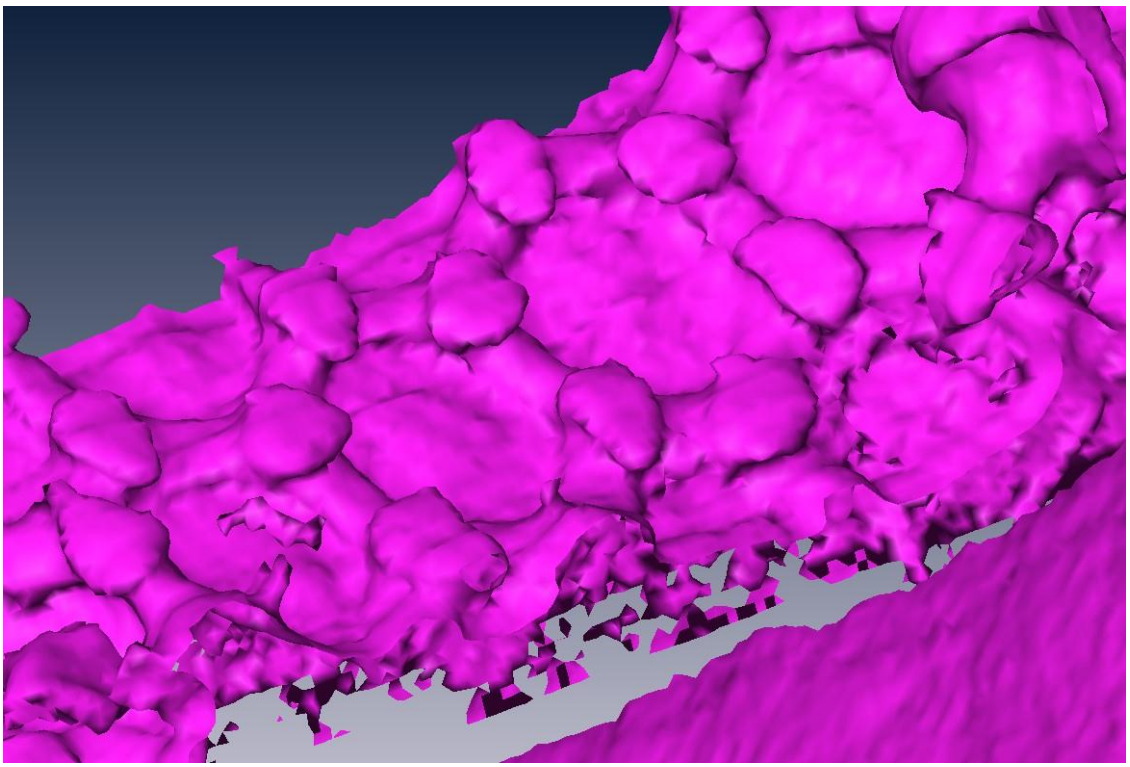

Figure 18A – 3D model of sample 4, unmeshed surface

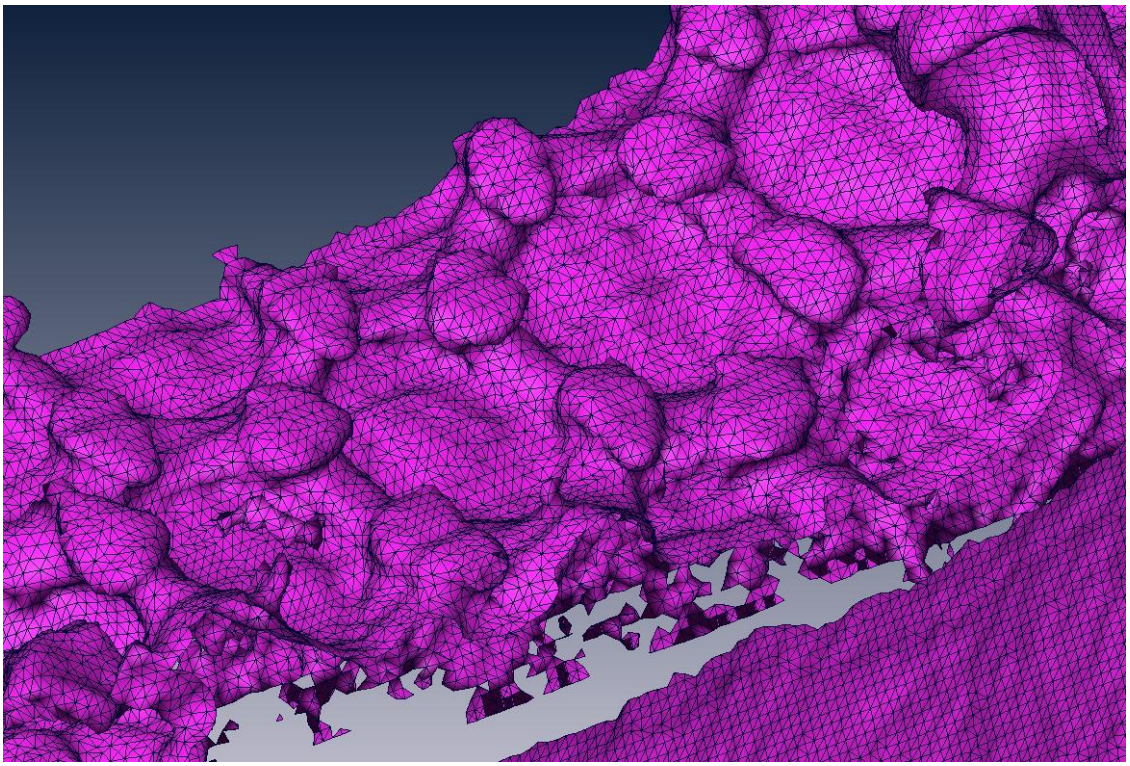

Figure 19A – 3D model of sample 4, meshed surface

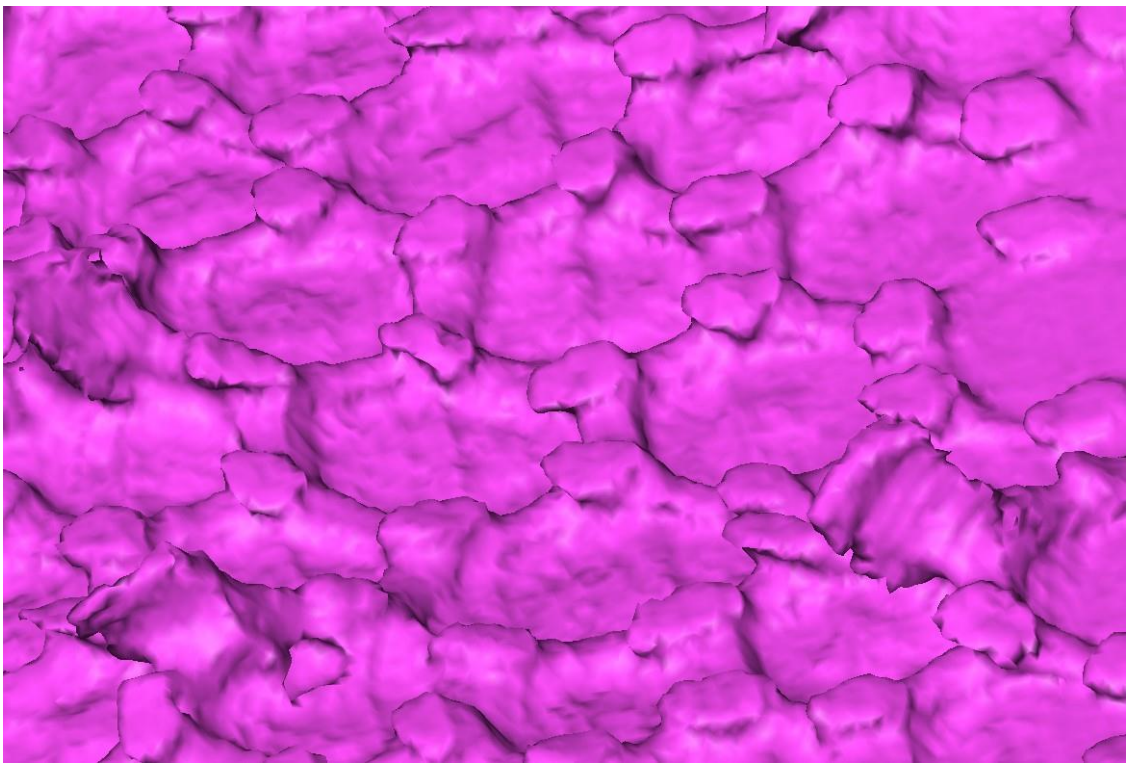

Figure 20A – 3D model of sample 4, unmeshed surface

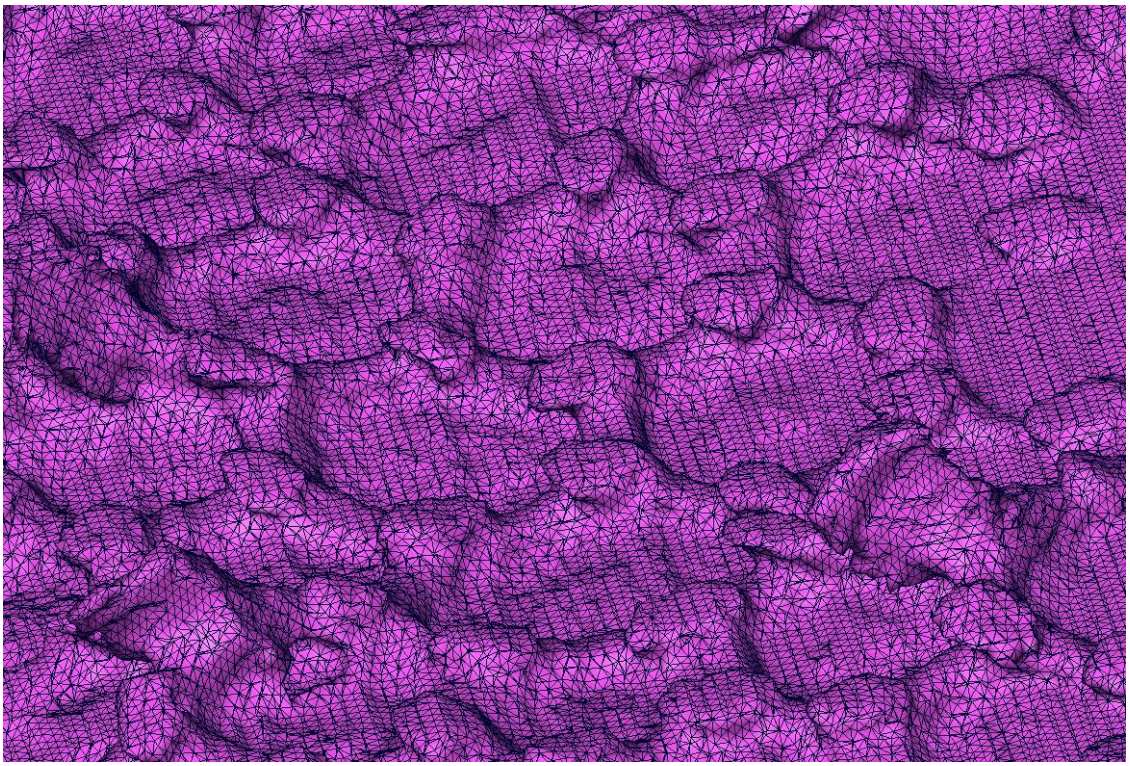

Figure 21A – 3D model of sample 4, meshed surface

Figure 22A-24A display the hairy cuticle of sample 7 and 8, thus the summer and winter adapted version of Cryptopygus clavatus. As sample 8 was almost covered by silver glue, no image that showed the hair density in its entirety was possible to obtain. Therefore no comparable images of the amount of hair on the cuticle can be presented for a possible evaluation of their contribution to hydrophobic properties.

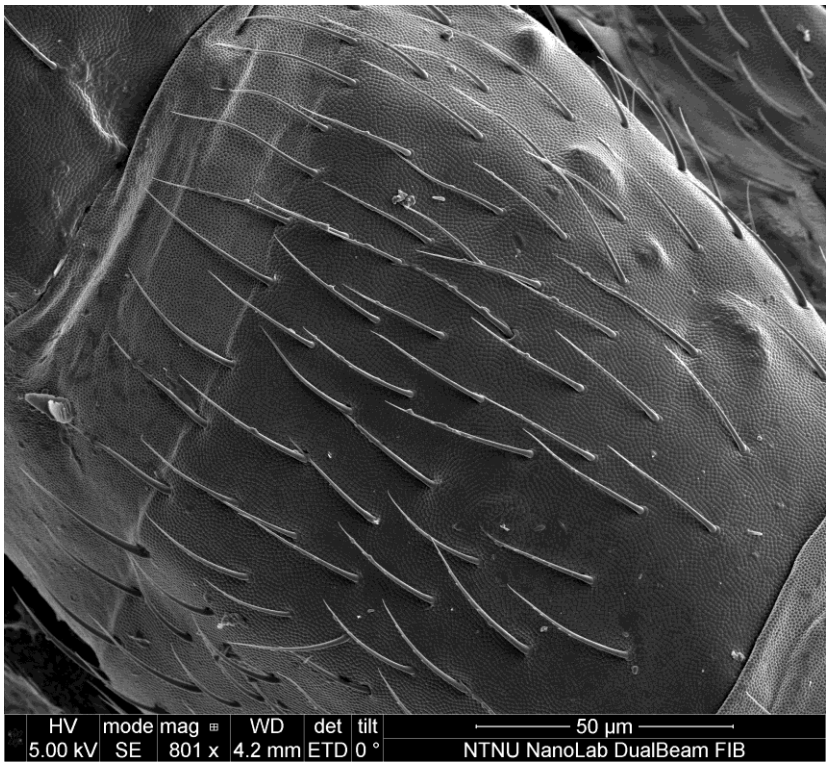

Figure 22A – Hairy surface of sample 7

Figure 23A – Hairy feet of sample 7

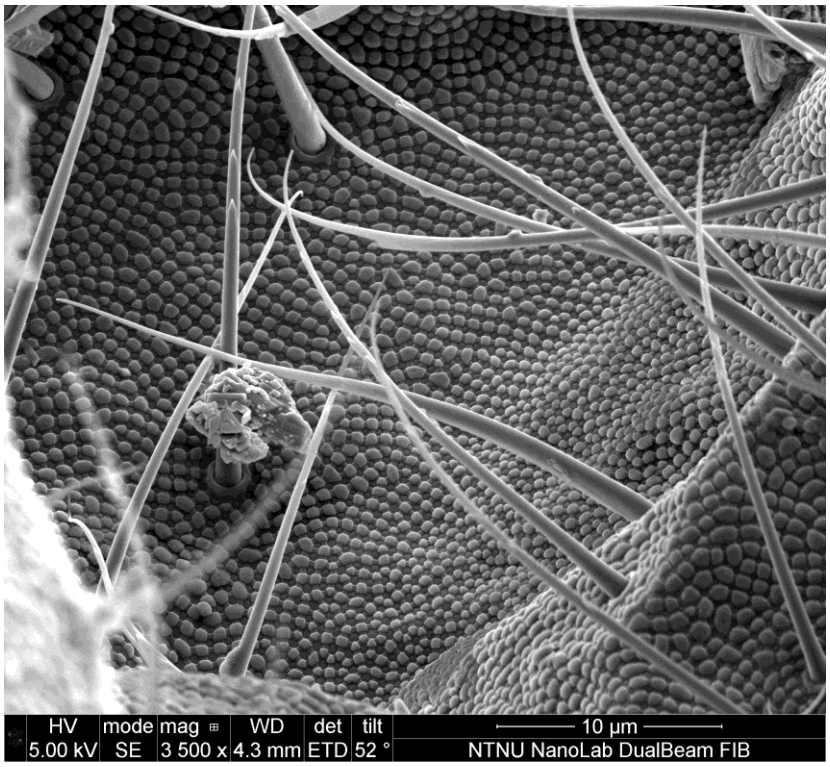

Figure 24A – Hairy surface of sample 8

There can be an internal variation of measurements on granules and belonging parameters on the same sample. This is illustrated in Figure 25A, and these values can be compared to those of Figure 47. For sample 1, 7 and 8 2-3 granules were measured and there is a variation of granule size on the same sample. How much the granules vary in size on the same sample is different, sample 1 has a more even granule size than sample 8. The latter showed a variation of 600 nm between to granules by looking at the results from Figure 47. Limitations of suitable images and results are the reason why not all samples and parameters are represented. As for Figure 47, the measurements are either done manually after FIB proceeding or by FIB software. The scale bar on the images used for measurements subsequently taken and calculated, varied from 500-8500 nm, see Figure 24A, and values collected from the smallest scale bars are still regarded as the most conservative.

	Sample 1			Sample 2	Sample 7		Sample 8	
	Granule 1	Granule 2	Granule 3	Granule 1	Granule 1	Granule 2	Granule 1	Granule 2
$g_{w,max}$	384.9	439.8	421.6	610.7	531.4	660	760.4	992.8
$g_{w,min}$	349	353.7	-	489.5	-	-	-	-
g_h	285.5	235.3	176	323.1	131.9	151	116.3	126.9
w_g	1089.6	686.8	778.6	-	588	886	-	-
ξ	76	30	-	213.1	-	-	-	-

Figure 25A – Measurements of surface features, sample 1, 2, 7 and 8 [nm]

	Colour codes for measurement					
500 nm	1000 nm	2000 nm	4000 nm	6400 nm	8500 nm	Measured by FIB software

Figure 26A – Color codes for Figure 24A